MOLECULAR DYNAMICS SIMULATION OF INTERACTIONS BETWEEN CLAY MINERALS AND A CONTROLLED ORGANIC PHASE

A Thesis
Presented to
The Academic Faculty

by

Qian Zhao

In Partial Fulfillment
of the Requirements for the Degree
Doctor of Philosophy in the
School of Civil and Environmental Engineering

Georgia Institute of Technology
May 2013

MOLECULAR DYNAMICS SIMULATION OF INTERACTIONS BETWEEN CLAY MINERALS AND A CONTROLLED ORGANIC PHASE

Approved by:

Dr. Susan E. Burns, Advisor
School of Civil and Environmental Engineering
Georgia Institute of Technology

Dr. Haiying Huang
School of Civil and Environmental Engineering
Georgia Institute of Technology

Dr. W. Crawford Elliott
Department of Geosciences
Georgia State University

Dr. Christian Huber
School of Earth and Atmospheric Sciences
Georgia Institute of Technology

Dr. J. David Frost
School of Civil and Environmental Engineering
Georgia Institute of Technology

Dr. J. Carlos Santamarina
School of Civil and Environmental Engineering
Georgia Institute of Technology

Date Approved: May 01, 2013

To my family

ACKNOWLEDGEMENTS

First and foremost, I would like to express my sincere gratitude to my advisor Dr. Susan Burns. It has been a great honor to work with her, the enthusiasm she has for her research is and will always be inspirational to me. I also feel grateful of being mentored by her patient and professional guidance, insightful suggestions. And I really appreciate the constant support throughout my study at Georgia Institute of Technology.

I would like to extend my appreciation to other members of my thesis committee, Dr. W. Crawford Elliott, Dr. J. David Frost, Dr. Haiying Huang, Dr. Christian Huber and Dr. J. Carlos Santamarina for their interests and insightful advice in my research. Other faculty members of Geosystems Group at Georgia Tech are also acknowledged for their contribution to my education. I also want to thank Dr. Ching-hua Huang, Dr. Michael E. Perdue and Dr. Andrew G. Stack for introducing me to the area of Geochemistry.

Special thanks are given to graduate students of the Geosystems Group, particularly to fellow students in Geoenvironmental group for the thought-provoking discussions. Everyone of you makes me feel blessed to be a member of this big Geo-family.

I am indebted to my parents who raised me with a love of engineering and supported me in all my pursuits. And most of all my supportive, encouraging, and patient wife Jing. I would never come this far without you.

TABLE OF CONTENTS

LIST OF TABLES

LIST OF FIGURES

Page

SUMMARY

Engineered organoclays are 2:1 phyllosilicate clay minerals synthesized with a controlled organic coating to provide controlled mechanical and chemical properties when compared to unmodified naturally occurring clays. Organoclays synthesized with montmorillonite as the base clay have demonstrated increased frictional strength, decreased compressibility, and enhanced sorption compared to the unmodified clay. Previous studies have examined the impact of the organic coating on the physical and mechanical properties of organoclays; however, the geochemical behavior for application in geoenvironmental engineering has remained relatively unquantified. This study investigated the behaviors of montmorillonite modified by quaternary ammonium cations (QAC clays), chosen with controlled structure and density of loading. The geochemical processes were modeled in the QAC clay interlayer using molecular dynamics simulations, and included organic cation structure and arrangement, organic compound sorption and mass transport, and surface electrokinetics of suspended QAC clay particles.

The interlayer arrangement of QAC was demonstrated to be a function of both the number and type of intercalated organic cations. In systems without water, the clay basal surface coverage increased and shifted from monolayers of carbon to multiple layers of carbon in the clay's interlayer, as the organic carbon loading increased. Monolayer, bilayer, and paraffin structures of organic carbon arrangement were observed in the interlayer, in agreement with previous studies. Furthermore, this study indicated that the transition of the micro-layer structures was essentially controlled by the interlayer

organic carbon content, or total organic carbon content (TOC) at the macro-scale. Consequently, when the interlayer organic coating was known, the interlayer surfactant microstructure can be estimated.

The interlayer sorption of a model organic compound, benzene, to different types of organoclays showed two major types of sorption mechanism: adsorption, with the dominant sorption mechanism being interaction between the clay surface and the organic molecule. Adsorption was observed for organoclays synthesized from smaller QACs, and demonstrated that as the number of small QACs decreased, the synthesized clay had a higher number of surface sites available for sorption, resulting in increased sorption capacity as the cation density decreased. In contrast. partitioning behavior was observed for organoclays synthesized with long chain cations, and the dominant mechanism of interaction was between the surfactant chain and the organic molecule. For these organophilic clays, as the organic carbon content increased, the organic carbon matrix formed from the cation chains had larger volume to dissolve organic molecules, resulting in increased sorption capacity.

The mass transport of an organic molecule, benzene, in HDTMA clay was simulated in both QAC clays and unmodified montmorillonite clay. The interlayer diffusion rate demonstrated that non-polar organic species tended to diffuse more slowly because they were subjected to interaction with the interlayer organic carbon chains, while non-interactive species like water had a higher diffusion rate. Additionally, as the interlayer pore spacing increased, or the molecular size decreased, the target diffusive species demonstrated increased diffusion rate. When applied to a modified compartment

model to estimate the bulk diffusion rate, the results indicated that the bulk diffusion rate of organic species in organoclays was controlled by the interlayer diffusion rate.

The surface electrokinetics of a suspended HDTMA montmorillonite particle were simulated for comparison with a sodium montmorillonite particle surface. The simulation results demonstrated that HDTMA cations were more likely to form inner-sphere complexes than sodium cations; consequently, they were more effective in neutralizing the layer charge of clay. The effective surface charge and electrical potential adjacent to a clay surface with either sorbed sodium or sorbed HDTMA were quantified. The HDTMA clay surface had lower charge, with an electrical potential closer to zero. The organic coating also had an impact on the thickness of the diffusive layer and the distribution of inorganic anions. The locations of the interfacial planes were predicted based on averaged species density profile and water alignment.

CHAPTER 1
ORGANIC COATED CLAYS AND THEIR ENGINEERING BEHAVIOR

Montmorillonite and clays with natural organic matter

Clay minerals are fine-grained soils that include a group of layered aluminum silicates or magnesium silicates, also known as phyllosilicates. The mineral montmorillonite consists of an alumnia octahedral sheet sandwiched between two silica tetrahedral sheets, and is referred to as a 2:1 clay mineral. Montmorillonite is the major component of bentonite, which is a mixed mineral soil used frequently for geotechnical applications. Montmorillonite is a highly plastic, swelling clay mineral with high specific surface area (Mitchell, 1976; Santamarina, 2001), which may result in significant sorptivity for certain species (Cases et al., 1992; Stadler and Schindler, 1993; Kraepiel et al., 1999). The layer charge of montmorillonite results primarily from isomorphic substitution within the mineral crystal, and typically yields an excess of negative charge, which is counteracted by cations that are present in the interlayer of the clay mineral. Most commonly, this excess negative charge has two primary results: interlayer attraction of inorganic metallic cations (e.g., Na^{+}, Ca^{2+}) that hydrate strongly, and the development of highly ordered water layers within the interlayer space (Young and Smith, 2000; Tambach et al., 2006). If environmental conditions change, cation exchange reactions may occur within the particle interlayer. Cation exchange in the interlayer does not affect the mineral solid phase; however, the physical-chemical properties of the clay mineral may vary significantly due to changes in the structure within the clay's interlayer (Celis et al., 1997; Bhattacharyya and Sen Gupta, 2006).

For fine grained soils, the mineralogy and soil fabric are the primary controls on the interfacial behavior of the soil. For 2:1 clay minerals, because of their relatively large amount of

specific surface and layer charge, intermolecular forces (both long-range and short-range forces) start to dominate the interactions between soil particles of colloidal size, as opposed to contact interactions observed for coarse-grained particles. Additionally, interlayer cation hydration will control the soil's swelling tendency (Pashley and Quirk,1984; Smith, 1998), while interlayer species and surface sites are responsible for the uptake of inorganic/ organic sorbates (Mortland et al., 1986; Boyd et al., 1988). The mechanical response will be controlled by inter-particle net forces (Yong and Selig, 1961; Santamarina, 2003). Notably, the force equilibrium between the mineral phase, water, and interlayer cations is also complicated, and can be altered with change of pore fluid. When the naturally occurring inorganic cations of the clay are replaced by organic cations, organic-clay complexes can be formed. The quantity and the nature of the exchanged organic cations may contribute to the altered properties of the new complexes.

The interaction between clay minerals and organic matter represents one major type of surface and colloid reaction in the geosystem. The organic matter in geosystems primarily originates from biological materials or industrial wastes, and migrates to water bodies, soils, and sediments (Cerri et al., 1991; Shen, 1999). The interaction between natural organic matter (NOM) and clay minerals typically results from physical or chemical bonding, resulting in organic-clay complexes, or organo-rich clays. Natural organic matter in soils is often a collective term to describe decomposed organic matter that comes from plants and animals in the environment, and includes both humic and non-humic fractions. Large molecules of NOM can be formed from the polymerization of different parts of already broken down matter. The relative size, shape, and composition of a molecule of NOM are heterogeneous (Stumm and Morgan, 1996), and the content of NOM in surface soils can range from 0.5% to 100% (Sparks, 2003). Also, due to the complexity of the types of clay minerals and organic matter, the interaction

mechanism between the phases can differ substantially. Most commonly, cation exchange and adsorption are the two major types of interactions between organic matter and clay minerals. In nature, those two processes are always heterogeneous and complicated and can significantly modify the engineering behavior of the soils.

Organoclay engineered with QAC surfactant

Engineered organic-coated clays are synthesized under laboratory controlled conditions, which allows selection of specific cation structure and density of loading on the mineral surface. Because engineered organoclays can be synthesized with selected organic coatings to optimize strength, lower compressibility, and to increase the retention of organic compounds in the environment, they are of engineering interest and have been investigated extensively during last decades (Weiss, 1963; Lagaly, 1981; Boyd et al. 1988b; Jaynes and Boyd 1991a; Smith et al., 1990; Sheng and Boyd, 1996). Most commonly, organoclays are created by exchanging quaternary ammonium cations (QACs) onto the clay surface (Burns et al., 2006; Bate, 2010). QACs are composed of an ammonium head group, with four exchangeable positions that can be occupied by organic functional groups of varying size and structure. The process of intercalating quaternary ammonium organic cations onto the montmorillonite surface by replacing their naturally occurring inorganic cations can be referred to as primary adsorption of organic cations.

By varying the molecular structure and quantity of the QACs that are loaded onto the clay's interlayer during primary adsorption, the interfacial characteristics of the resulting clay mineral can be controlled, resulting in changes in properties such as surface hydrophobicity, frictional interaction (Burns et al., 2006), and dynamic behavior. Additionally, the organoclay's sorptivity for nonpolar organic compounds (i.e., secondary sorption), will also exhibit variable

behavior as a function of the exchanged organic cation structure or amount of loading (Redding et al., 2002; Bartelt-Hunt et al., 2003). For engineering purposes, it is necessary to quantify organic-modified clay behavior as a function of its organic coating, in terms of both cation type and quantity. Geotechnical characterization of clays modified with quaternary ammonium cations (QAC) demonstrated that organic-coated clays exhibit varying engineering behaviors according to their different intercalated organic surfactants in interlayer (Soule and Burns, 2001; Burns et al., 2006).

After intercalation of organic cations into the interlayer of a clay-organic composite, the charge distribution, interlayer distance, and polarity of interlayer species can be altered, resulting in differences in interlayer structure as a function of the type and amount of sorbed cation. The interlayer surfactant also affects the particle-particle interactions and mineral surface characteristics, which contribute to the modified engineering properties of organoclays (Jaynes and Boyd, 1991; Lo et al., 1997). Consequently, fundamental understanding of the microstructure of organic-coated soils is critical to interpret in order to predict the engineering behaviors of organoclays in practice.

While extensive work has been performed to quantify the behaviors of organoclays (Weiss, 1963; Lagaly, 1981; Janek and Smrcok 1999), exploration of the fundamental mechanisms responsible remains challenging due to the complex interlamellar structure in the organoclays. Significant insights have been gained through experimental investigation of the intercalated QAC structure, including X-Ray Diffraction (XRD) (Lagaly, 1981), Fourier transform infrared spectroscopy (FTIR) (He et al., 2004a), and thermo-gravimetric measurement (TG) (Xie et al., 2002; Yariv, 2004). These studies have greatly enhanced the fundamental understanding of the microstructures of interlayer surfactants, providing insights into issues such

as the orientation of the aliphatic chain, and the transition from monolayer arrangement to the paraffin complex. However, it is often difficult for experimental approaches to explore molecular interactions among mineral, intercalated organic cations, and water in the interlayer. For fundamental understanding of organoclay behavior controlled by the interlayer surfactant, two questions merit examination: First, how to relate intercalated surfactant structure to base clay and surfactant type? A model aimed at describing the arrangement pattern of surfactants based on clay prototype and intercalated organic cations is needed. Second, how to interpret and predict the engineering properties (sorptivity, strength, conductivity) of organo-clay composites from their surfactant arrangement patterns?

Geotechnical characterization of QAC- montmorillonite

While organic matter can exert a significant influence on soil properties, the physical, chemical, and mechanical behavior of a soil coated with organic phases still needs to be quantified from the perspective of geotechnical and geoenvironmental engineering. Multiple studies have tested soils with controlled interlayer organic phases under laboratory conditions. Clays synthesized with quaternary ammonium cations (QAC) are the most commonly tested materials in terms of geotechnical characterization (Boyd et al. 1988; Smith et al., 1995; Bartelt-Hunt et al., 2005; Lorenzetti et al., 2005). The engineering characterization and behavior, including Atterberg limits, strength, sorptivity, compressibility, and hydraulic conductivity of montmorillonite modified with organic cations will be discussed briefly.

The interactions between organoclays and the pore liquid is significantly different from that of unmodified clay. While pure montmorillonite exhibits high water content at its liquid limit (water content several times solid mass), the liquid limit for organic-coated montmorillonite

is measurably lower, due to the presence of non-polar, as opposed to ionic, interlayer cations (Soule and Burns, 2001). In contrast, when the pore liquid is changed from water to low polarity fluid (i.e. methanol), organolays synthesized from larger QACs (i.e. $HDTMA^+$, $ODTMA^+$) exhibited stronger pore liquid holding capacity, and their liquid limit as percentage of organic pore liquid versus solid increases.

Clays with interlayer organic matter typically have increased strength because intercalating organic cations onto 2:1 clay minerals reduces the amount of interlayer water and can also facilitate binding of silica sheets. The increase in strength is observed for both the critical and peak shear strengths of the organic modified clays. Direct shear tests performed on unmodified bentonite, BTEA-bentonite, TMA-bentonite, DTMA-bentonite, and HDTMA bentonite demonstrated that organo-modified bentonite had a significantly higher friction angle (in the range of 34~37 degrees), compared with unmodified bentonite (approximately 7 degrees) (Soule and Burns, 2001). Notably, when those organobentonites were consolidated to the same effective stress before shear, they had water contents ranging from 50~55%, while unmodified bentonite had a water content greater than 300%. Consolidated undrained triaxial tests were also performed to study the strength of organoclays synthesized from QACs with varying chain length and branch structures (Bate, 2010). The critical state frictional angles of modified clays ranged from 34~60.8 degrees and increased as the total organic carbon (TOC) content increased.

The adsorption efficiency of pure montmorillonite as a sorbent for nonpolar organic compounds is low due to its hydrophilic interlayer species (Boyd et al., 1988; Smith et al., 1990). In contrast, organoclays may exhibit much stronger capacity of uptake of nonpolar organic compounds when compared with unmodified montmorillonite. It has been demonstrated that organoclays synthesized from small QACs (e.g., TMA^+; TEA^+; $BTEA^+$), demonstrate

surface adsorption for small organic molecules (i.e. benzene) and can be modeled using a Langmuir adsorption isotherm (Burns et al., 2006), while organoclays intercalated by long chain QACs (e.g., $HDTMA^+$), exhibit partitioning behavior and are best modeled with a linear sorption isotherm (Burns et al., 2006; Mortland et al., 1986). Experimental evidence has indicated that as the size of the organic cation was increased, either by increasing the length of the carbon chain in one functional group position or by increasing the chain length equally in all four functional group positions, the secondary sorption of nonionic organic chemicals transitioned from an adsorption mechanism to a partitioning mechanism (Boyd et al., 1988). Thus, it is possible that the sorption capacity and type are essentially controlled by the arrangement of interlayer organic carbon.

According to 1D consolidation test results (ASTM D2435-96, Test method A, Soule and Burns, 2001), organoclays synthesized from QACs have significantly lower compressibility when compared with unmodified clays. The compression index can be reduced by an order of magnitude and the swell index is also tens of times lower. At same stage of loading, organoclay with the highest organic content, or more layers of interlayer carbons, exhibit the most compression (i.e. HDTMA-clay) while those that have the least amount of organic carbon, or a monolayer carbon surfactant (i.e. TMA-clay) would experience the least compression. Additionally, organoclays exhibit less tendency to expand, with swell indices ranging from 0.035~0.083 (Soule and Burns, 2001), compared with a swell index of 1.5 for unmodified montmorillonite clay.

Organoclays have relatively higher hydraulic conductivity than unmodified montmorillonite clays. Falling-head permeability tests with flexible-wall permeameters (Lorenzetti et al., 2005) were performed to compare the hydraulic conductivities of unmodified

clay, GCL clay, and GCL with organoclay amendments. Test results indicated that only a small increase in hydraulic conductivity was observed for both types of amended GCLs with up to 20% organobentonite amendment. However, at higher organobentonite contents, measured hydraulic conductivity for amended GCLs increased by as much as three orders of magnitude. Similar trends have been observed for the hydraulic conductivities of Na-bentonite, BB-40 (Na-bentonite modified by dicetyldmethylammonium), and CDV (completely decomposed volcanic rock) (Lo and Yang (2001). Among the three types of soils, organic bentonite BB-40 had the largest hydraulic conductivity and was 3 orders of magnitude larger than the unmodified Na-bentonite. However, when the conductivity tests were performed with gasoline, the trend was reversed: Na-bentonite had the largest conductivity to gasoline and BB-40 was about 3 orders of magnitude smaller.

Current Engineering applications of organoclays

Because of their increased strength, lower compressibility, and enhanced sorption capacity for organic compound, organically modified clays can be used for a variety of applications, including waste stabilization, water purification, oil and hydrocarbon spill control, and as components of engineered earthen barriers. Organoclays, especially montmorillonite based organoclays, can be blended with natural soil for the construction of engineered barrier systems (Lo and Yang, 2001; Lorenzetti et al., 2005; Lee et al., 2012). Many studies have demonstrated the possibility of using organoclays as sorbents for organic contaminants in a wide variety of environmental applications (Alther et al., 1988; Harper & Purnell, 1990; Stockmeyer, 1990; Park & Jaffe, 1993; Sheng & Boyd, 2000). Clay liners are effective for control of advective transport of dissolved aqueous species, but are ineffective at controlling the diffusive

transport of organic molecules, and may also allow increased flow in the presence of concentrated organic liquids. (Gangadharan et al., 1988) (Brown et al., 1983). Because organoclays are organophilic, they demonstrate a lower conductivity when exposed to concentrated organic liquid (e.g., petroleum products).

Scope of this study

While many of the properties of organoclays have been quantified at the macroscale, there remain significant questions regarding nanoscale structure and transport within the interlayer of the clay organic composites. Consequently, this study used molecular dynamics (MD) modeling to examine the geochemical properties of montmorillonite minerals with single chain quaternary ammonium cations (QAC) intercalated into the clay's interlayer. The simulations were performed using the Large-scale Atomic/Molecular Massively Parallel Simulator (LAMMPS) (Plimpton, 1995) and results were processed in Visual Molecular Dynamics (VMD) (UIUC, March 2011) and Materials Studio 5.5 (Accelrys Inc.).

The prototypes of unmodified clays were Na-montmorillonite with varying charge densities, intercalated with three types of single chain QACs (Figure 1-1): tetramethylammonium (TMA); decyltrimethylammonium (DTMA) and hexadecyltrimethylammonium (HDTMA) (chemical structures are shown in the figure below), to synthesize the organoclay composites. The effect of increasing one carbon chain length of the QAC on the organoclay behaviors was investigated, including: surfactant arrangement and microstructure of the resultant organoclays (Chapter 3); secondary sorption behavior of organoclays as a function of surfactant structures and amount of organic loading (Chapter 4); mass transport of an organic compound in long chain QAC clays (Chapter 5); and surface electrokinetics of suspended QAC clay particles (Chapter 6).

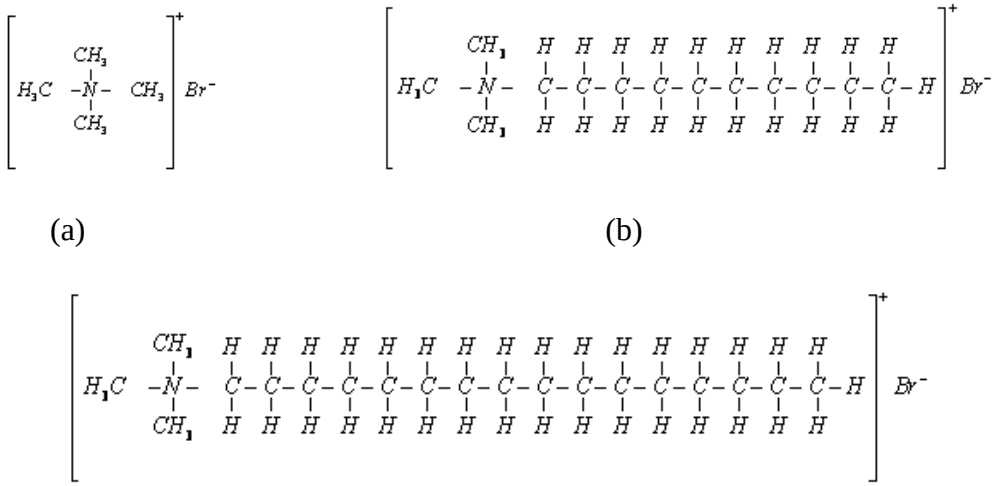

Figure 1-1. Molecular structure of modeled QAC organic cation structure: (a) TMA, (b) DTMA, (c) HDTMA.

CHAPTER 2
MOLECULAR DYNAMICS SIMULATION OF INTERACTION BETWEEN CLAY, WATER AND ORGANIC SURFACTANT- COMBINED FORCE FIELD

Insight into geochemical processes at the nanoscale level of the organoclay is difficult to obtain, and is typically inferred from a relatively small number of carefully controlled experimental and analytical investigations (Zhou et al., 2007; Zhou et al., 2008); however, due to complexities of the micro-structure of layered phyllosilicate minerals and to the difficulties of observation and measurement at such a small scale, it is necessary and important to apply theoretical molecular models to yield insight into phenomena that occur at the atomistic level. Molecular modeling combines theoretical methods and computational techniques in order to model or mimic the behavior of molecules, or groups of molecules in a system, and it has various applications in chemical, biological engineering, material sciences, and the pharmaceutical industry. These techniques are becoming more mature and robust, such that molecular modeling is an important supplement to experimental approaches. In geochemistry, geoenvironmental engineering, and environmental engineering (Cygan, 2001; Cummings, 2002), molecular models have played an important role in understanding interfacial and nano-scale properties and processes.

Computer simulation techniques have been involved in the study of the clay and clay-organic composites, including: Discrete Element Method (DEM) (Anandarajah, 1999), Monte Carlo (MC) (Skipper et al., 1995a,b), and molecular dynamics (MD) (Greathouse and Cygan, 2005; Liu et al., 2007) simulations. To best simulate the properties of organic-coated clays at the nano-scale, molecular dynamics modeling permits the simulation of mineral-organic interaction at the molecular level, and provides quantitative information for atomistic interactions, as well as

thermodynamic information for the simulated system (Hou et al., 2000; Greathouse and Cygan, 2005; Liu et al., 2009). Applications of MD simulation can be used as an important supplement to aid in the interpretation of experimental studies. Because MD simulations can be performed in three dimensions, on the time scale of nano-seconds, it is sufficient for the study of intercalated surfactant in interlayer of the montmorillonite mineral.

In this study, the combined force field of ClayFF (Cygan et al., 2004a) plus the Constant-Valence Force Field (CVFF, Dauber-Osguthorpe et al., 1988) plus the Flexible SPC water model (Teleman et al., 1987) were used to model the molecular interactions. While MD simulations for organic materials is a mature field, only very recently has a clay force field been proven to work well for all clay minerals, and more importantly to produce robust results when the clay is interacting with other phases (e.g. water, organic cations, or non-polar molecules). Cygan et al. (2004) proposed a general force field ClayFF to provide a basis for simulation of hydrated and multi-component mineral systems and their interfaces with aqueous solutions. The fundamentals of this approach include: flexible SPC water model, ionic metal-oxygen interaction which is the combination of LJ potential and coulombic interaction, and bonded terms for hydroxyl (bond stretch and angle bend). This system is different from the traditional force field in that the non-bonded terms are used to treat most inter-atomic interactions, which means that all atom positions are not fixed within the mineral crystal. Instead of a too "rigid" crystal structure defined by previous force fields, ClayFF achieves the stability of crystal structure by using pair potential functions that also allows flexibility of the atoms. Additionally, ClayFF also decreased the surface potential of the mineral, resulting in an impact on interlayer species that is likely more realistic (Bourg and Sposito, 2010).

ClayFF has been demonstrated to be good for simulations based on not only clay minerals, but also for clay minerals intercalated by interlayer components. Combined with Constant Valence Force Field (CVFF, Dauber-Osguthorpe et al., 1988), it has been proven to be a powerful tool to model intercalated species in clay. Based on ClayFF, Liu et al. (2007) and Liu et al. (2009) performed hexadecyltrimethyl-ammonium, alkylammonium and acetate ions intercalation into smectite, Cygan et al.(2004) modeled methane hydrate complexation in montmorillonite, and Greathouse et al. (2005) simulated adsorption equilibria onto a montmorillonite surface.

Force field

In the context of classical molecular dynamics, a force field defines the potential functions and parameters used to describe the interaction between particles. Force fields are usually fitted from experimental approaches; consequently, they are considered empirical. An advanced force field is compatible with other force fields, can be applied to more cases and is expected to produce results that are consistent with experimental results.

In order to run a force-field based molecular dynamics simulation, it is necessary to define how two atomic or molecular species, A and B, interact with each other. Their bonds include different types of “strong” and “weak” bonds that describe the nature of intermolecular forces (Rapaport, 1995). Strong intermolecular bonds include covalent and metallic bonds, while weak bonds include the hydrogen bond and other non-covalent “bonds” (or pair interactions) (e.g., van der Waals force). In this study, the term "van der Waals force" solely refers to the London/dispersion force. The Lennard-Jones potential is interpreted as the approximate model for the isotropic part of the total (repulsion plus attraction) van der Waals force. All the “weak”

and “strong” interactions contribute to the total energy of the system, and the minimum of total energy often corresponds to the optimized structure of the system. For a pair of atoms, the minima of interaction energy indicate the first derivative of energy, or total force between them, is zero.

The algorithm for equilibrium MD is based on Newton’s second law. When the system is first treated with energy minimization, the dynamics is performed by calculating the total force acting on each atom. The total force includes all valid types of interactions that come from bonded atoms or any atom that is located within the cutoff distance (for Coulombic force, cutoff is often set to infinite by using the summation technique). The total force on an each atom divided by its own weight yields the current acceleration of the atom. In the next timestep, the velocity and displacement of the atom is calculated from the current position, velocity, and acceleration. The total force is then updated at the new position, and the calculation continues by repeating the same procedure. The time scale is approximately a femtosecond (10^{-15} s) for one timestep, and the overall simulation time can be nanoseconds (10^{-9} s).

The combined force field of ClayFF & CVFF

The combined ClayFF and CVFF force field combines those energy terms that contribute to the total energy, while the total energy can be divided into a non-bonded (or pair) term and bonded term. The non-bonded term includes van der Waals interaction and Coulombic interaction, while the bonded energy consists of 2, 3, and 4 body interactions that contributed to the covalent interactions:

$$E_{total} = E_{pair} + E_{bond}$$

Pair potential energy

Without considering covalent bond making or breaking, the most common case is the "ionic" interaction between any two charged atoms, which is described by pair potential. It is important to note that not only the oxygen and metallic atoms have this pair interaction, any two atoms in the simulated system can have pair interaction. The pair potential energy is the combination of Lennard-Jones (LJ) and Coulombic potential energy:

$$E_{pair} = E_{LJ} + E_{coul}$$

$$E_{coul} = \frac{e^2}{4\pi\varepsilon_0} \sum_{i \neq j} \frac{q_i q_j}{r_{ij}}$$

$$E_{LJ} = \sum_{i \neq j} D_{0,ij} \left[\left(\frac{R_{0,ij}}{r_{ij}} \right)^{12} - 2 \left(\frac{R_{0,ij}}{r_{ij}} \right)^{6} \right]$$

Where: D_o = depth of the potential well, and R_0 is the distance corresponds to the minimum potential energy

Two charged atoms would attract each other via electrical force if they carry reverse charges. For VDW term, the r^{-12} term describes Pauli repulsion at short ranges due to overlapping of electron orbitals and the r^{-6} term describes attraction at longer ranges (van der Waals force, or dispersion force). Figure 2-1 shows an example of the pair potential energy between bridging oxygen and silicon as a function of interaction distance within the clay. It can be noticed that the two atoms always have electrical attraction to each other since they carry reverse charges and their VDW interaction energy depends on the separate distance. The sum of the two is the total pair energy and it determines whether the two atoms attract or repulse each other. The radius at minimum potential energy also corresponds to the equilibrium state of interaction (total force equals to zero) since:

$$\sum F = -\frac{dE}{dr}$$

It is important to note that the radius at equilibrium of two atoms is not necessarily the radius at equilibrium in a group of atoms. The local minimum energy also does not necessarily correspond to the global minimum energy, due to the non-linearity of the super-imposed energy terms.

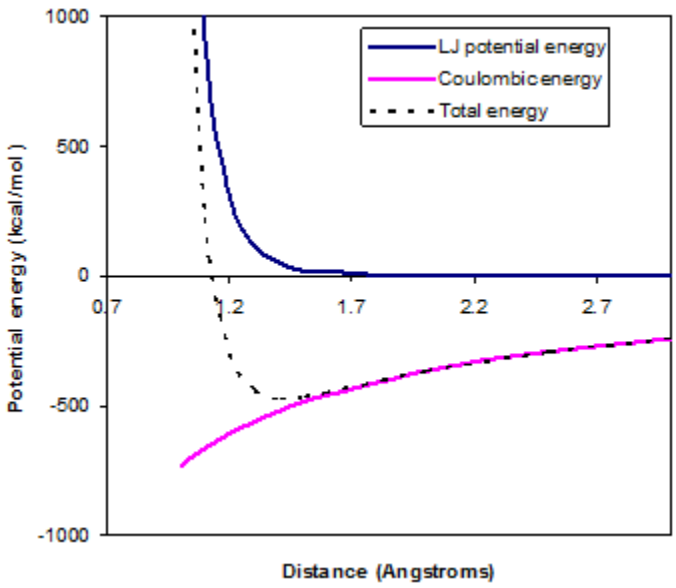

Figure 2-1. Pair potential energy vs. distance between single bridging oxygen and single silicon in clay.

Bond potential energy

Bonded energy terms are usually used to describe the energy price required to deform covalently bonded atoms. They are commonly used for organic cations, anions, and molecules. Note the interactions are not restricted to two interacting atoms and for each type of deformation, the specific form to describe the deformational energy could be different:

$$E_{bond} = E_{bond\_stretch} + E_{angle\_bend} + E_{improper} + E_{dihedral}$$

Bond stretch energy

Hooke's Law may be adequate to describe the stretch energy of certain covalent bonds (e.g. OH bond of water, hydroxyl), then each bond stretch between atom types A and B makes a contribution to the total molecular potential energy in harmonic notation:

$$E_{bond\_stretch} = k(r - r_0)^2$$

where k is the force constant, r is the instantaneous bond length, and r_0 is the equilibrium bond length. This is the most common expression for stretch energy of the O-H bond in hydroxyl, water. Alternately, the Morse potential term (e.g. C-N; C-H bonds in organic cations) can be used:

$$E_{bond\_stretch} = D\left[1 - e^{-\alpha(r - r_0)}\right]^2$$

Where r_0 is the equilibrium bond distance, alpha is a stiffness parameter, and D determines the depth of the potential well. There are also many other terms to address bond stretch energy (e.g. FENE; Class 2, and hybrids of those).

Angle-bending energy

When three atoms form an angle that consists of two covalent bonds, the energy to bend the angle can be described by a harmonic function (theta represents the angles):

$$E_{angle\_bend} = k(\theta - \theta_0)^2$$

Dihedral and improper energy

There are also 4-body interaction energy terms (e.g., dihedral and improper terms for CVFF) that are not considered if the center atoms are carbon and nitrogen (as in the TMA molecule), but they are necessary for molecules with longer carbon chains (e.g., DTMA and HDTMA). The dihedral terms for QACs were considered as harmonic type, while for benzene were considered as charmm type:

$$E_{dihedral} = k[1 + d\cos(n\phi)]$$ (harmonic)

where k is constant and d = ±1, n is integer >=0.

$$E_{dihedral} = k[1 + \cos(n\phi - d)]$$ (charmm)

where k is constant and d is integer value of degrees, n is integer >=0.

The improper (out-of-plane) term for four interacting atoms has its energy described as:

$$E_{improper} = k(\chi - \chi_0)^2$$

where k is constant and has the unit of (energy/radian^2); χ_0 and χ are in unit of degrees (note: LAMMPS converts degree to radians internally).

Parameters

The parameters were obtained from ClayFF and CVFF and their values were converted from the equations given in the following references (Table 2-1). Note the same equations might have different expressions in LAMMPS, so the parameter values might vary but they are interchangeable.

Table 2-1. Overall pair potential parameters for MD simualtions

	species	symbol	charge (e)	D_0[e] (kcal/mol)	R_0[f] (Å)
ClayFF[a]	water hydrogen	h*	0.4100[b]	0	0
	water oxygen	o*	-0.8200[b]	0.1554	3.5532
	hydroxyl hydrogen	ho	0.4250	0	0
	hydroxyl oxygen	oh	-0.9500	0.1554	3.5532
	bridging oxygen	ob	-1.0500	0.1554	3.5532
	bridging oxygen with octahedral substitution	obos	-1.1808	0.1554	3.5532
	bridging oxygen with tetrahedral substitution	obts	-1.1688	0.1554	3.5532
	bridging oxygen with double substitution	obss	-1.2996	0.1554	3.5532
	hydroxyl oxygen with substitution	ohs	-1.0808	0.1554	3.5532
	tetrahedral silicon	st	2.1000	1.8405×10^{-6}	3.7064
	octahedral aluminum	ao	1.5750	1.3298×10^{-6}	4.7943
	tetrahedral aluminum	at	1.5750	1.8405×10^{-6}	3.7064
	octahedral magnesium	mgo	1.3600	9.0298×10^{-7}	5.9090
	hydroxide magnesium	mgh	1.0500	9.0298×10^{-7}	5.9090
	octahedral calcium	cao	1.3600	5.0298×10^{-6}	6.2484
	hydroxide calcium	cah	1.0500	5.0298×10^{-6}	6.2484
	octahedral iron	feo	1.5750	9.0298×10^{-6}	5.5070
	octahedral lithium	lio	0.5250	9.0298×10^{-6}	4.7257
	aqueous sodium ion	Na	1.0000	0.1301	2.6378
	aqueous potassium ion	K	1.0000	0.1000	3.7423
	aqueous cesium ion	Cs	1.0000	0.1000	4.3002
	aqueous calcium ion	Ca	2.0000	0.1000	3.2237
	aqueous barium ion	Ba	2.0000	0.0470	4.2840
	aqueous chloride ion	Cl	-1.0000	0.1001	4.9388
CVFF[c]	head carbon	sp3	0.1000	0.1597	3.9006
	CH_2 carbon	c2	-0.2000	0.1478	4.0599
	CH_3 carbon	c3	-0.3000	0.1478	4.0599
	nitrogen	n	-0.5000	0.1668	3.9286
	hydrogen	h	0.1000	0.0360	2.7670
SPC/E water model[d]	water hydrogen	hscp	0.4238	0	0
	water oxygen	oscp	-0.8476	0.1554	3.5532

[a]Pair potential parameters from ClayFF (Cygan et al., 2004)

[b]Parameters are consistent with SPC model (Berendsen, 1984)
[c]Pair potential parameters from CVFF (Dauber-Osguthorpe et al., 1988)
[d]Pair potential parameters from SPC/E (extended) water model (Berendsen, 1984)
[e,f] When given the notation of LJ potential of $E_{LJ} = \sum_{i \neq j} D_{0,ij} \left[\left(\frac{R_{0,ij}}{r_{ij}} \right)^{12} - 2 \left(\frac{R_{0,ij}}{r_{ij}} \right)^{6} \right]$**, if LJ potential is notated as** $E_{LJ} = \sum_{i \neq j} 4\varepsilon_{ij} \left[\left(\frac{\sigma_{0,ij}}{r_{ij}} \right)^{12} - \left(\frac{\sigma_{0,ij}}{r_{ij}} \right)^{6} \right]$**, then** $D_{0,ij} = \varepsilon_{ij}$**;** $R_{0,ij} = 2^{1/6} \sigma_{0,ij}$

The parameters listed in Table 2-1 are for the two same species ii. For different species ij, their interacting LJ potential energy parameters are decided by mixing the parameters of two individual types of atoms. The new parameter is decided according to arithmetic mean rule for the distance parameter and geometric mean rule for the energy parameter (Lorentz-Berthelot rules):

$$R_{0,ij} = \frac{1}{2}(R_{0,i} + R_{0,j})$$
$$D_{0,ij} = \sqrt{D_{0,i} D_{0,j}}$$

The covalent potential energy parameters include that for bond stretch (either harmonic or morse), angle bend (Table 2-3), and four body interactions (torsional and out-of-plane, Table 2-4, Table 2-5). The covalent bond in QACs are morse type while the others are harmonic (Table 2-2).

Table 2-2a. Bond stretch energy parameters – harmonic terms

species		$k_{bond\_stretch}$	r_0
i	**j**	**(kcal/mol Å^2)**	**(Å)**
water oxygen	water hydrogen	554.1349	1.0000
hydroxyl oxygen	hydroxyl hydrogen	554.1349	1.0000
hydroxyl oxygen with substitution	hydroxyl oxygen with substitution	554.1349	1.0000
benzene carbon	benzene carbon	480.0000	1.3400
benzene carbon	benzene hydrogen	363.4200	1.0800

Table 2-2b. Bond stretch energy parameters – morse terms

species		D	α	r_0
i	**j**	**(kcal/mol Å^2)**		**(Å)**
QAC carbon	QAC hydrogen	108.6	1.771	1.105
QAC carbon	QAC carbon	88.0	1.915	1.526
QAC carbon	QAC nitrogen	72.0	2.290	1.460

Table 2-3. Angle bending energy parameters

species			k_{angle_bend}	θ_0
i	**j**	**k**	**(kcal/mol rad^2)**	**(deg)**
metal	hydroxyl oxygen	hydroxyl hydrogen	30.0	109.47
metal	hydroxyl oxygen with substitution	hydroxyl hydrogen with substitution	30.0	109.47
water hydrogen	water oxygen	water hydrogen	30.0	109.47
QAC hydrogen	QAC carbon	QAC carbon	44.4	110.00
QAC carbon	QAC carbon	QAC carbon	46.6	110.50
QAC carbon	QAC carbon	QAC nitrogen	50.0	109.50
QAC carbon	QAC nitrogen	QAC carbon	37.0	120.00
QAC hydrogen	QAC carbon	QAC nitrogen	51.5	109.47
QAC hydrogen	QAC carbon	QAC hydrogen	39.5	106.40
benzene carbon	benzene carbon	benzene hydrogen	37.0	120.00
benzene carbon	benzene carbon	benzene carbon	90.0	120.00

Table 2-4a. Dihedral (torsional) energy parameters – harmonic terms

species				$k_{dihedral}$	d	n
i	**j**	**k**	**l**	**(kcal/mol)**		
QAC hydrogen	QAC carbon	QAC carbon	QAC carbon	0.14225	1	3
QAC carbon	QAC carbon	QAC carbon	QAC carbon	0.14225	1	3
QAC carbon	QAC carbon	QAC carbon	QAC nitrogen	0.14225	1	3
QAC carbon	QAC carbon	QAC nitrogen	QAC carbon	0	1	3
QAC carbon	QAC nitrogen	QAC carbon	QAC hydrogen	0	1	3
QAC hydrogen	QAC carbon	QAC carbon	QAC hydrogen	0.14225	1	3
QAC hydrogen	QAC carbon	QAC carbon	QAC nitrogen	0.14225	1	3

Table 2-4b. Dihedral (torsional) energy parameters – charmm terms

species				$k_{dihedral}$	d	n
i	**j**	**k**	**l**	**(kcal/mol)**		
benzene carbon	benzene carbon	benzene carbon	benzene carbon	12.000	-1	2
benzene carbon	benzene carbon	benzene carbon	benzene hydrogen	12.000	-1	2
benzene hydrogen	benzene carbon	benzene carbon	benzene hydrogen	12.000	-1	2

Table 2-5. Improper (out-of-plane) energy parameters

species				$k_{improper}$	χ_0	χ_0
i	**j**	**k**	**l**	**(kcal/mol)**	**degrees**	**rad**
QAC hydrogen	QAC carbon	QAC carbon	QAC carbon	0.37		0.00
QAC carbon	QAC carbon	QAC carbon	QAC carbon	0.37		0.00
QAC carbon	QAC carbon	QAC carbon	QAC nitrogen	0.37		0.00
QAC carbon	QAC carbon	QAC nitrogen	QAC carbon	0.37		0.00
QAC carbon	QAC nitrogen	QAC carbon	QAC hydrogen	0.50		0.01
QAC hydrogen	QAC carbon	QAC carbon	QAC hydrogen	0.50		0.01
QAC hydrogen	QAC carbon	QAC carbon	QAC nitrogen	0.37		0.00
benzene carbon	benzene carbon	benzene carbon	benzene carbon	0.37		0.00
benzene carbon	benzene carbon	benzene carbon	benzene hydrogen	0.37		0.00
benzene hydrogen	benzene carbon	benzene carbon	benzene hydrogen	0.37		0

Boundaries, relaxation and ensemble dynamics

Periodic boundary

For any simulation box with limited size, all atoms inside will be in motion if the temperature is not zero. So some atoms, either due to interaction with surrounding atoms or closer distance to the boundary of the simulation box, are more likely to pass through the simulation box boundary and get lost, which will reduce the density of the atoms within the

simulation box (Rapaport, 1995). This undesirable effect can be avoided by introducing a simulation box with periodic boundaries, as illustrated in the figure below. When the simulated system is surrounded with a large number of identical images/copies, and image boxes are truly identical at the atomic level, the movement of a "true" atom is the same with that of its copies/images. When an actual atom (dark grey) leaves the simulation box, one of its image will enter the simulation box and this keeps the density constant of atoms in the box. Then the inter-atomic forces is calculated again as the sum of all the forces imposed by adjacent atoms based on the updated atomic positions (within the cutoff distance).

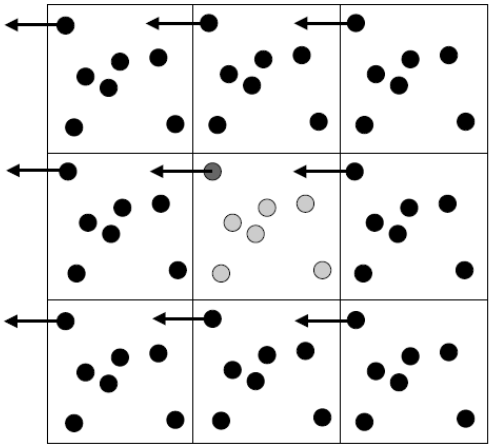

Figure 2-2. Particle passing through periodic boundary: note the grey atoms in the center are in simulated system, the black atoms are images (Hinchliffe, 2003).

Relaxation

The initial configuration of the simulated system is often not at the best organization. This can be the result of ill-defined structures of different species, or due to mixing of different phases (e.g. solid-liquid). Consequently, dynamics performed directly on the un-treated initial condition can bring undesirable results. To avoid such sequences, energy minimization of the initial system is usually performed before running dynamics, such that the individual group of atoms can achieve their optimized structure or the systems with highly overlapped atoms (large

energies and forces) can be relaxed by pushing the atoms off of each other. Alternate means of relaxing a system are to run dynamics with limited timestep, or to impose constrains on kinetic energy of the atoms (e.g. decrease temperature to 0 K). This procedure is spatially necessary when the initial positions of some atoms are not appropriate.

Conventionally, energy minimization of the system is performed by iteratively adjusting atom coordinates. Iterations are terminated when one of the stopping criteria is satisfied (e.g., tolerance of energy difference, maximum steps of iteration). At that point, the configuration will likely be in a local potential energy minimum. More precisely, the configuration should approximate a critical point for the objective function of total energy E (as shown below), which may or may not be a local minimum.

$$E(r_1, r_2, ...r_n) = \sum_{ij} E_{pair}(r_i, r_j) + \sum_{ij} E_{bond}(r_i, r_j) + \sum_{ijk} E_{angle}(r_i, r_j, r_k) + \sum_{ijkl} E_{dihedral}(r_i, r_j, r_k, r_l) + \sum_{ijkl} E_{improper}(r_i, r_j, r_k, r_l) + \sum_{i} E_{fix}(r_i)$$

For a complicated system that contains clay, water and interlayer cations, relaxation needs to be carried out before running dynamics. One reason for this is that the structures (especially clay) within the simulation system must be optimized to bring in best simulation results. The other reason is that the interface between clay and interlayer species sometimes are not perfectly constructed.

Ensembles and dynamics

The equilibrium of interaction between atoms or groups of atoms can be achieved in the system; however, the thermodynamic properties of all atoms contained in the system must also meet the characteristics of the ensemble. It means that the system must maintain a certain amount of particles, and the statistical properties of all particles must meet certain boundary conditions. The boundary conditions could be constraints on volume, temperature, pressure, or combinations

of them. Only when the properties of the ensemble are compatible with the constraints is the individual particle movement in the system meaningful. In this study, the common ensemble types can be divided into several types:

Isothermal-Isobaric (NPT) ensemble

NPT time integration of a certain amount of time steps can be carried out using Nose/Hoover temperature thermostat and Nose/Hoover pressure barostat. The systems remained at constant pressure and constant temperature during the time integration.

Canonical ensemble (NVT)

Similar to NPT integration, the systems remained at constant volume and constant temperature during the time integration.

Microcanonical ensemble (NVE)

Similar to NPT integration, the systems remained at constant energy and constant temperature during the time integration.

So when the atoms in the system are running dynamics, the additional constraints of the ensemble property is also included. This means the atoms' movement not only follows Newton's second law but also the prerequisite that statistically they need to behave like a group with certain bulk properties.

Validation

This part was intended to compare simulation results of species diffusion, ion hydration and interlayer species arrangement in clay using the combined force field with experimental observations. Simulation results including hydration shell size, self-diffusion rate and interlayer spacing were compared with previous physical chemical data to validate the force field used for all the following studies.

In first example, the dissolved sodium chloride in bulk solution was simulated (Figure 2-3a). the interaction between sodium and chloride ions vs. water were observed and their self-diffusion in bulk liquid at 1 atm, 298K. The simulation cell included 700 water molecules, 2 sodium and 2 chloride ions. The concentration of both ions is at 0.172mol/L. Energy parameters of ions and water was based on the values for dissolved ions and water from clayFF. The simulation cell had the size of 32.8Å×31.3 Å ×18.8 Å, after went through 1ns of NPT and 1ns of NVT time integration. After system reached equilibrium, the density of solution, the distance from ion to first hydration shell (Figure 2-3b) and coordination number of water were obtained and they showed good agreement with experimental measurements (Table 2-6). Additionally, Simulated self-diffusion coefficient of sodium and chloride ions were calculated from their mean-squared displacement (MSD) and verified by previous studies.

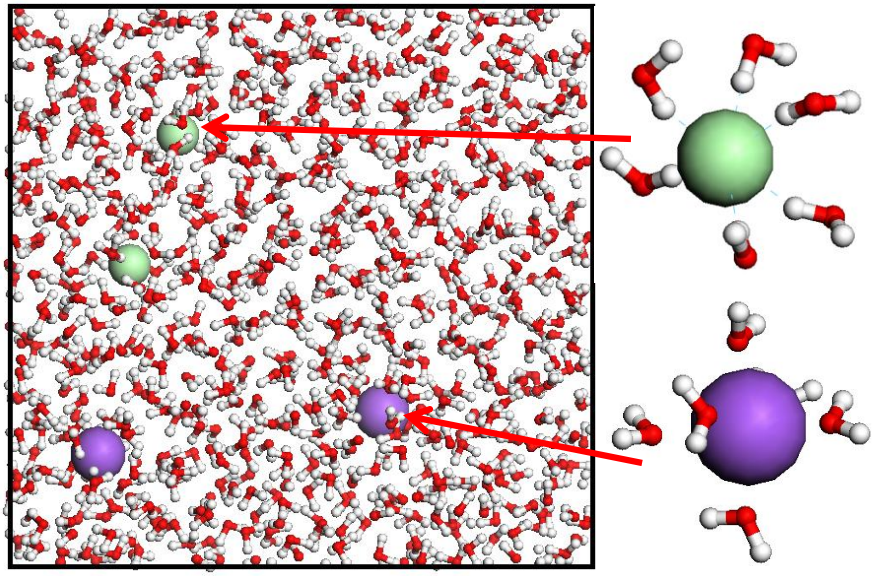

(a)

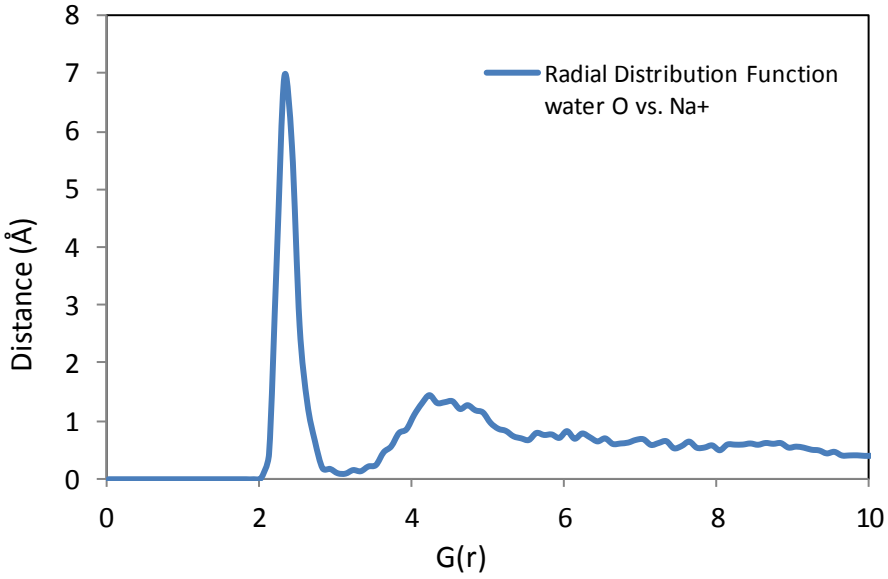

(b)

Figure 2-3. (a)sodium and chloride ions solvated by water molecules (b) radial distribution function (RDF) of water oxygen vs. sodium.

Table 2-6. Physical-chemical output of simulated ion hydration

	simulation results	Previous study
Density of solution	1.06kg/L	1.02kg/L
Diffusion coefficient Na^+	$15.1\times10^{-10}m^2/sec$	$13.3\times10^{-10}m^2/sec$[a]
Diffusion coefficient Cl^-	$17.8\times10^{-10}m^2/sec$	$20.3\times10^{-10}m^2/sec$[a]
Hydration shell radii Na^+	2.4Å (Na^+ to H_2O O)	2.35~2.46Å[b]
Coordination number Na^+	5.5-6.0	5.8[c]
Hydration shell radii Cl^-	3.1Å (Cl^- to H_2O O)	3.2Å[d]
Coordination number Cl^-	7.0-7.5	7.2[c]

[a]Sharma, 2004
[b]Azam et al., 2009
[c]Koneshan et al., 1998
[d]Zhao et al., 2010

In second example, interlayer swelling simulation of Na-Montmorillonite was carried out to compare with XRD study by Fu et al. (1990). The XRD results of Fu et al. (1990) was proven to be precise measurement of Na-Montmorillonite swelling when interacting with vapor or liquid phases. It was served as benchmark for us to compare with the simulation work. In this case, we recorded basal spacing (001 d-spacing) of Na-Montmorillonite as a function of amount of interlayer water. And the swelling curve of Na-Montmorillonite, recorded as relation between basal spacing and given weight ratio of interlayer water vs. clay. Our initial condition was a dry system with the presence of two parallel clay platelet and interlayer cations only. For each successive simulation, an increment of 30 water molecules was introduced into the simulation box and followed by the same procedure to obtain new basal spacing after equilibrium. This process was repeated until the total number of water molecules reached 300. Basal spacing versus the weight ratio of added water/clay platelet was recorded.

The type of montmorillonite which was chosen as the base clay for intercalation was Wyoming montmorillonite. The chemical formulae of the clay (unit cell) was $0.58Na^{+}(Mg_{0.5}Al_{3.5})(Al_{0.08}Si_{7.92})O_{20}(OH)_4$, where sodium represented the interlayer compensation cations. The simulated clay had 0.58 e of charge per unit cell, which can be attributed to both tetrahedral and octahedral substitution of metal ions within the clay framework. The super cell of clay was created by expanding the unit cell horizontally: 8 times in x direction and 4 times in y direction, so the thickness of the super cell was also the thickness of the 2:1 clay sheet. The structure of clay was first created and then exported from Material Studio (Accelrys Inc.) software.

The swelling curves of Na-Montmorillonite exhibited two clearly-defined expanded stages. For dry base clay, a small increment of interlayer water molecules started to solvate the free sodium ions and the clay surface, and as more water molecules were introduced, they formed a multiple-layer network which was stabilized by hydrogen bonds. This process prevailed until two hydrated layers were developed and it explains two observed stages of the base clay swelling curve. The simulated swelling tendency was in good agreement with XRD observations.

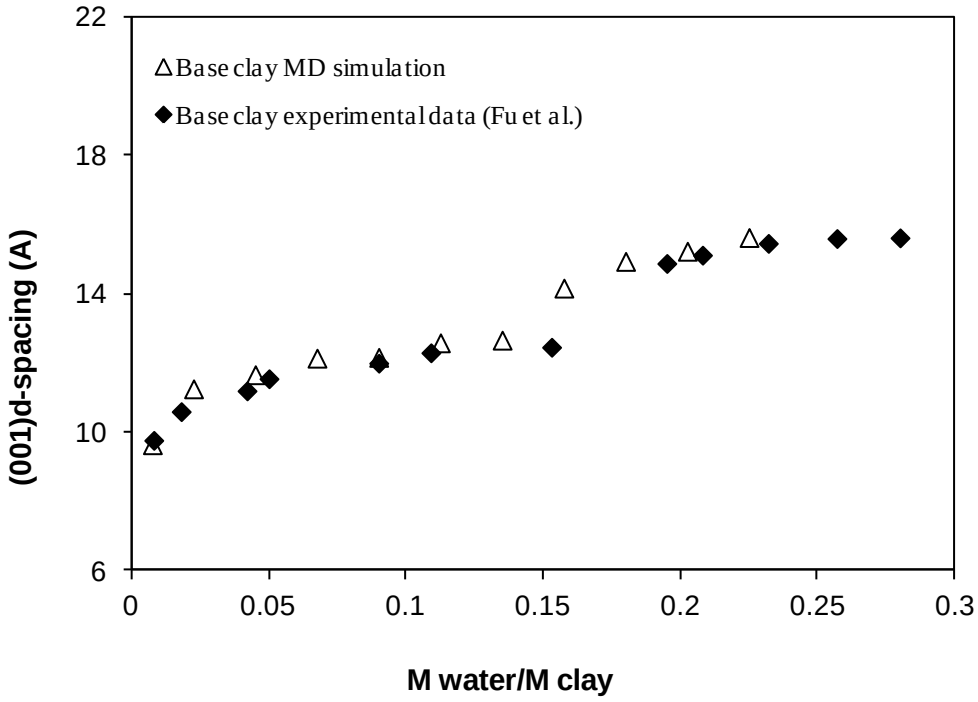

Figure 2-4. simulated swelling of Na-montmorillonite vs. experimental data.

Coding

Two scripts were needed in order to run a MD simulation in LAMMPS. The first one was a data file to store the initial conditions of the system, including: initial simulation box size, coordination, charge, type (or element) ID (unique for each atom in the system) of all atoms, bonding information for all types of covalent interaction (bond, angle, improper and dihedral interaction of any possible combination of atoms, recorded with their ID). The parameters of all energy terms can be stored either in the data file or input file.

The second script is an input file stored with the commands of running the simulation. It defines the dimension and periodicity of the system, units, parameters of all energy terms, neighboring criteria and grouping information, and initial velocity of all atoms. In the simulation command part, it often includes the definition of time step and energy minimization criteria, and commands for running dynamics with controlled ensemble properties and for output of simulation results.

Sample input and data files can be found in the Appendix. The example shows the coding format and model of benzene sorption in the HDTMA clay interlayer.

CHAPTER 3
MOLECULAR DYNAMICS SIMULATIONS OF QUATERNARY AMMONIUM CATION MORPHORLOGY IN MONTMORILLONITE INTERLAYER

Introduction

Organic coated clays are of engineering interests because the organic coating can exert significant influence on the both the mechanical and chemical behavior of clay (Yeung et al. 1996; Perret et al. 2000; Smith and Jaffe 1994). Changes in the structure of the base clay (e.g., charge), organic surfactant, and density of loading can result in significant differences in the structure of the organoclay, with the resulting clays exhibiting a wide range of behaviors. In nature, the components of the coatings made from natural organic matter are complicated and highly heterogeneous; thus, the resultant properties of the soil-organic complex are difficult to interpret. For engineering purposes, specific types of organic coated clays can be synthesized under very controlled conditions in order to control the resultant chemical and mechanical properties. Combing a given base clay with an organic cation of specific structure can facilitate the development of an organoclay with predictable engineering properties. Most commonly, Na-montmorillonite is used as the base clay and its sodium cations can be exchanged with quaternary ammonium cations (QAC) (Soule and Burns, 2001; Burns et al., 2006). QAC coated montmorillonite exhibits enhanced strength, lower compressibility and stronger retention of organic compounds (Lo, 2001; Burns et al., 2006) in the environment, yielding a variety of potential applications in waste containment, landfill liners, and slurry walls (Park and Jaffe, 1993; Smith and Jaffe, 1994; Sheng and Boyd, 2000; Lorenzetti et al. 2005).

Numerous previous studies have focused on the characterization of QAC arrangement and conformation after intercalation of the QAC in interlayer of layered silicates (Lagaly, 1981;

Vaia et al., 1994; Wen et al., 2006). Both experimental and simulation techniques have been performed, including: X-ray powder diffraction (XRD) (Lagaly, 1981;); NMR spectroscopy (Osman et al., 2004; Zhu et al., 2005); Monte-Carlo simulations (Skipper et al., 1995a, 1995b), and molecular dynamics simulations (Heinz et al., 2007; Liu et al., 2009). However, due to the complexity of comparison of different material origins and components, as well as characterization of interlayer organic loading, most previous experimental research was based on either one type of base clay or one type of organic cation. The numerical simulations have been very successful at yielding insight into experimental results; however, the development of a packing model that can be applied to predict arrangement of any given combination of clay and single chain QAC is still limited. The fundamental understanding of the transition of the organoclay microstructure that corresponds to the modification of their surface characteristics and bulk properties is still challenging. Consequently, it remains useful to identify the QAC surfactant packing modes, along with the onset of transitions between modes, based on the molecular interactions between clay-QACs in interlayer.

The objective of this chapter is to simulate the arrangement of single chain QAC-surfactants of varying structures and quantities in the interlayer of different montmorillonite clays, and compare the results with previous experimental data. Additionally, a model to predict single chain QAC surfactant arrangement in montmorillonite interlayer for given clay prototype and organic molecule loading will be derived. To meet this objective, molecular dynamics (MD) simulations were performed to address the intercalated surfactant structure at the molecular level: surfactant arrangement of three single chain QACs (tetramethylammonium (TMA^+), decyltrimethylammonium ($DTMA^+$), and hexadecyltrimethlyammonium ($HDTMA^+$)) were quantified for different systems, and the effect of amount and type of intercalated organic cation

was examined. Finally, the surfactant structures were summarized as a function of total organic carbon loading in interlayer.

Background

For swelling clays like Na-montmorillonite, the clay normally carries a negative layer charge, and the interlayer species encountered in nature are usually hydrophilic inorganic cations. Their interlayer structures are maintained by metallic cation hydration, mineral surface hydration, and development of hydrogen bonds within interlayer (Young and Smith, 2000; Tambach et al., 2006). However, the naturally occurring interlayer species of the base clay can be modified by exchanging their naturally occurring metallic cations with organic cations, resulting in organic-clay complexes, known as organoclays. The microstructure of the intercalated surfactant essentially controls many engineering behaviors of synthesized organoclays, especially when the quantity of intercalated organic carbon is high. It has been reported that increased TOC of organoclay yields higher zeta potential (Bate and Burns, 2010), enhanced strength, lower compressibility (Burns et al., 2006), and linear sorption pattern for organic contaminants partitioning into long chain surfactant phases (Redding et al., 2002).

Significant experimental and numerical simulation results have demonstrated that the organic carbon of intercalated surfactants tends to form integral number of layers, oriented parallel to the basal surface of clay (He et al., 2005; Liu et al., 2009). For montmorillonite intercalated with quaternary ammonium cations (QAC), there are several possible patterns of QAC surfactant arrangement as the organic carbon loading increases, including: lateral monolayer of organic carbon (basal spacing 13.0~15.0 Å); lateral bilayer of organic carbon (basal spacing 17.7~19.8 Å) and pseudo-trilayer/paraffin-monolayer structures (basal spacing

>22 Å) (Lagaly, 1981; Zhu et al., 2003; He et al., 2004; Liu et al., 2009). Typically, the paraffin bilayer arrangement is observed in clays with very high charge density, and it often corresponds to a percentage of cation exchange that exceeds 100%. The transition from a lateral monolayer structure to a paraffin complex, which is typically indicated by increased basal spacing, corresponds to an increased amount of organic loading that props open the interlayer spacing and creates a more organophilic organic phase in the interlayer.

The amount of organic carbon that can be exchanged into the interlayer of a 2:1 clay is controlled by several factors, including the charge density of the base clay, the percentage of interlayer cation being exchanged, and the molecular structure (carbon number) of the intercalated organic cation. Substitutions in the structure of montmorillonite can alter its chemical makeup and layer charge; however, most commonly, sodium montmorillonite has the chemical formula of $nNa\ (Mg_xAl_{4.0-x})(Al_ySi_{8.0-y})O_{20}(OH)_4$, where x and y represent the number of octahedral and tetrahedral substitutions per unit cell, respectively. Larger number of substitutions in the silica sheet indicates more charges carried by the unmodified base clays, which increases the capacity to accommodate more cations (inorganic or organic) in the interlayer. Also, the process of exchanging inorganic cations for organic cations may occur partially. The higher percentage of cation exchange indicates more organic cations have been intercalated in the clay's interlayer. The quantity of organic carbon in the QAC also affects the amount of intercalated carbon. Consequently, the transition between the modes of arrangement of surfactant in the clay interlayer is attributable to the overall effect of the clay's layer charge, percentage of cation exchanged, and the structure of the organic cation. Though the three factors have been studied individually in previous work, this work seeks to examine how the total organic carbon loading affects the interlayer QAC arrangement pattern.

In this study, the mode of surfactant arrangement of three organoclays was studied. Clays with varying properties were chosen as the base clay, and the organic cations were chosen to represent a range of sizes, from small quaternary ammonium cations such as tetramethylammonium (TMA^+), to larger quaternary ammonium cations with increased length in one alkyl chain, including decyltrimethylammonium ($DTMA^+$) and hexadecyltrimethlyammonium ($HDTMA^+$). Molecular dynamics simulations were used to study the interaction between interlayer species at the molecular level. Different surfactant structures were obtained and then compared with those that have been quantified by both experimental and previous simulation work. Additionally, a surfactant arrangement model is derived from the simulation results, with the purpose of predicting QAC surfactant arrangement in the montmorillonite interlayer for given clay prototype and organic cation loading.

Computational Methods

Base clay & organic surfactant model

Montmorillonite (MMT) with varying charge density was considered as the base clay for this study (Table 3-1). The organoclay simulations were based on the chemical formulae of XQAC $(Mg_YAl_{4-Y})(Al_{0.071}Si_{7.929})O_{20}(OH)_4$, where X represents the number of interlayer compensation cations per unit cell and Y represents the octahedral charge contributed to the Al-Mg substitution in octahedrons. A constant charge of 0.071e from tetrahedral substitution was assumed. The three clay prototypes had total layer charges ranging from 0.5e~1.071e per unit cell, corresponding to clays with charges ranging from approximately 69~148meq/100g, which covers most types of montmorillonite commonly encountered in nature. For simulated clay

model, the layer charge was most contributed by the octahedron substitutions. The super cell of montmorillonite consisted of 28 duplicates of unit cells and had a basal surface area of 35.72 Å × 35.04 Å in size, which was also the dimension of the simulation box in the x and y direction, respectively.

For each charge density of montmorillonite, QACs were intercalated into the interlayer of montmorillonite, assuming 100% cation exchange. Three types of QACs with the same structure of nitrogen head group, but with varying chain length (TMA, DTMA, and HDTMA) were intercalated.

Table 3-1. QAC Structure as a Result of Clay Charge Density, CEC, and QAC Type

Clay prototype[1,2,3]	QAC Type	CEC (%)	No. of QAC	Equilibirum basal spacing (Å)	Organic carbon arrangement
0.500QAC $(Mg_{0.429}Al_{3.571})(Al_{0.071}Si_{7.929})O_{20}(OH)_4$	TMA^+	100	14	14.08 ± 0.046	Lateral monolayer
	$DTMA^+$	100	14	14.36 ± 0.034	Lateral monolayer
	$HDTMA^+$	100	14	18.21 ± 0.066	Lateral bilayer
0.643QAC $(Mg_{0.572}Al_{3.429})(Al_{0.071}Si_{7.929})O_{20}(OH)_4$	TMA^+	100	18	14.12 ± 0.063	Lateral monolayer
	$DTMA^+$	100	18	17.71 ± 0.041	Lateral bilayer
	$HDTMA^+$	100	18	18.79 ± 0.062	Lateral bilayer
1.071QAC $(Mg_{1.000}Al_{3.000})(Al_{0.071}Si_{7.929})O_{20}(OH)_4$	TMA^+	100	30	14.19 ± 0.051	Lateral monolayer
	$DTMA^+$	100	30	19.44 ± 0.043	Lateral bilayer/trilayer
	$HDTMA^+$	33	10	14.45 ± 0.046	Lateral monolayer
	$HDTMA^+$	66	20	18.98 ± 0.056	Lateral bilayer
	$HDTMA^+$	80	24	22.73 ± 0.053	Lateral trilayer
	$HDTMA^+$	100	30	24.12 ± 0.068	Paraffin monolayer

[1] 0.500e per unit cell corresponds to a charge density of approximately 69.1meq/100g

[2] 0.643e per unit cell corresponds to a charge density of approximately 88.9meq/100g

[3] 1.071e per unit cell corresponds to a charge density of approximately 148.0meq/100g

Force field applied

Force-field based, equilibrium molecular dynamics simulations were performed in this study. The interactions between clay- QACs were modeled by the combined force field of ClayFF (Cygan et al., 2004) and Consistent-Valence Force Field (CVFF, Dauber-Osguthorpe et al., 1988). Clay FF includes the potential energy terms and their parameters for all types of atoms in the clay framework, while CVFF defines those of the organic cations. When combined together, the interaction between any groups of atoms in the system is calculated from interaction potential energies based on the mixing rule of the parameters. The combined force field

maintained the structures of the different phases and most importantly, guaranteed flexibility and full interactions between clay and QACs.

The total energy components of the simulated system were expected to be the combination of Coulombic interaction, van der Waals interaction, and bonded interaction (detailed information in Table 3-2):

$$E_{total} = E_{VDW} + E_{Coulombic} + E_{bond\_stretch} + E_{angle\_bend} + E_{torsion} + E_{improper}$$

Table 3-2. Potential Energy Terms for This MD Simulation

Energy term	Potential function	Equation	Interacting atoms	Applied to
Van der Waals	Lennard-Jones (12-6)	$E_{VDW} = D_{0,ij}\left[\left(\frac{R_{0,ij}}{r_{ij}}\right)^{12} - 2\left(\frac{R_{0,ij}}{r_{ij}}\right)^{6}\right]$	2	Any 2 atoms
Coulombic	Coulombic	$E_{Coulombic} = \frac{e^2}{4\pi\varepsilon}\sum_{i\neq j}\frac{q_i q_j}{r_{ij}}$	2	Any 2 atoms
Bond stretch	Harmonic	$E_{bond\_stretch} = k_1(r_{ij} - r_0)^2$	2	O-H bond
	Morse	$E_{bond\_stretch} = D(1 - e^{-\alpha(r_{ij} - r_0)})^2$	2	organic cations
Angle bend	Harmonic	$E_{angle\_bend} = k_2(\theta_{ijk} - \theta_0)^2$	3	metalic atom-O-H; organic cations
Torsional	Harmonic	$E_{torsion} = k_3[1 + d\cos(n\phi)]$	4	organic cations
Improper	Harmonic	$E_{improper} = k_5(\chi - \chi_0)^2$	4	organic cations

The non-covalent interaction is universal for any two atoms and it was represented by the summation of the conventional Lennard-Jones potential (usually referred to as 12-6 potential) and Coulombic potential energy terms. Lennard-Jones potential represents the van der Waals energy term, which is significant at short range while Coulombic interaction becomes dominant at long range. The parameters for non-covalent interactions were obtained from Cygan et al., 2004 and Dauber-Osguthorpe et al., 1988. For bonded interactions, different terms were used to describe 2 body (bond stretch), 3 body (angle bend) and 4 body (torsional; improper) interactions, in accordance with the nature of the bonding atoms and the bulk property of individual molecules. The first four terms of the total energy were involved in the energy

calculation of the clay framework and all the terms were considered as energy components of the QACs.

Simulated system

The intercalation of organic cations into the interlayer space of montmorillonite was simulated at the nanoscale. To best mimic the interlayer species, each combination of clay-QAC structure was simulated in two stages. The first stage was to obtain equilibrium basal spacing for the clay-QAC. Initially, the basal spacing was set to more than 35 Å in order to accommodate all the intercalated organic cations, which were placed randomly in the interlayer spaces. The interlayer was sandwiched between 2 MMT platelets while the two external surfaces of MMT were also covered with appropriate amount of QAC to maintain electrical neutrality of the system (Figure 3-1a). In order to allow free equilibrium of the gallery spacing, the simulation box remained open in the z direction (Heinz et al., 2004). After 1000 picosecond (ps) of NPT time integration (1atm, 25 ℃) was performed, a new simulation box containing two MMT platelets and two interlayer species were created in stage 2, constructed from equilibrium trajectories of MMT platelets and sandwiched layer during stage 1 (Figure 3-1b). During stage 2, 3d periodic boundaries were applied without a vacuum gap, with successive 500ps NPT and 1000ps NVT integration performed on the system. For same type of base clay, but with different amounts of QAC loadings, each type of QAC was started with maximum loading (1.071e), then the equilibrium structure was chosen and appropriate number of cations was removed, while the number of octahedral substitution within clay framework was also adjusted. Then the new system was simulated in stage 1 again.

The conceptual models of the simulated system including characteristics of the clay prototype and cation type are given in Table 3-1. The model was first created in Materials Studio (Version 5.5, Accelrys Inc.), and all MD simulations were performed in the Large-scale Atomic/Molecular Massively Parallel Simulator (LAMMPS) (Plimpton, 1995). During all simulation stages, the time step was set at 0.5 femtosecond and energy minimization was performed before running the dynamics. During the last 100 picosecond of NVT time integration, samples were taken in order to obtain trajectories and radial distribution functions for post-analysis. The mean-squared displacement was recorded during the whole NVT integration.

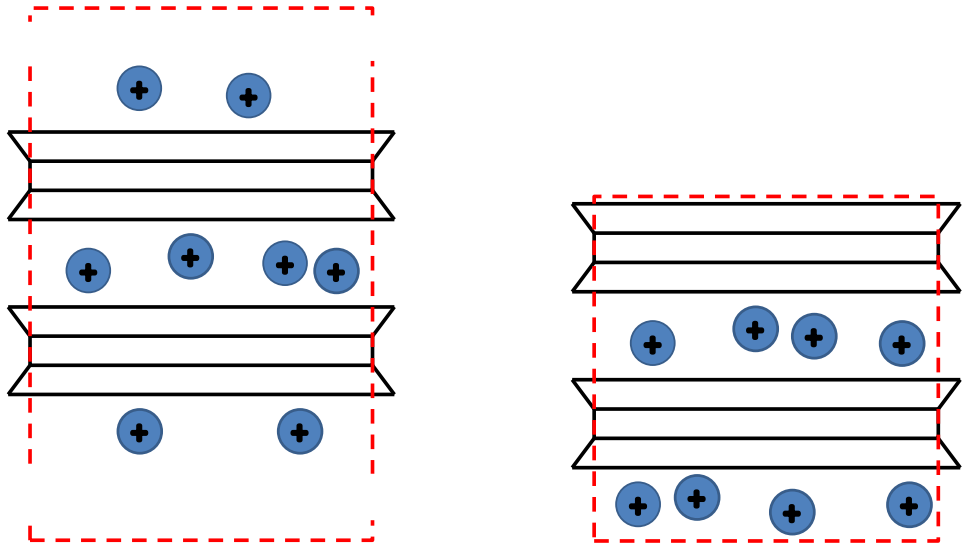

(a) (b)

Figure 3-1. Simulation cell for two stages: (a) Stage 1, 1000 ps NPT ; (b) Stage 2, 500 ps NPT + 1000 ps NVT

Analysis

Snapshot of interlayer species after equilibrium

The 3-D structure of interlayer species was visualized as snapshots from the recorded trajectories after the system reached equilibrium (based on last 20ps of NVT time integration) (Figure 3-2). The coordinates and bonding of all the atoms were imported to Materials Studio 5.5 (Accelrys Inc.) and recovered for analysis.

Radial Distribution Function (RDF) of different atoms

Examination of the radial distribution function (RDF) for species B around A yielded an estimate of the density of species B around species A at a given distance, with the peaks of the RDF representing higher occurrence frequency of species B around A. The higher occurrence frequency can be used to infer interaction/bonding between species B and species A. The RDF was determined according to (Allen & Tildesley, 1987):

$$G_{AB}(r) = \frac{1}{4\pi\rho_B r^2}\frac{dn_{AB}}{dr}$$

Where ρ_B = number density of species B, and dn_{AB} = average number of B in the range of *r* to *r* + *dr* from A. In this study, the RDF was obtained during the sampling stage and calculated as the average of several successive timesteps.

Mean Squared Displacement (MSD) of atoms

The mean squared displacement (MSD) of the group of certain species was calculated every 200 steps, during the NVT time integration. The MSD is the square of the displacement of each atom, averaged over all the atoms in the group. The displacement of an atom from its original position and its MSD can be calculated by:

$$MSD = \frac{1}{N}\frac{1}{N_{t_0}}\sum_{i=1}^{N}\sum_{N_{t_0}}[\boldsymbol{X}_i(t-t_0)-\boldsymbol{X}_i(t_0)]^2$$

Where N is the number of atoms in the group; N_{t0} is the number of time origins used; X_i is the coordinate of molecule i. The slope of the mean squared displacement versus time is proportional to the diffusion coefficient of the diffusing atoms, which allows calculation of the diffusion coefficient (D) of atoms within the interlayer according to the Einstein relation (Allen & Tildesley, 1987):

$$MSD = 2dDt$$

Where d = 2 for the diffusion in 2d space and t is the simulation time that corresponds to the recorded mean-squared displacement.

Results& Discussions

Mineral surface vs. QAC head and chain

The results were interpreted in the context of the interaction between the mineral surface and QAC surfactant in terms of bonding between the mineral surface and the QAC head group, the conformation of the cation, the layered arrangement of the QAC aliphatic chains, and the dynamics of the QAC head and chain. The overall results of simulated QAC clays are visualized in Figure 3-2 and their structural properties are summarized in Table 3-1.

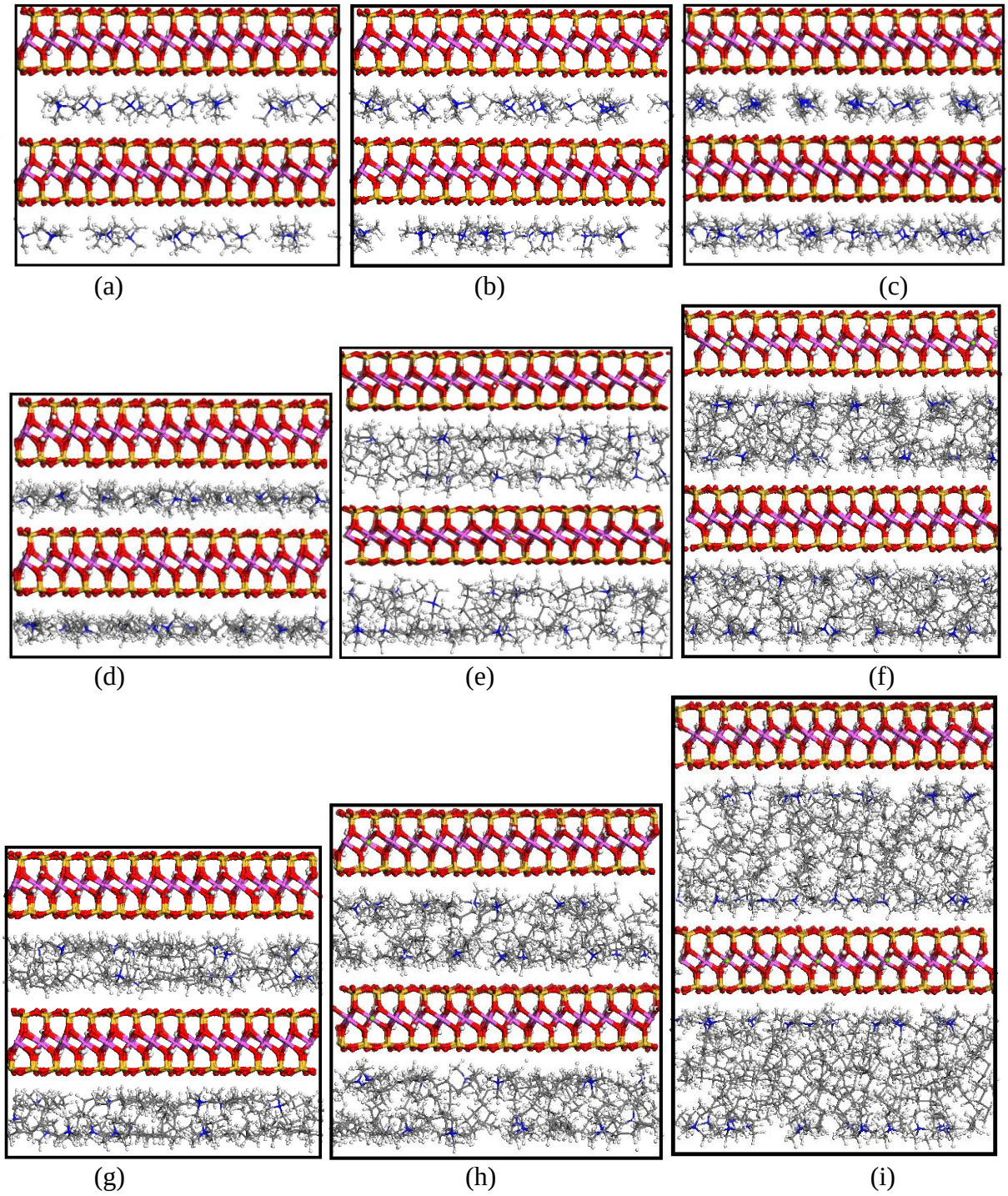

Figure 3-2. System trajectories at equilibrium: (a) TMAclay with 0.5e/UC; (b) TMAclay with 0.643e/UC; (c) TMAclay with 1.071e/UC; (d) DTMAclay with 0.5e/UC; (e) DTMAclay with 0.643e/UC; f) DTMAclay with 1.071e/UC; (g) HDTMAclay with 0.5e/UC; h) HDTMAclay with 0.643e/UC; i) HDTMAclay with 1.071e/UC; Note: for all species, C = gray, N = blue, H = white, O = red, Si = yellow, Na = purple, Al = pink, Mg = green.

Morphology of Nitrogen head

The head group of the QACs, which carries the positive charge of the organic cation, was attracted to the clay surface via electrostatic forces (QAC-head and mineral interface is shown in Figure 3-3a). The RDF of the clay surface oxygen vs. QAC nitrogen indicated the minimum distance of QAC nitrogen and hydrogen to the surface oxygen were 3.85 and 2.65 Å, respectively. In contrast to previous observations for the $R\text{-}NH_3^+$ group (Heinz et al., 2004), no hydrogen bond was formed between the QAC methyl group (CH_3) and the clay surface oxygen (Figure 3-3b), which also indicated that the QAC head group could have lateral rearrangement across cavities (Heinz et al., 2003). However, by comparing the MSD of the QAC head group and carbon tails (Figure 3-4), the simulation results indicated that the QAC head could be considered as an immobile phase near the clay surface, when compared with the non-polar carbon tails, which is in agreement with Liu et al. (2009).

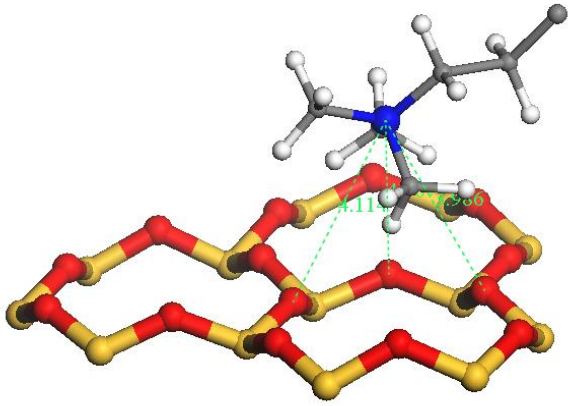

(a)

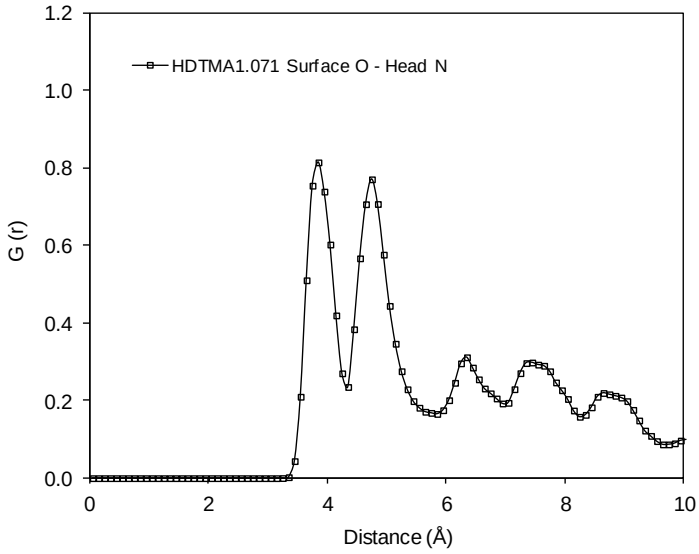

(b)

Figure 3-3. Interaction between QAC head group and clay surface oxygen. (a) QAC head vs. clay basal surface; (b) surface oxygen to QAC nitrogen.

Aliphatic carbon-surface oxygen

For clay interlayers without interlayer water molecules, the aliphatic carbon chains of alkylammonium cations tend to form integral numbers of layers, aligned parallel to the clay basal surface. In general, as the number of intercalated aliphatic carbons was increased, the arrangement transitioned from lateral-monolayer carbon to lateral-bilayer, pseudo tri-layer, or even paraffin-monolayer structure (Lagaly, 1976). The transition between interlayer structures was triggered by the increase of van der Waals area required by increasing the size of the alkylammonium cations, as it exceeded the area per electron charge on the basal plane (Sposito, 1984). That is, at the critical point, the monolayer structure was no longer stable and it transitioned to a bilayer arrangement. Consequently, the organic carbon arrangement was controlled by both the layer charge of the phyllosilicate and the intercalated QAC. The number of carbon layers demonstrated a step increase as the interlayer organic carbon reached the threshold of maximum packing density.

For the three QACs studied Table 3-3 gives a rough estimation of the carbon layers, along with their van der Waals area, which was equal to $(5.7(n_c+3)+14)$ $Å^2$ (where n_c is the number of aliphatic carbons on the chain). The threshold transition for the single carbon layer was determined by the ratio of van der Waals area of each QAC, divided by MMT surface area per electron (total area divided by total charge). The relationship demonstrated that QAC carbon would form a monolayer if the ratio was less than 1, while bilayers would form in the range of 1~2, and tri/paraffin layers would form if the number was larger than 2. The estimated arrangement patterns had excellent agreement with the simulation results (Table 3-3, Figure 3-2).

Table 3-3. QAC Arrangement Estimated from VDW Area

QAC type	VDW area of QAC ($Å^2$)	VMD area/area per e^- on MMT		
		0.5e/UC	0.643e/UC	1.071e/UC
TMA	36.8	0.41 (Mono)	0.52 (Mono)	0.87 (Mono)
DTMA	88.1	0.97 (Mono)	1.25 (Bi)	2.08 (Bi-Tri)
HDTMA	122.3	1.35 (Bi)	1.73 (Bi)	2.89 (Tri-Paraffin)

Mobility of QAC head group & carbon chain

The mobility of the QAC head group and chain were examined separately, and were recorded as the averaged MSD of all the head group nitrogen and chain carbons. Because the chain length controlled the degree of freedom of the chain, only HDTMA clay was examined. The mobility of head group and chain were inferred from the respective MSD during NVT time integration.

It can be noticed that the nitrogen head group had little mobility throughout the NVT integration. For the paraffin monolayer structure, the nitrogen head had a mean squared displacement of less than $2Å^2$ over 1 ns. The ratio of MSD over time yielded a self-diffusion coefficient of the nitrogen head group of less than $2\times10^{-11}m^2/s$, which confirmed that nitrogen head group was essentially an immobile phase near the mineral surface. However, the aliphatic carbon chain demonstrated much larger mobility (self diffusion coefficient was approximately $1\times10^{-10}m^2/s$) compared with head group and the mobility increased as the organic loading was increased (Figure 3-4). The aliphatic chains of monolayers structure also had less mobility compared with that in the paraffin structure due to their constrained movement in interlayer space.

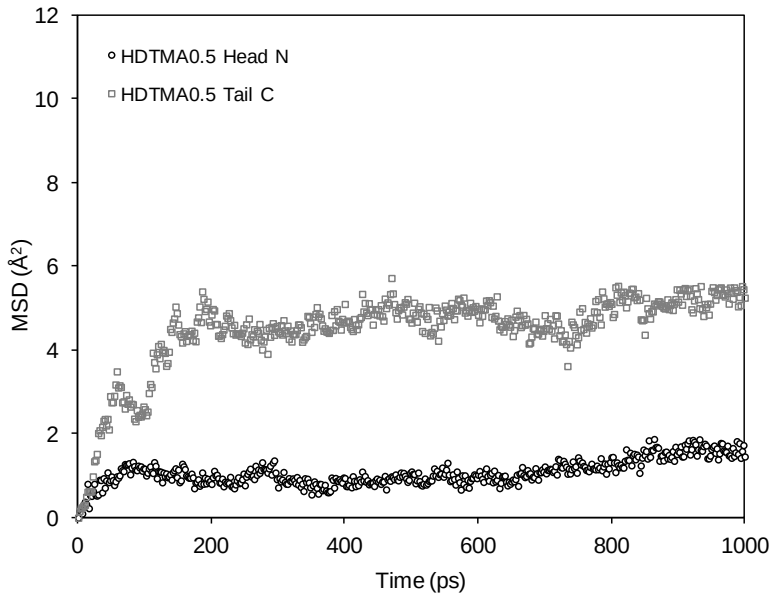

(a)

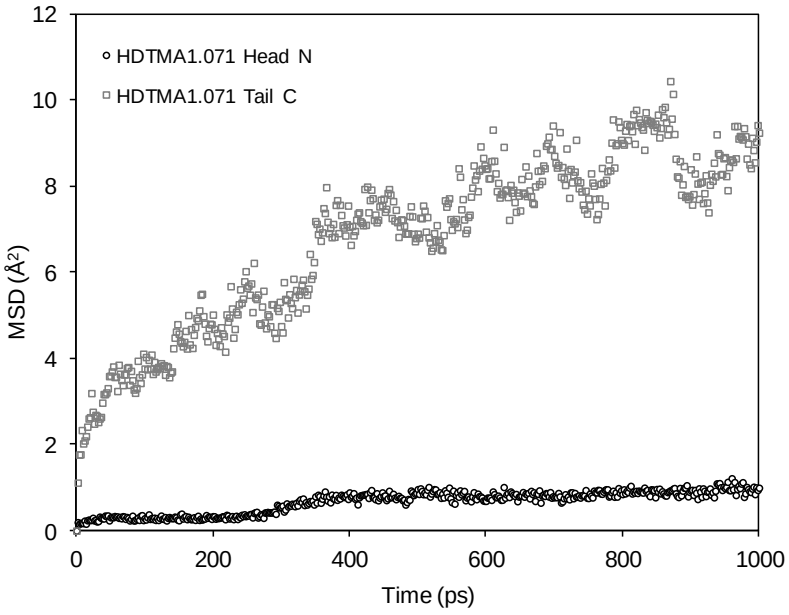

(b)

Figure 3-4. MSD of interlayer species: (a) HDTMAclay with charge density of 0.5e/unit cell; (b) HDTMAclay with charge density of 1.071e/unit cell.

QAC surfactant structure vs. clay charge, QAC type

Effect of increased charge density

The effect of increasing the charge density of base clay was also examined. For each surfactant, the base clays for intercalation had permanent structural charges of 0.5e, 0.643e, and 1.071e per unit cell which resulted in the numbers of intercalated QACs in the interlayer of 14, 18, and 30 for the resultant organoclay complexes, respectively (assuming 100 percent cation exchange).

The simulations demonstrated that when the charge density was increased, it was easier for long-chain QACs (i.e. HDTMA) to form more carbon layers (mono to bi and bi to tri/paraffin), while no substantial change was observed for the small QAC clays (Figure 3-2). For low-charge montmorillonite (0.5e), the QAC arrangement was either monolayer (TMA and DTMA) or bilayer (HDTMA), with simulated basal spacing of less than 19Å. As layered charge increased, the TMA clay retained a monolayer organic carbon structure by covering a significant amount of clay surface, while DTMA clay and HDTMA clay both significantly increased the layers of carbon. For the case of long-chain QACs with high charge clay (1.071e), more clay basal surface was taken by the head groups due to the increase in the number of head groups. Consequently, the aliphatic chains had little chance to conform to the clay surface, and instead, they were released from the surface and pushed to the interlayer space. The bulk aliphatic carbons were aggregated via short range forces and formed multiple-layered structures (Figure 3-2), with a much larger resultant basal spacing (e.g., basal spacing of HDTMA clay = 24.12 Å).

Effect of increased percentage of cation exchange

Another factor that affected the quantity of organic cation loaded into the interlayer was the percentage of metallic cations that were replaced by organic cations. For the case of Na-montmorillonite, the higher percentage of cation exchange indicated more organic cations were loaded onto mineral surface. Thus, the effect of increasing the percentage of cation exchange was similar to that of increased clay charge density, and as the amount organic carbon was increased the number of carbon layers also increased as a result (Table 3-1).

Effect of increased chain length

The effect of increasing the carbon chain length of intercalated QACs was examined by intercalating TMA^+; $DTMA^+$ and $HDTMA^+$ into same base clay with a charge density of 0.5e per unit cell in the case of dry system (Figure 3-2). The results demonstrated that both TMA^+ and $DTMA^+$ formed a monolayer of organic carbon and interacted with both the upper and lower clay surfaces. Most notably, the TMA^+ only formed discrete pillars that propped up the interlayer space, while the $DTMA^+$ cation chains were arranged parallel to the basal surface, covering a significant portion of the surface area. The simulation results also suggested that for a 0.5QAC per unit cell of loading, TMA clay was far from surface saturation, while the DTMA clay was very close to the transitional zone of monolayer to bilayer arrangement. In contrast, $HDTMA^+$ cations did not form a monolayer arrangement, but instead formed a bi-layer structure with significant surface coverage as well.

Because individual HDTMA cations have much larger van der Waals area compared with the smaller QACs, it was always favorable for the HDTMA surfactant to

form multiple organic carbon layers in montmorillonite, even in the case of low charge montmorillonites (Figure 3-2). A paraffin arrangement of interlayer HDTMA cations was observed for montmorillonite with charge density of 1.071e per unit cell, with a significant amount of basal spacing occupied by HDTMA cations. When $HDTMA^+$ was loaded at high density, the long aliphatic chain also formed a significant volume of porous, hydrophobic media in interlayer, which could facilitate partitioning of non-polar species in interlayer (Zhao and Burns, 2012). Consequently, montmorillonite intercalated with HDTMA cations typically have larger basal spacings and exhibit organophilic behavior.

QAC surfactant structure vs. TOC

At nano-scale, for univalent cations like QACs, the van der Waals area and area per electron on clay are two of the controlling factors for QAC arrangement in the montmorillonite interlayer. Previous studies have shown that the basal spacing of synthesized QAC-montmorillonite increased as a result of both increased carbon number on the chain (Osman et al., 2004; Osman et al., 2005; Heinz et al., 2007), as well as increased number of cations in the interlayer (He et al., 2005; Liu et al., 2009). This suggests that at macro scale, the basal spacing or the packing style of interlayer QAC was controlled by the total amount of organic loading, or total organic carbon content of the intercalated QAC. In contrast, this study used the weight ratios between the QAC and the clay as the only variable:

$$\frac{m_{QAC}}{m_{MMT}} = \frac{n \times CEC\% \times M_{(QAC)}}{M_{(UC)}}$$

Where: n is the charge per unit cell of clay.

$CEC\%$ is the percentage of organic cations exchanged into the interlayer

$M_{(QAC)}$ is the molar mass of intercalated QAC

$M_{(UC)}$ is the molar mass of the clay unit cell

The relation between basal spacing and weight ratio was plotted based on compiled data of previous work (Zeng et al., 2003; Osman et al., 2004; Osman et al., 2005; Heinz et al., 2007; Liu et al., 2009), as well as this study (Figure 3-5). Most notably, for the simulated dry systems in this study, the basal spacing and number of organic carbon layers of synthesized organoclays increased as the total organic carbon loading increased, which is in agreement with both previous experimental and simulation studies. The total organic content/loading onto the clay surface could be attributed to either increased length of the carbon chain of QACs (carbon content per molecule) or increased percentage of cation exchange and the higher charge density of the unmodified base clay (more intercalated QAC). Simulation results also indicated that the increase of basal spacing versus increased TOC (or m_{QAC}/m_{clay}) was stepwise rather than continuous for low and intermediate organic loading (Figure 3-5). The "steps" of observed basal spacing corresponded to integral numbers of organic carbons that arranged parallel to the clay basal surface, starting from a monolayer of carbon (14.0~15.0Å), that transitioned to a bilayer of carbon (17.7~19.5Å), then eventually formed multiple layers of carbon (>22.5Å). The weight ratios for the three cases were 0~0.15, 0.2~0.3, >0.32, respectively. The trend worked reasonably well compared with the theoretical transition calculated based on the maximum packing density of aliphatic carbons, as indicated by dashed lines in Figure 3-5. Consequently, knowledge of the mass ratio of QAC vs. clay allowed

prediction of the packing style of the QAC carbon, assuming the intercalation of QAC was homogeneous within the mineral interlayer.

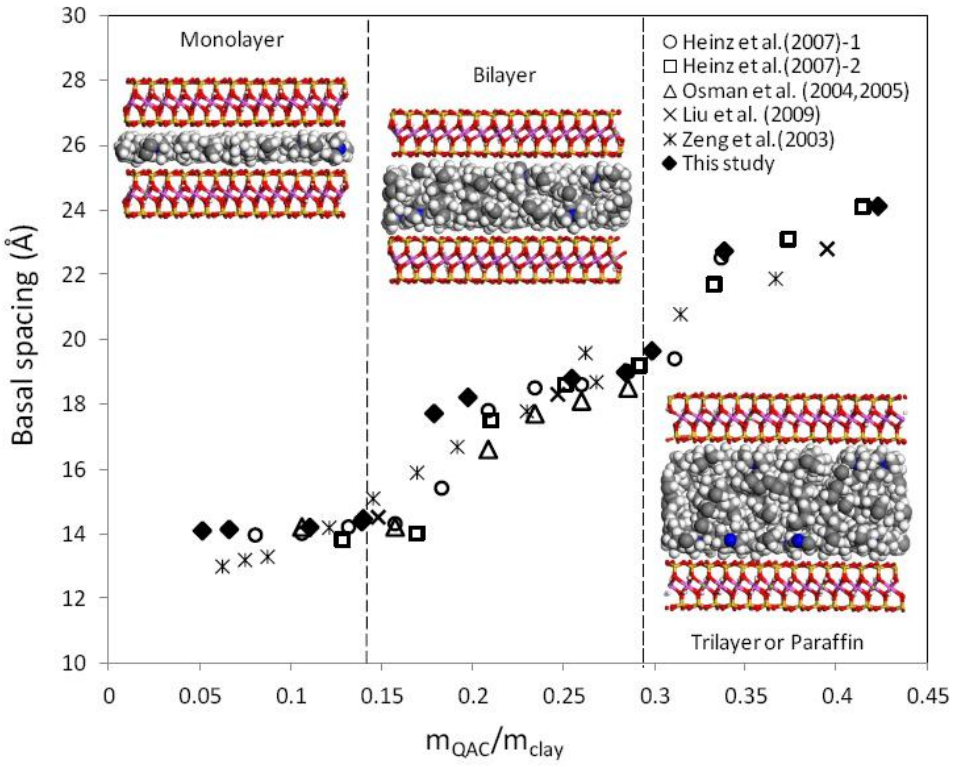

Figure 3-5. Basal spacing as a function of interlayer oragnic carbon content.

Conclusions

The morphology of single chain quaternary ammonium cations (QAC) in the montmorillonite interlayer was examined through a series of molecular dynamics (MD) simulations, and compared to previous experimental and simulation studies. The amount of clay layer charge, the cation exchange percentage, and the QAC type were used as the controlling factors for the resultant microstructure of interlayer QAC. Overall results confirmed that for different amount of organic loading, the interlayer organic carbon would have different arrangement, including lateral monolayer, lateral bilayer, and paraffin structure, in agreement with previous observations. Furthermore, this study indicated that the transition of the micro-layer structures was essentially controlled by the interlayer organic carbon content, or total organic carbon content (TOC) at macro-scale. Consequently, when the interlayer organic coating is known, interlayer surfactant microstructure can be roughly estimated based on this relationship.

CHAPTER 4
MOLECULAR DYNAMICS SIMULATIONS OF ORGANIC COMPOUND SORPTION IN QUATERNARY AMMONIUM CATION INTERCALATED MONTMORILLONITE

Introduction

Clay mineral surfaces, such as montmorillonite, have relatively low sorption affinity for nonpolar organic compounds due to the hydrophilic/organophobic interlayer volume that results from the permanent structural layer charge of the mineral (Boyd et al., 1988; Smith et al., 1990). In montmorillonite, the layer charge results primarily from isomorphic substitution within the mineral crystal, and typically yields an excess of negative charge. The resulting layer charge is counteracted by cations that are present in the interlayer of the clay mineral. Most commonly, this excess negative charge has two primary results: interlayer attraction of inorganic metallic cations (e.g., Na^{+}, Ca^{2+}) that hydrate strongly, and the development of highly ordered water layers (Young and Smith, 2000; Tambach et al., 2006) within the interlayer space. The limited uptake capacity of natural montmorillonite for nonpolar organic compounds can be improved by exchanging their naturally occurring inorganic cations with organic cations. Increasing the total organic content in the interlayer of the clay mineral changes the interlayer space from organophobic to organophillic, resulting in an interlayer space that may exhibit much larger uptake capacity for organic compounds (Chiou et al., 1983; Jaynes and Boyd, 1991; Upson and Burns, 2006; Richards and Bouazza, 2007). The enhanced sorption capacity of organoclays for organic compounds results in their potential applications in

waste containment, landfill liners, and slurry walls (Park and Jaffe, 1993; Smith and Jaffe, 1994; Sheng and Boyd, 2000).

The process of intercalating quaternary ammonium organic cations onto the montmorillonite surface by replacing their naturally occurring inorganic cations will herein be referred to as primary adsorption of organic cations. By varying the molecular structure and quantity of the organic cations that are loaded onto the clay's interlayer during primary adsorption, the interfacial characteristics of the resulting clay mineral can be controlled, resulting in changes in properties such as surface hydrophobicity, frictional interaction (Burns et al., 2006), and dynamic behavior. Additionally, the organoclay's sorptivity for nonpolar organic compounds (i.e., secondary adsorption), will also exhibit variable behavior as a function of the exchanged organic cation structure or degree of loading (Bartelt-Hunt et al., 2003). Extensive work has been performed to quantify the adsorption behavior of nonpolar organics on organoclays (Smith et al., 1990; Bartelt-Hunt et al., 2003; Redding et al., 2002). Notably, it has been demonstrated that organoclays synthesized from small QACs (e.g., TMA^+; TEA^+; $BTEA^+$) demonstrated surface adsorption for benzene and could be modeled using a Langmuir adsorption isotherm, while organoclays made with long chain QACs (e.g., $HDTMA^+$), exhibited partitioning behavior and were best modeled with a linear adsorption isotherm. Experimental evidence has indicated that as the size of the organic cation was increased, either by increasing the length of the carbon chain in one functional group position (Boyd et al., 1988) or by increasing the chain length equally in all four functional group positions (Fuller et al., 2007), the secondary sorption of nonionic organic chemicals transitioned from an adsorption mechanism to a partitioning mechanism. This suggested

that total organic carbon (TOC) in the interlayer, not the cation structure, was the controlling factor in the adsorption mechanism. Furthermore, it has been demonstrated that clays that had been treated with HDTMA cations demonstrated increased sorption capacity for organic molecules as the quantity of total organic carbon was increased (Burns et al., 2006; Mortland et al., 1986), while organoclays made from small QACs showed a decrease in sorption capacity as the total organic carbon was increased (Burns et al., 2006); both trends are consistent with a shift from surface adsorption to partitioning as the size of the organic cation was increased.

While extensive work has been performed to quantify the uptake of nonpolar organic compounds by organoclays, exploration of the fundamental mechanisms responsible for sorption remains challenging due to the complex interlamellar structure in the organic phase. Significant insights have been gained through experimental investigation of the intercalated QAC structure. However, while the experimental approaches aid interpretation of the sorption behavior of modified clays, it remains useful to identify molecular interactions between the mineral, the sorbed organic cations, and the organic sorbates. Computational methods, such as molecular dynamics, permit the simulation of this interaction at the molecular level, and provide quantitative information for atomistic interactions, as well as thermodynamic information for the simulated system (Hou et al., 2000; Greathouse and Cygan, 2005; Liu et al., 2009), and can be used as an important supplement to aid in the interpretation of experimental studies.

In this study, the adsorption of a nonpolar organic to three organoclays was studied. Benzene was chosen as the representative organic sorbate, and the cations were chosen to represent a range of sizes, from small quaternary ammonium cations such as

tetramethylammonium (TMA^+), to larger quaternary ammonium cations with increased length in one alkyl chain, including decyltrimethylammonium ($DTMA^+$) and hexadecyltrimethlyammonium ($HDTMA^+$). Molecular dynamics (MD) simulations were used to study the interaction between phases at the molecular level without the presence of water, and yielded insight into different sorption isotherms that have been quantified at the macroscale (Burns et al., 2006; Bartelt-Hunt et al., 2003). Additionally, the microstructure of the sorbed surfactants and the characteristics that controlled the secondary adsorption of benzene were analyzed quantitatively.

Computational methods

Force field applied

The force field was applied to define the interaction between three phases: clay-organic cations (QACs) and organic sorbate, was the combination of ClayFF (Cygan et al., 2004) and the Consistent-Valence Force Field (CVFF, Dauberosguthorpe et al., 1988), following the methods of Liu et al. (2009). Clay FF includes the potential energy terms and its parameters for all types of atoms in the clay framework, while CVFF defines those of the organic phases (organic cation and organic sorbate, benzene). When combined together, the interaction between any groups of atoms in the system is quantified and interaction potential energies can be calculated based on the mixing rule of the parameters. The combined force field maintained the structures of the different phases and most importantly, guaranteed flexibility and full interactions between the phases.

The total energy in the simulation was expected to have the components of Coulombic interaction, van der Waals interaction, and bonded interaction (detailed information in Table 4-1):

$$E_{total} = E_{VDW} + E_{Coulombic} + E_{bond\_stretch} + E_{angle\_bend} + E_{torsion} + E_{improper}$$

Table 4-1. Potential Energy Terms of Surfactant Arrangement Simulation

Energy term	Potential function	Equation	Interacting atoms	Applied to
Van der Waals	Lennard-Jones (12-6)	$E_{VDW} = D_{0,ij}\left[\left(\frac{R_{0,ij}}{r_{ij}}\right)^{12} - 2\left(\frac{R_{0,ij}}{r_{ij}}\right)^{6}\right]$	2	Any 2 atoms
Coulombic	Coulombic	$E_{Coulombic} = \frac{e^2}{4\pi\varepsilon}\sum_{i\neq j}\frac{q_i q_j}{r_{ij}}$	2	Any 2 atoms
Bond stretch	Harmonic	$E_{bond\_stretch} = k_1(r_{ij} - r_0)^2$	2	O-H bond
	Morse	$E_{bond\_stretch} = D(1 - e^{-\alpha(r_{ij} - r_0)})^2$	2	C-N,C-C,C-H bonds of organic cations
Angle bend	Harmonic	$E_{angle\_bend} = k_2(\theta_{ijk} - \theta_0)^2$	3	metalic atom-O-H; organic molecules
Torsional	Harmonic	$E_{torsion} = k_3[1 + d\cos(n\phi)]$	4	organic cation
	Charmm	$E_{torsion} = k_4[1 + \cos(n\phi - d)]$	4	benzene
Improper	Harmonic	$E_{improper} = k_5(\chi - \chi_0)^2$	4	organic cation; benzene

where: D and D_0 are the depth of the potential well; r_{ij} is the separation distance of atoms i and j; θ_{ijk} is the angle of atoms i, j and k; $R_{0,ij}$ is radius that corresponds to the minimum LJ potential energy; q_i, q_j are partial charges of two atoms; ε is the dielectric constant, r_0 and θ_0 are equilibrium values of radius and angles; $k_1 \sim k_5$ are prefactors; α is a stiffness parameter (equal to1/L); $d = \pm 1$, n is an integer ≥ 0, and χ_0 is the equilibrium value (degrees).

The non-covalent interaction is universal for any two atoms and it was represented by the summation of the conventional Lennard-Jones potential (usually referred to as 12-6 potential) and Coulombic potential energy terms. Lennard-Jones potential represents the van der Waals energy term, which is significant at short range while Coulumbic interaction becomes dominant at long range. For bonded interactions, different terms were used to describe 2 body (bond stretch), 3 body (angle bend) and 4 body (torsional; improper) interactions, in accordance with the nature of the bonding atoms and the bulk property of individual molecules. The first four terms of the total

energy were involved in the energy calculation of the clay framework and all the terms were considered as energy components of the organic phases.

Simulated system

The secondary adsorption of organic compounds by organoclays occured mainly in the interlayer space, rather than on the external surfaces of the particles (Jaynes and Vance, 1999). Consequently, a periodic simulation box consisting of two clay platelets and two interlayer species was created in Materials Studio (Version 5.5, Accelrys Inc.). Characteristics of all species in the system, including the clay prototype and cation type are given in Table 4-2. For the simulation, all three QAC-clay complex have basal surface area of 35.72Å × 35.04Å in size, which is also the dimension of simulation box in x and y direction, respectively. Initially, each basal spacing was set to more than 30~36 Å in order to accommodate all the intercalated QACs (number of cations equals to 28 × charge per unit cell), which were placed randomly in the interlayer spaces. Next, four benzene molecules (approximated based on weight ratio from experimental studies) were also intercalated into each interlayer of the QAC-clay complex. Then the initial configuration of the clay-QAC complex and benzene was imported to the Large-scale Atomic/Molecular Massively Parallel Simulator (LAMMPS) (Plimpton, 1995) for the MD simulation. During the simulation, the time step was set at 1.0 femtosecond and energy minimization was performed before running the dynamics. During the first stage of simulation, the NPT time integration was performed (1atm, 25 ℃) for 1000 picosecond and system was allowed to reach equilibrium. Then a further 1000 picosecond NVT time integration was performed with approximately 100 picoseconds of a sampling stage in order to record the trajectories for post-analysis (for RDF and species density only, MSD

was obtained during the whole NVT integration). In order to obtain the trajectories of clay- QAC complex for comparison, a separate but similar simulation was performed, except no benzene molecules were added and system was treated with 1000 picosecond of NPT time integration only (Figure 4-1).

Table 4-2. Clay Prototype Models

Chemical formulae of clay unit cell[1]	Duplicates[2]	Charge density/Unit cell	Organic cation type
$0.500Na^{+}(Mg_{0.429}Al_{3.571})(Al_{0.071}Si_{7.929})O_{20}(OH)_4$	28	0.5e	TMA
$0.643Na^{+}(Mg_{0.571}Al_{3.429})(Al_{0.071}Si_{7.929})O_{20}(OH)_4$	28	0.643e	DTMA
$1.071Na^{+}(Mg_{1.000}Al_{3.000})(Al_{0.071}Si_{7.929})O_{20}(OH)_4$	28	1.071e	HDTMA

[1] modified after Heinz et al. (2005)
[2] 28 duplicates for each 2:1 clay platelet

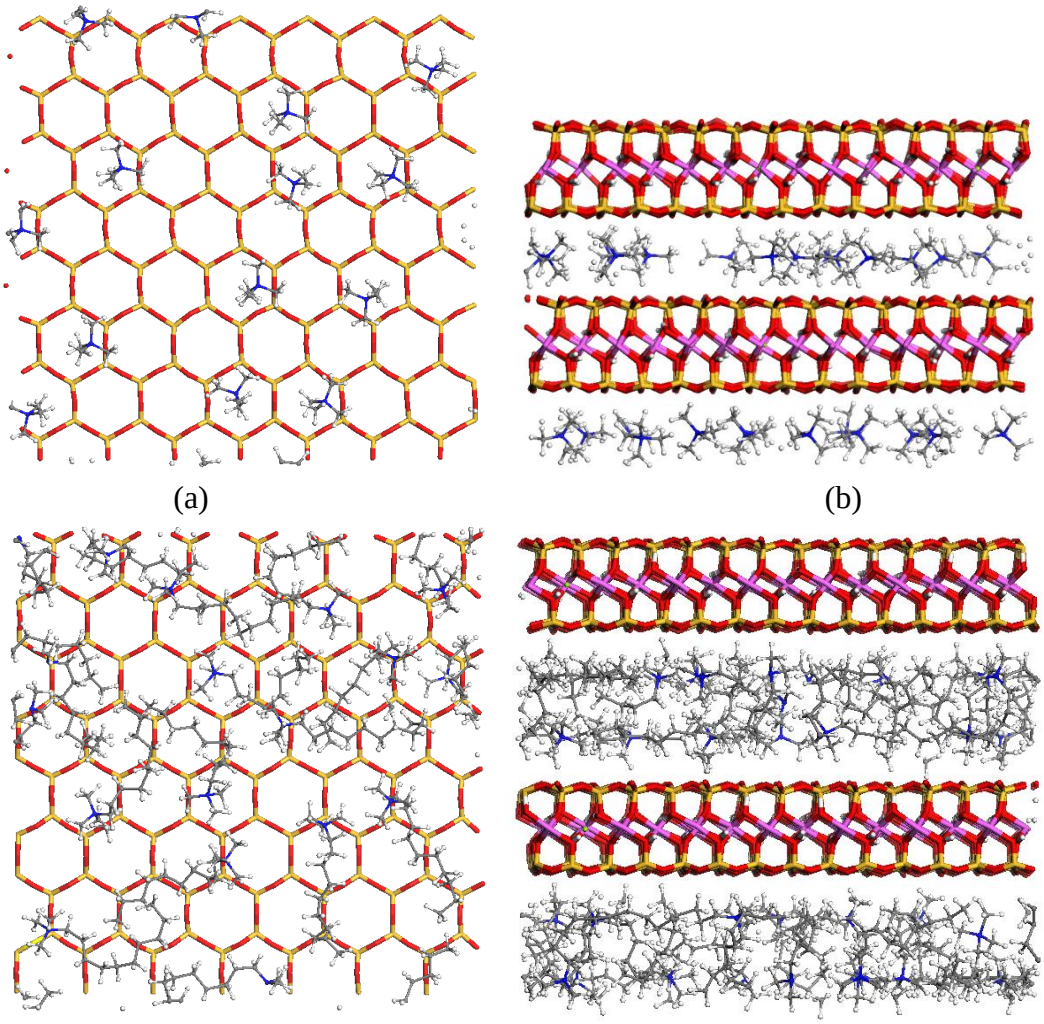

(a) (b)

(c) (d)

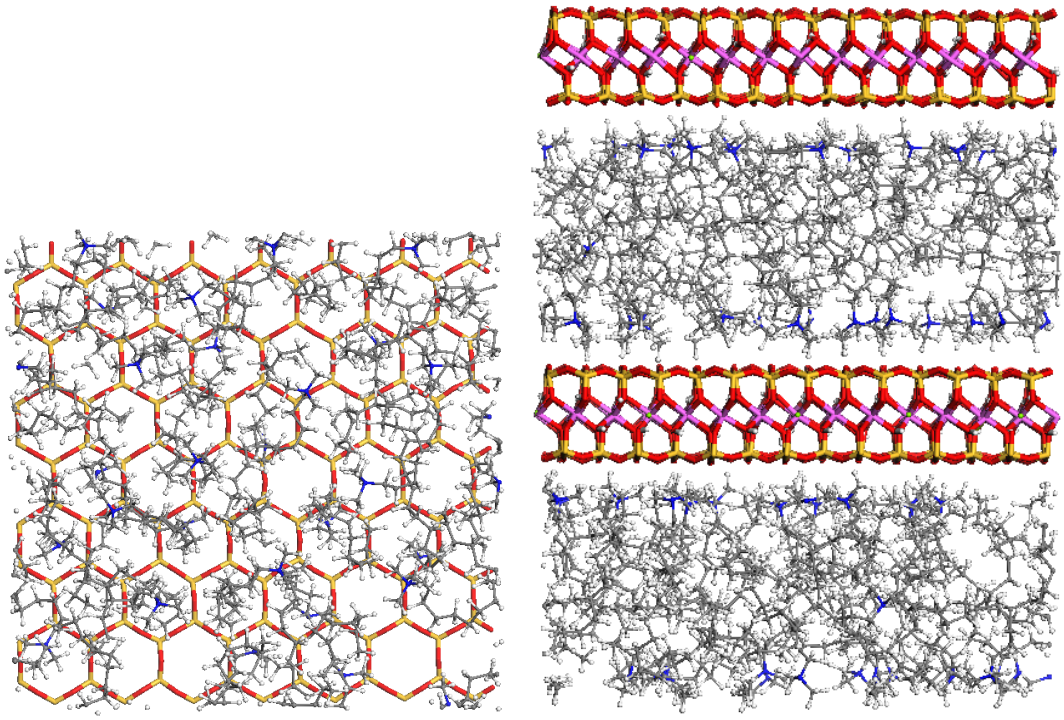

(e) (f)

Figure 4-1. Organic surfactant structure after primary adsorption of clay-QAC: a) TMA plane view; b) TMA side view; c) DTMA plane view; d) DTMA side view; e) HDTMA plane view; f) HDTMA side view. Note: for all species, C = gray, N = blue, H = white, O = red, Si = yellow, Na = purple, Al = pink, Mg = green.

Analysis

Snapshot of interlayer species after equilibrium

The 3-D structure of clay and interlayer species, including the organic cations and the benzene molecules, was visualized as snapshots from the recorded trajectories after the system reached equilibrium. The coordinates and bonding of all the atoms were imported to Materials Studio 5.5 (Accelrys Inc.) and recovered at different stages of the simulation for analysis.

Spatial density of species in the interlayer space

In the interlayer space, the density of each atom was quantified as its histogram along the Z direction, normal to the clay basal surface, in the interlayer spacing:

$$N(X_i, z) = n(z - \frac{\delta}{2}, z + \frac{\delta}{2})$$

Where z is the coordinate of atom along Z direction; n is the count of atom type X_i; δ = 0.2 or 0.1 Å is the interval of bin array.

Radial Distribution Function (RDF) of different atoms

Examination of the radial distribution function (RDF) for species B around A yielded an estimate of the density of species B around species A at a given distance, with the peaks of the RDF representing higher occurrence frequency of species B around A. The higher occurrence frequency can be used to infer interaction/bonding between species B and species A. The RDF was determined according to (Allen and Tildesley, 1987):

$$G_{AB}(r) = \frac{1}{4\pi\rho_B r^2}\frac{dn_{AB}}{dr}$$

Where ρ_B = number density of species B, and dn_{AB} = average number of B in the range of r to $r+dr$ from A. In this study, the RDF was obtained during the sampling stage and calculated as the average of several successive timesteps.

Mean Squared Displacement (MSD) of benzene molecules

The mean squared displacement (MSD) of the group of benzene molecules was calculated every 200 steps, during the whole NVT time integration. The MSD is the

square of the displacement of each atom, averaged over all the atoms in the group. The displacement of an atom from its original position and its MSD can be calculated by:

$$MSD = \frac{1}{N}\frac{1}{N_{t_0}}\sum_{i=1}^{N}\sum_{N_{t_0}}[\boldsymbol{X}_i(t-t_0)-\boldsymbol{X}_i(t_0)]^2$$

Where N is the number of atoms in the group; N_{t0} is the number of time origins used; X_i is the coordinate of molecule i. The slope of the mean squared displacement versus time is proportional to the diffusion coefficient of the diffusing atoms, which allows calculation of the diffusion coefficient (D) of benzene molecules within the interlayer according to the Einstein relation (Allen and Tildesley, 1987):

$$MSD = 2dDt$$

Where d = 2 for the diffusion in interlayer space and t is the simulation time that corresponds to the recorded mean-squared displacement.

Results& Discussions

Surfactant structure after primary adsorption

Simulation results of montmorillonite intercalated by only three organic cations, TMA, DTMA, and HDTMA, were recorded and the interlayer structures were visualized after equilibrium was achieved (Figure 4-1). Additionally, basal spacing for each of the three organoclays was determined (Table 4-3). When TMA cations were exchanged into the interlayer, they tended to form discrete aggregations on the surface oxygen plane (Figure 4-1a), covering approximately 15% of the area of the oxygen plane. Although this study was performed in the absence of water molecules, previous studies performed at low water contents have demonstrated that the cations interacted with both top and bottom oxygen planes and acted as pillars, holding the clay platelets apart at a given interlayer space (Barrer, 1989). Low water content simulations performed prior to this study also demonstrated the pillar effect (data not shown). The small size of the TMA cation resulted in a relatively small resultant interlayer spacing before benzene sorption (14.14 Å) (Table 4-3).

Table 4-3. Structural Properties of Simulated Organoclays. 1After NPT time integration, simulation results of HDTMA clay agree with experimental study of (Burns et al., 2006); 2Calculated as number of carbons per unit area of clay basal surface

Cation type	Carbon on the chain	Number of cations	Basal spacing (Å)[1]	Carbon/Area (Count/Å^2)[2]
TMA^+	1	14	14.136 ± 0.0695	0.04
$DTMA^+$	10	18	17.711 ± 0.0854	0.17
$HDTMA^+$	16	30	24.320 ± 0.0875	0.52

DTMA cations with a size intermediate to TMA and HDTMA, demonstrated preferential orientation of the aliphatic chain and aligned parallel to the clay surface covering the oxygen plane, even when the cation loading on the clay was low (Figure 4-1b). In this study, the DTMA cation formed a bilayer structure in the interlayer, with carbon atoms concentrated in two planes, preferentially oriented near the upper and lower clay surfaces, and not significantly distributed within the interlayer space. It is important to note that a large percentage of the clay basal surface was covered when the DTMA cations were exchanged (approximately 80%), even though a relatively small number of cations were exchanged onto the surface. The basal spacing of the DTMA clay before benzene sorption was 17.71 Å (Table 4-3).

In contrast, the sorption of HDTMA cations to the clay surface was significantly different than that observed for TMA and DTMA. The hydrophilic nitrogen head of the HDTMA cation, which was the functional group where positive charge was concentrated, always interacted with the surface oxygen; however, the saturated aliphatic chain, which was organophilic, exhibited different arrangements on the clay surface as cation density was increased. As more HDTMA cations were loaded onto the clay surface (through higher charge density or by increasing the percentage of cation exchange, data not shown), the density of head groups near the clay surface increased and allowed the aliphatic chains to move away from the clay surface, interacting with each other in the interlayer space via short range forces and entanglement mechanisms (Figure 4-1c). At high HDTMA loadings, the concentration of cations was large enough to form a paraffin structure and resulted in the basal spacing equal to 24.32 Å (Table 4-3).

Secondary sorption mechanism

Because the TMA cations covered only approximately 15% of the area of the oxygen plane, a large area of the surface was available as active sorption sites. Subsequently, during the process of secondary adsorption of benzene to the TMA modified clay, the nonpolar benzene molecules oriented parallel to the clay surface, interacting with the oxygen rings that were not covered by the TMA cations (Figure 4-2a). It is believed that as more benzene molecules are adsorbed, the number of available sites would decrease and eventually reach the limit of nearly 100% of surface coverage (Barrer, 1989), which corresponds to the ultimate sorption capacity as indicated by the Langmuir adsorption theory. These results are consistent with experimental studies that demonstrated lower secondary sorption of organic compounds as the quantity of quaternary organic cations (or TOC) sorbed to the clay surface was increased (Redding et al., 2002), although it is important to note that this was true only in case when small QACs, such as TMA, were sorbed to the clay.

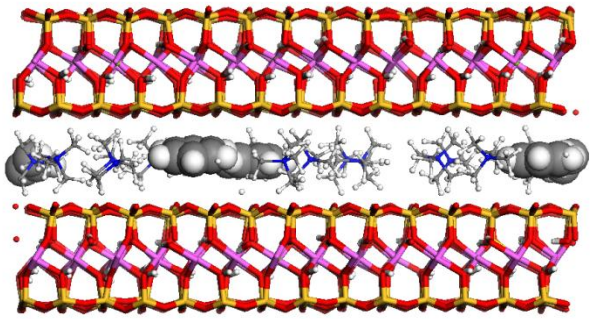

(a)

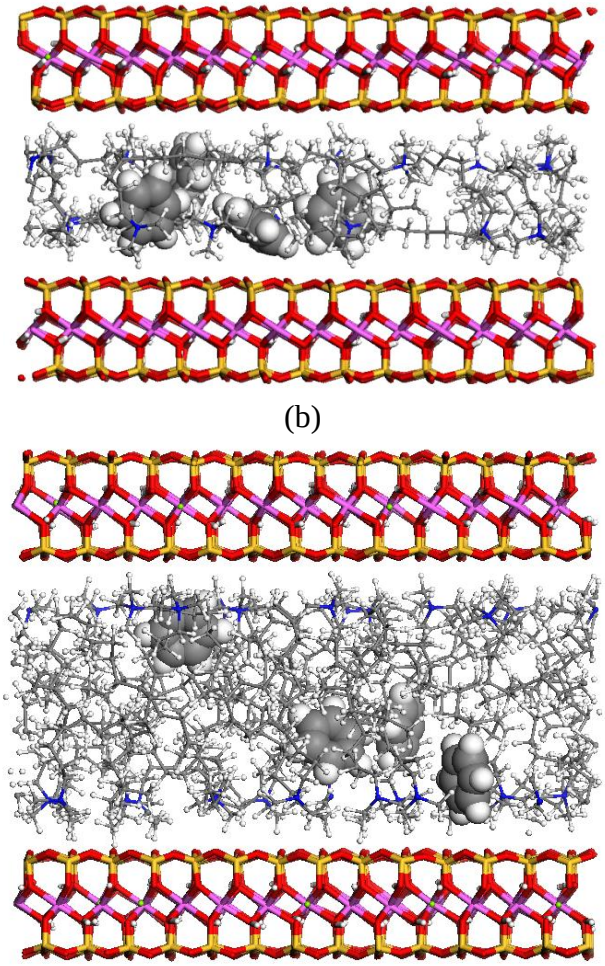

(b)

(c)

Figure 4-2. Interlayer species after overall system NVT equilibrium (only one interlayer is shown): a) TMA surfactant and benzene molecules; b) DTMA surfactant and benzene molecules; c) HDTMA surfactant and benzene molecules. Note: for all species, C = gray, N = blue, H = white, O = red, Si = yellow, Na = purple, Al = pink, Mg = green.

Sorption of DTMA cations to the clay surface resulted in a significant increase in surface coverage of the clay when compared to TMA, even though the number of sorbed DTMA cations was low. Increasing the tail length of the cation resulted in significant coverage of the clay surface, at approximately 80%. Because a large percentage of the clay surface was covered with the aliphatic carbon chain, availability of the oxygen rings as sorption sites for benzene was reduced. Instead, benzene molecules interacted with a

combination of both surface oxygen and aliphatic chains, as indicated by their vertical orientation when sorbed to DTMA clay (Figure 4-2b). Compared with TMA clay, DTMA clay clearly showed a dual mechanism of uptake of benzene, which was a combination of surface oxygen attraction of benzene molecules, as well as aliphatic chains, which aggregated and surrounded benzene based on van der Waals interaction. The sorption mechanism for DTMA represented a transition from purely adsorptive behavior to partitioning of the benzene molecules.

Sorption of benzene molecules to HDTMA clay demonstrated a significantly different mechanism from TMA and DTMA because the HDTMA molecules formed a paraffin-type organic structure within the interlayer. The bulk of the aliphatic chains of HDTMA developed a porous, amorphous organophilic matrix in the interlayer that behaved like a solvent during the partition of the organic benzene solute. The amount of aliphatic carbon in the HDTMA chain was large, such that van der Waals interaction dominated, and benzene molecules were more likely to be contained in aliphatic chains via short-range forces; consequently, the uptake of benzene molecules was a partitioning mechanism (Figure 4-2c). Also, when compared to the limited surface sorption sites observed for TMA clays, pore space in the porous aliphatic interlayer medium could be created when benzene molecules penetrated the interlayer, resulting in a linear isotherm (Bartelt-Hunt et a., 2003). Consequently, increasing the total organic carbon content in the interlayer resulted in increased sorption of the benzene molecules, which was consistent with experimental observations (Redding et al., 2002).

Density of different species in interlayer

A snapshot of the species density histogram along the z direction (normal to the clay basal surface) was obtained for the carbon and nitrogen atoms in the organic cations and for the carbon atoms in the benzene molecules. The distribution of the atoms demonstrated that the aliphatic carbon along the z direction (The upper and lower bound in the z direction represents the two adjacent clay basal surfaces) clearly divided into an integral number of peaks, which verified the monolayer (Figure 4-3a), bilayer (Figure 4-3b) and paraffin (Figure 4-3c) arrangement of QAC carbon for TMA, DTMA, and HDTMA, respectively. For all types of organoclays, the nitrogen head group was associated with the clay surfaces, as indicated by the peaks of the N atom count near the upper and lower boundaries of the clay particles. The density distribution of benzene carbon provided direct evidence of the shifted mechanisms for the uptake of benzene molecules: in the case of TMA clay, the benzene carbons were located closer to the clay surface than the nitrogen atoms (Figure 4-3a); however, when the QAC was DTMA, benzene tended to locate midplane and not to interact with clay surface significantly (Figure 4-3b). Finally, in the case of HDTMA clay, the benzene molecules clearly had the maximum distance from the clay surface, forming alternating layers with the aliphatic carbons in the HDTMA cations (Figure 4-3c).

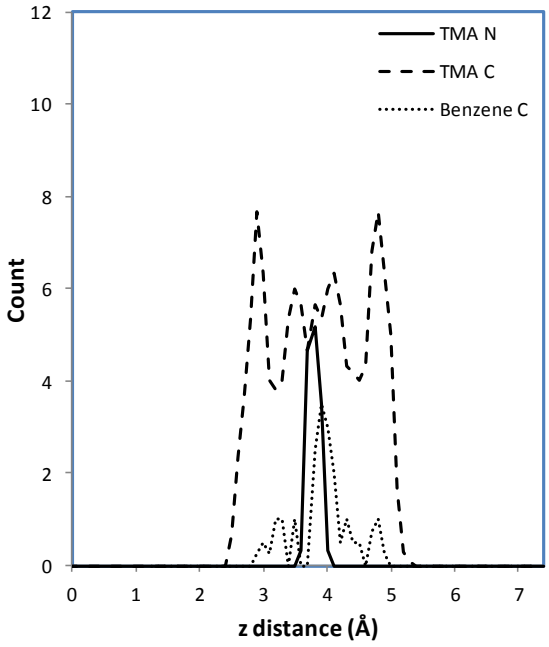
TMA N
TMA C
Benzene C
Count
z distance (Å)
0
2
4
6
8
10
12
0
1
2
3
4
5
6
7

(a)

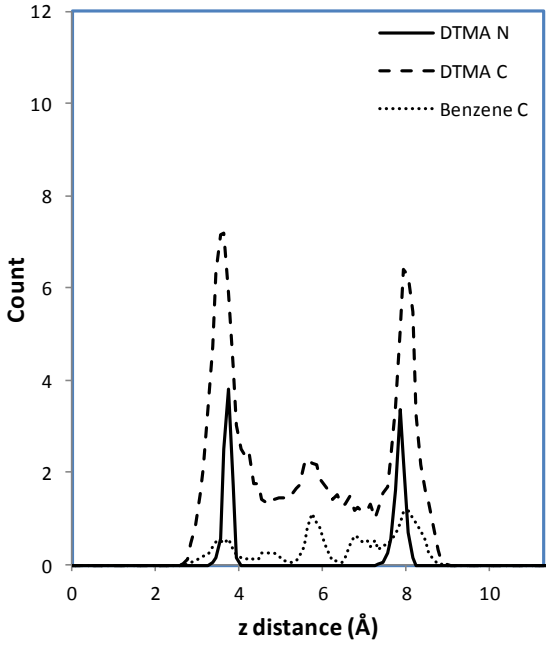
DTMA N
DTMA C
Benzene C
Count
z distance (Å)
0
2
4
6
8
10
12
0
2
4
6
8
10

(b)

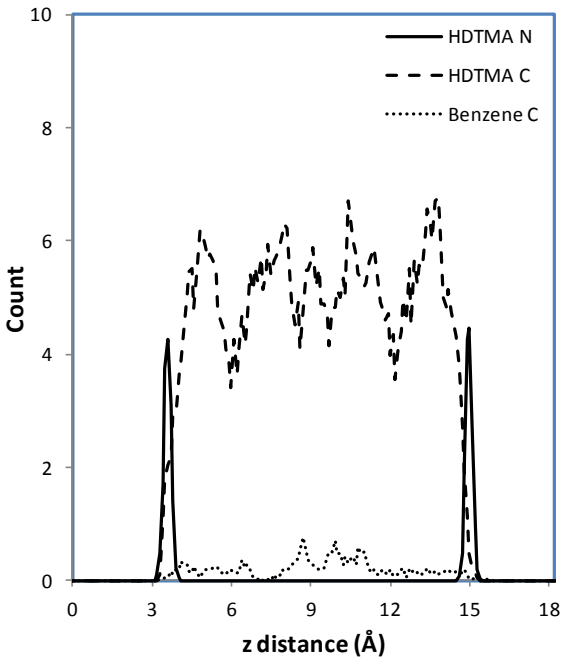

(c)

Figure 4-3. Species density histogram; z distance is normal to the clay basal surface. Note: For TMA clay, all carbons were counted, for DTMA and HDTMA clays, only aliphatic carbons were counted.

Radial Distribution Function

The Radial Distribution Functions (RDF) were derived to quantify interactions between certain species, and also to yield insight into the adsorption type of three organoclays (Figure 4-4). To obtain a representative result, the average RDF of 1000 instantaneous trajectories was produced, and the interaction was quantified through the RDF between the clay surface oxygen atoms and the benzene hydrogen atoms. For TMA clay, benzene molecules tended to interact with surface oxygen, which is evident in the close and relatively uniform distribution of benzene hydrogen relative to the surface oxygen (Figure 4-4a). In contrast, for HDTMA clay, the peak at approximately 2.65 Å indicated that surface adsorption did occur at some point in the simulation, but was not the dominant mechanism of uptake because benzene molecules were most likely to be contained in the bulk aliphatic chains, at approximately 8~12Å from the clay surface (Figure 4-4a). For the case of DTMA clay, it clearly showed some transitional characteristics between TMA clay and HDTMA clay, with interaction between surface oxygen weakened compared with TMA (in the range of 2~4Å) and the short range interaction between organic cation and benzene becoming more significant (8~10Å) (Figure 4-4a).

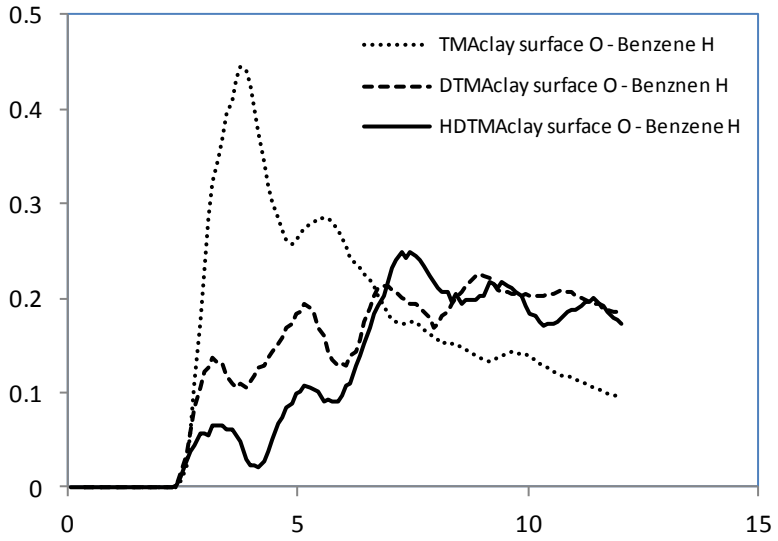

(a)

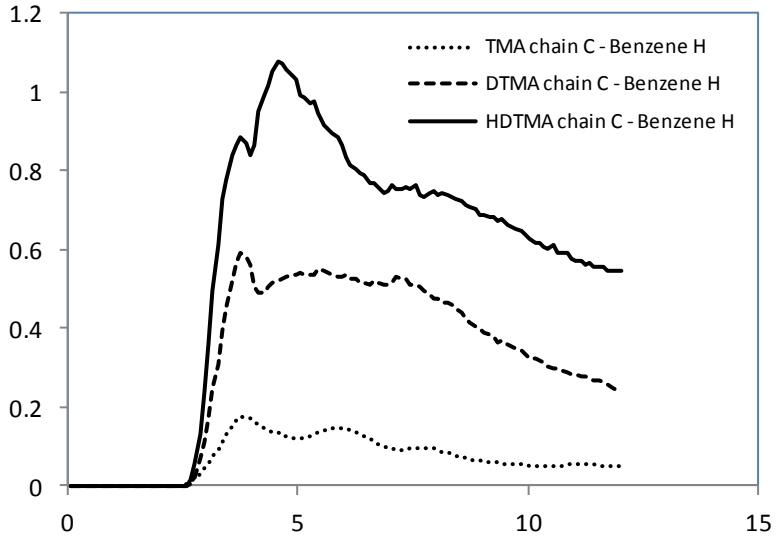

(b)

Figure 4-4. Radial distribution function of selected atoms: a) clay surface oxygen versus benzene hydrogen; b) aliphatic carbon versus benzene hydrogen.

The RDF of the QAC aliphatic carbon and benzene hydrogen was also quantified to examine the short-range interaction between benzene molecules and QAC chains. The simulation demonstrated that the carbon on the HDTMA aliphatic chains surrounded the benzene molecules, and this short-range interaction (2.6~5Å) between aliphatic carbon and benzene decreased for DTMA and TMA (Figure 4-4b). It was also observed that the

distance between the QAC chain carbon and the benzene hydrogen was largest for TMA and smallest for HDTMA, which indicated increased interaction between the benzene and the HDTMA chains, further supporting the low probability of surface adsorption of benzene onto HDTMA modified clays.

Mean squared displacement

The Mean Squared Displacement (MSD) of benzene molecules was calculated as the average value of displacement of benzene molecules in the group (Figure 4-5), with the slope of the MSD versus time used to calculate the self-diffusion coefficients of benzene molecules in the interlayer of TMA DTMA and HDTMA clays (Table 4-4). The calculated interlayer diffusion coefficient in TMA clay and HDTMA clay would be expected to differ from bulk values due to differences in diffusion within the inter- and intra-pore space; however, the simulation results were on the order of 10^{-6} cm^2/s, which was consistent with previous experimental results (Table 4-4). The similar magnitude of the interlayer and bulk diffusion coefficients suggests that interlayer diffusion represents the rate-limiting step in diffusion of benzene through organoclays. Note that the benzene molecules in HDTMA clay had the largest MSD over time, which suggested that the benzene molecules had larger mobility within the interlayer space. It is believed that this is a result of the relative ease of displacement of the HDTMA aliphatic chain in the interlayer.

Table 4-4. Self-diffusion Coefficients of Benzene Molecules in Different Porous Media

Source	Method	Sorbent	Sorbate		Temperature	Diffusion Coefficient
This study	MD	100%HDTMA-montmorillonite	Benzene	Interlayer	298 K	$2.71\times10^{-6}cm^2/s$
	MD	100%DTMA-montmorillonite	Benzene	Interlayer	298 K	$1.38\times10^{-6}cm^2/s$
	MD	100%TMA-montmorillonite	Benzene	Interlayer	298 K	$1.04\times10^{-6}cm^2/s$
Lorenzetti et al., 2005	Experimental	70%BTEA-bentonite	Tritium	1D bulk	room temperature	$3.80\times10^{-6}cm^2/s$
	Experimental	70%HDTMA-bentonite	Tritium	1D bulk	room temperature	$3.60\times10^{-6}cm^2/s$
Headley et al., 2001	Experimental	Sand+Bentonite+Organophilic clay	Benzene	1D bulk	293K	$0.50\sim1.50\times10^{-6}cm^2/s$
Hou et al., 2000	MD	Zeolite 12MR	Benzene	crystal	650 K	$2.32\sim2.56\times10^{-6}cm^2/s$
Sastre et al., 1999	MD	Zeolite 12MR	Benzene	crystal	650 K	$4.62\times10^{-6}cm^2/s$
Johnson et al., 1989	Calculated	Clay liner sample	Benzene	Field	283K	$3.00\times10^{-7}cm^2/s$

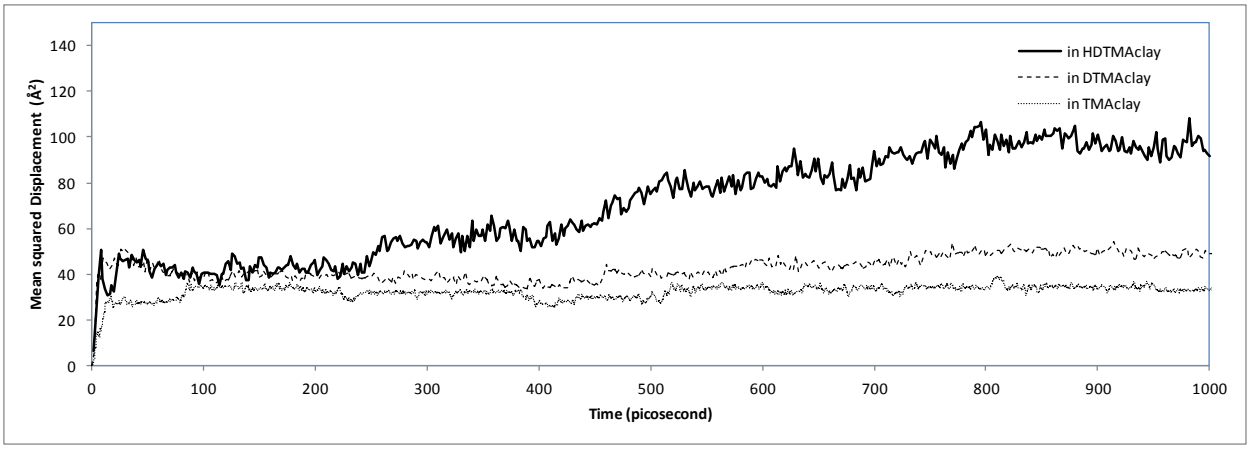

Figure 4-5. Average mean squared displacement of benzene moleclues versus time.

Conclusions

In summary, this chapter simulated the secondary sorption behavior of benzene to organoclays through modeling with three different quaternary ammonium cations. Simulation results indicated that the arrangement of surfactants resulted in integral layers of aliphatic carbons as a function of organic carbon loading, and that the number of layers of carbon controlled the interaction type between benzene molecules and the clay surface. The simulation indicated that benzene molecules interacted directly with the clay surface in the presence of TMA cations, resulting in an uptake mechanism of surface adsorption. Consequently for TMA clay, an increase in total organic carbon would result in a decrease in the sorption capacity of the clay due to decreased surface sites that were accessible for sorption. In contrast, HDTMA clay, with layered aliphatic carbon, would exhibit increased sorption capacity as total organic carbon was increased because the HDTMA cations formed a partitioning medium that retained benzene molecules via short-range forces in the aliphatic chains. The molecular dynamics simulation yielded insight that supported the observed experimental evidence of TMA clay as a surface adsorptive mechanism and HDTMA clay as a partitioning mechanism. Further, the simulation demonstrated that the sorption mechanism was mixed, demonstrating properties of adsorption and partitioning, for DTMA clay with a chain length intermediate to TMA and HDTMA.

CHAPTER 5
MOLECULAR DYNAMICS SIMULATIONS OF BENZENE SORPTION AND DIFFUSION IN HDTMA CLAY INTERLAYER PORES

Introduction

Organic contaminants in groundwater can originate from a variety of sources such as industrial manufacture, human activities, and improper waste disposal practices (Bedding et al., 1982; Focazio et al., 2008). Because many of these compounds are toxic and/or carcinogenic, the release of organic contaminants to the environment, along with their interaction with soil sediments, transport, and final fate is of great concern (Weber et al., 1991; Pignatello and Xing, 1996). Organic-coated clays, or organoclays, can be used as amendments in engineered barriers or geosynthetics clay liners for retardation, sorption, and isolation of organic compounds due to their strong capacity for uptake of non-polar organic compounds (Lo and Yang, 2001; Lee et al., 2012) (Smith and Jaffe, 1994; Yang et al., 2003). Most commonly, organic-coated clays are created by exchanging organic cations onto the clay surface, through replacement of the naturally occurring inorganic metallic cations of the base clays. When organic cations replace inorganic cations on the clay surface, organoclays usually exhibit increased saturated hydraulic conductivity compared to that of unmodified clays; however, their conductivity for water is still low (magnitude of 10^{-8} m/s) and may even be reduced for separate phase organic fluids (Lo and Yang, 2001). Consequently, the rate of advective transport remains low, and the molecular diffusion caused by concentration gradients in porous media like an organoclay can be the critical component in the overall rate of mass transport. In many instances, diffusion controls the quantity and rate of organic

compound that passes through a barrier system, especially in conditions of low hydraulic gradient (Lorenzetti et al., 2005).

The organoclay capacity to uptake non-polar solutes allows retardation of the diffusive transport of the solute, and leads to a diffusion regime that can be considered as a transient process (Fetter, 1999; Sharma, 2004). Typically, non-polar compound diffusion through clays with sorption is described using Fick's law coupled with a "sink term" that accounts for sorption of the non-polar solute (Boving and Grathwohl, 2001; Bourg et al., 2002):

$$\varepsilon \frac{\partial C}{\partial t} = D_e \frac{\partial^2 C}{\partial x^2} - \rho \frac{\partial q}{\partial t} \quad \text{..... (5.1)}$$

Where $\rho \frac{\partial q}{\partial t}$ is the sink term that corresponds to the transient diffusion; ε and ρ denote the porosity and bulk density of organoclays, respectively; D_e is the effective diffusion coefficient considered as the overall effect of tortuous and restricted movement of solute in the porous media:

$$D_e = \frac{D_{\text{aq}} \varepsilon_e \delta}{\tau} \quad \text{..... (5.2)}$$

Where ε_e is effective porosity; δ and τ are constrictivity factor and tortuosity of the porous media, respectively. D_{aq} is the diffusion coefficient in bulk water.

For organophilic clays (Redding et al., 2002; Yariv and Cross, 2002), sorption of hydrophobic organic compounds in interlayer organic surfactants can be quantified by a simple distribution/partitioning coefficient K_d:

$$q = K_d C_{aq} \quad \text{..... (5.3)}$$

Where q is the mass of solute per unit dry mass of solid; C_{aq} is the concentration of solute in solution at equilibrium [mol/L].

After substitution of the above equation into equation (1), the apparent diffusion coefficient D_a can be defined:

$$\frac{\partial C}{\partial t} = \left(\frac{D_e}{\varepsilon + K_d \rho} \right) \frac{\partial^2 C}{\partial x^2} = D_a \frac{\partial^2 C}{\partial x^2} \quad \text{..... (5.4)}$$

The diffusion equation for a non-polar sorbate diffusing in an organoclay requires many parameters, some of which are difficult to obtain from experimental work. Additionally, many isotherms exhibit non-linearity as a function of concentration, which is not addressed in this model. Most importantly, the model was derived based on the bulk properties of the porous media; consequently, the interlayer pore characteristics and the equilibrium between macropores and interlayer pores are not reflected in this equation. As a result, the modeled parameters deviate from values obtained from experiments; for example, K_d values observed in diffusion experiments are inherently lower than the value of K_d obtained from batch sorption tests (Grathwohl, 1998). The overestimated K_d can be problematic when designing retardation capacity and equilibrium time of transient diffusion for barrier systems. Additionally, previous studies have shown that in organophilic pores (e.g. montmorillonite with organic coatings) surface diffusion of adsorbed species can also occur in interlayer pores. This requires an extra "surface diffusion" term be included in D_a to fit some experimental data which causes additional difficulties in the application of this model (Thomas and Clouse, 1990a,b,c).

Recently, a diffusion model that focuses on the interlayer diffusive behavior of species and connects interlayer "compartment" pore with continuum scale has been proposed by Bourg and Sposito (2010). They suggested the diffusion coefficient of object species (i) can be estimated by the weighted average of that in macropore and in interlayer nanopore:

$$\frac{D_{a,i}}{D_{aq,i}} = \frac{1}{G_i}(\alpha_{macropore,i} + \alpha_{nanopore,i}\delta_{nanopore,i}) \quad \text{..... (5.5)}$$

Where G is the "geometric factor" that accounts for pore characteristics and distribution; δ is the "constrictivity factor" that accounts for the constricted movement of species in interlayer. α is the molar fractions of species of interest in different types of pores.

Because the microstructure of the porous media (e.g. effective pore volume, tortuosity) remains constant, Bourg and Sposito (2010) suggested the geometric factor could be cancelled out by normalizing cation (i.e., Na^+, Sr^+, Cs^+) diffusion with water diffusion. The advantage of this approach is that when the molar fraction and diffusive properties of each species in interlayer nanopores is known, the diffusive properties of them in bulk can be predicted by normalizing by the water tracer. Similarly, the diffusion of non-polar compounds in organoclays can be predicted if the sorption in interlayer pores is taken into account in the equation. For organophilic partitioning clays, organic solutes are expected to have lower average diffusion rate in interlayer pores due to sorption by the interlayer organic carbon phase (e.g. HDTMA cations). Consequently, interlayer diffusion becomes the rate limiting step for overall mass transport due to the higher concentration of organic solute in organoclay interlayer, assuming no preferential transport paths for organic solute are available (Figure 5.1).

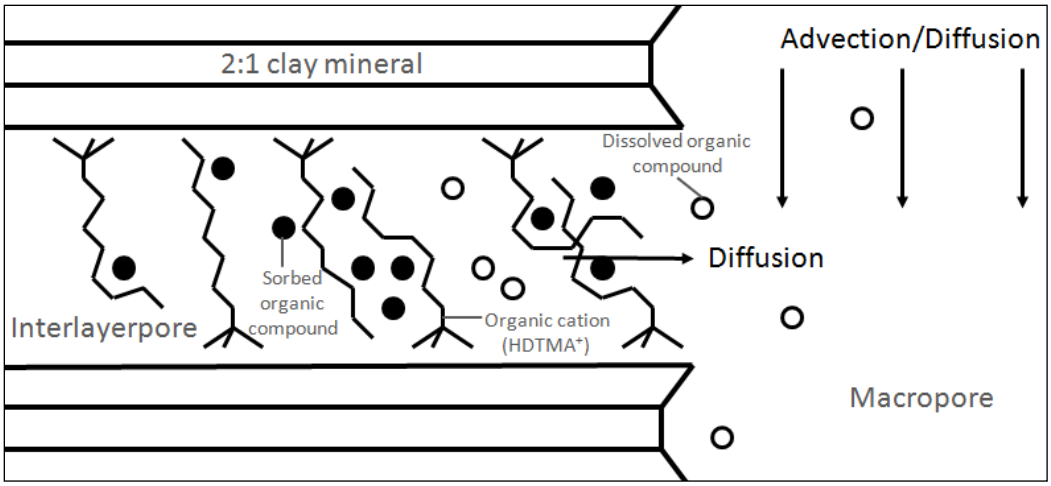

Figure 5-1. Interlayer diffusion process controlled by interaction between organic solute and interlayer organic surfactant.

It is the goal of this work to investigate the sorption and transport of benzene in interlayer pores of sodium montmorillonite (Na-MMT) and HDTMA ($((CH_3)_3N(CH_2)_{15}CH_3)$-modified clay (HDTMA clay), and relate the apparent diffusion coefficient of interlayer species $D_{interlayer}$ to the bulk diffusion coefficient D in organoclay. Equation (5) is modified to take into account of sorption of benzene, to be discriminated from non-interactive species like water or sodium:

$$\frac{D_{a,benzene}}{D_{aq,benzene}} = \frac{1}{G}\left(\alpha_{macropore,benzene} + \frac{\alpha_{nanopore,benzene}\delta_{nanopore,benzene}}{R}\right) \quad \text{(5.6)}$$

Where R is the term that accounts for the "confined movement" of benzene in HDTMA clay due to sorption.

Based on this model, molecular dynamics simulations were performed to study the interlayer diffusive behavior of water tracer and benzene in pure sodium-montmorillonite and HDTMA clays with different amounts of interlayer water. An advanced force field of clay was used, and each simulation was as long as 5 ns. Results of all simulations were compiled to examine the: (1) constrictivity on water tracer and

organic sorbate (benzene) in the interlayer nanopores of HDTMA clay; (2) sorption and diffusion dynamics of organic sorbate in interlayer by addressing the interactions between different phases and apparent diffusion coefficients of organic molecules; (3) relation of transport rate of organic compound in organoclay interlayer to apparent values in the bulk. Based on the results, the apparent bulk diffusion coefficient of organic sorbate in organophilic clays can be predicted when the diffusion coefficient of a water tracer is known.

Molecular dynamics simulations

Force Field

Force-field based, equilibrium molecular dynamics simulations of HDTMA clay interlayer were performed in Large-scale Atomic/Molecular Massively Parallel Simulator (LAMMPS) (Plimpton, 1995).The basis of the overall simulation was the combined force field of ClayFF(Cygan et al., 2004) + Constant Valence Force Field(CVFF, Dauberosguthorpe et al., 1988) + SPC water model (Berendsen et al., 1981; Allen, 1987). The combined force field of the three has been proved to be appropriate for the simulation of system contains clay, water and organic phases (Greathouse and Cygan, 2005; Liu et al., 2009; Zhu et al., 2011), also, the interaction among phases in interlayer, especially the diffusion behavior of species are addressed based on the combined force field, the accuracy of which process also verified by previous studies (Bourg and Sposito, 2010). The details of the energy terms of clay and HDTMA cations can be found in previous study (Zhao and Burns, 2012).

Physical Model

In order to compromise with long simulation time, the simulation box included only one interlayer space sandwiched between two half clay platelets (Figure 5.2), and had periodic boundary in all three directions. The prototype of clay was modified from MMT321 (southern clay, Heinz et al., 2005) and its chemical formula is $(Na)_{0.643}[Al_{0.071}Si_{7.929}O_{16}][Mg_{0.572}Al_{3.429}O_4(OH)_4]$, and the clay platelet consisted of 28 unit cells. Consequently, the initial size of the simulation cell was approximately 35.72 Å $\times$35.04 Å in the basal plane and approximately 22.5~28 Å in z direction, depends on the quantities of interlayer species. The net negative charge of clay platelet resulted from 18 random isomorphic substitutions, and the negative charge of the clay mineral framework was compensated by the interlayer organic cations (assuming 100% cation exchange) to maintain the electrical neutrality of the simulated system. The interlayer space consisted of species including water, HDTMA cation and benzene, for comparison, a Na-MMT system was also simulated. In order to avoid the complexity of discussion of quantity of interlayer water, three sets of simulations were performed for HDTMA clays, with their interlayer water content of $5H_2O$, 10 H_2O and 15 H_2O per unit cell (Table 5.1), which was approximately equivalent to the amount of water of one, two and three layer hydrates in Na-MMT (Bourg and Sposito, 2010).

Table 5-1. HDTMA Clay Properties and Interlayer Diffusion Coefficients

chemical formula of clay unit cell	clay type	cation	water molecules per unit cell	basal spacing[a] (Å)	interlayer diffusion coefficient[b] (m^2/s)
0.643cation $(Mg_{0.571}Al_{3.429})(Al_{0.071}Si_{7.929})O_{20}(OH)_4$	HDTMA clay1	$HDTMA^+$	approx. 5	22.468 ± 0.045	$1.40 \pm 0.33 \times 10^{-10}$ (benzene)
	HDTMA clay2		approx. 10	25.211 ± 0.041	$1.78 \pm 0.37 \times 10^{-10}$ (benzene) $1.18 \pm 0.27 \times 10^{-9}$ (tracer)
	HDTMA clay3		approx. 15	28.023 ± 0.054	$2.15 \pm 0.44 \times 10^{-10}$ (benzene)
	Na-MMT	Na^+	approx. 22.5	25.595 ± 0.050	$4.11 \pm 0.72 \times 10^{-10}$ (benzene) $1.30 \pm 0.19 \times 10^{-9}$ (tracer)

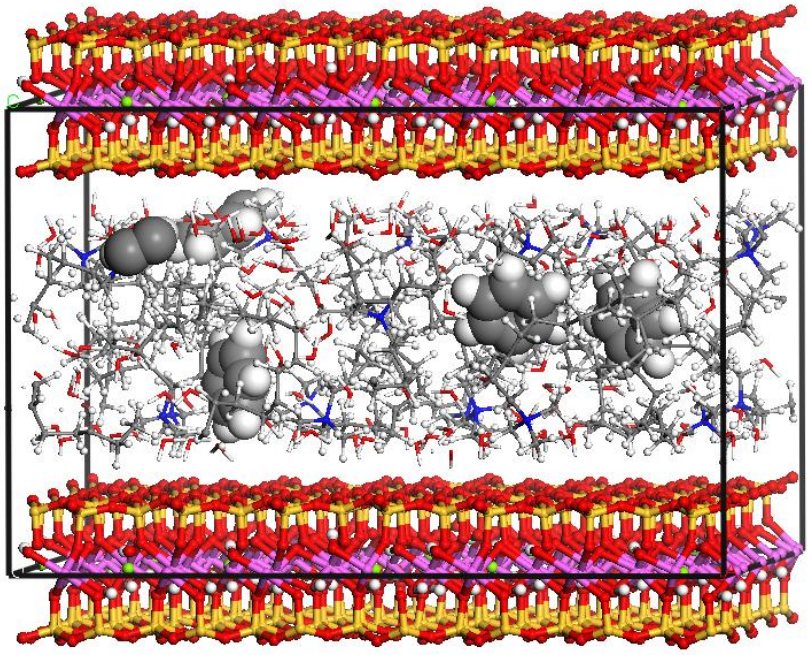

Figure 5-2. 3D view of stage 2 simulation box (Periodic boundaries highlighted by black lines).

Simulated System

Each simulated system included approximately 2500~4500 atoms and the overall simulation time was more than 5 nanoseconds. The first stage of simulation was to create a 2 clay 2 interlayer structures that subjected to NPT and NVT time integration and had free gallery spacing equilibrium, following the same method of Zhao and Burns (2012). Other than benzene molecules and HDTMA cations, water molecules were also intercalated into each interlayer space.

After the simulated system reached equilibrium after stage1, a new simulation cell was created by subtracting the previous 2 interlayer and 2 clay platelets to 1 interlayer and 1clay platelet (1/2 on top and bottom). This subtracted equilibrium scenario of sandwiched layer was then imported to LAMMPS and optimized again, followed by another 500ps of NPT time integration and 5 ns NVT time integration. During all stages, the time step was set at 1.0 femtosecond (fs), for stage 2 NVT time integration, trajectories were recorded every approximately 100 ps; the mean-squared displacement (MSD) of interlayer species were recorded every 1.0 ps for post-analysis.

Results& Discussions

Simulated systems at equilibrium

Trajectories of HDTMA-Organoclays and their nano-pore species were obtained at the end of NVT time integration. The interlayer species are visualized in Figure 5.3 and basal spacing at equilibrium is shown in Table 5.1. It can be noticed that the interlayer spacing increased from HDTMA clay1 to HDTMA clay3, indicating increased size of interlayer pore volume. The nitrogen head groups of HDTMA cations were

attracted to the clay surface while the aliphatic carbon chains were driven away from the clay surface as the amount of interlayer water molecules increased. The hydrogen bond (dashed blue line, Figure 5.3) formed by the water and HDTMA clay surface oxygen was increased significantly as the amount of interlayer water increased, the first layer of water molecules bonded to clay surface has lower mobility than others and they are in replacement of clay-aliphatic chain interaction. Also, it can be noticed that as the amount of interlayer water increases, they would develop H bond that connects adjacent water molecules, this H bond "percolation" phenomenon prevailed as more water molecules were introduced. Finally, interlayer volume partitioned into small domains of organic phase (HDTMA cation) and water (Figure 5.3d).

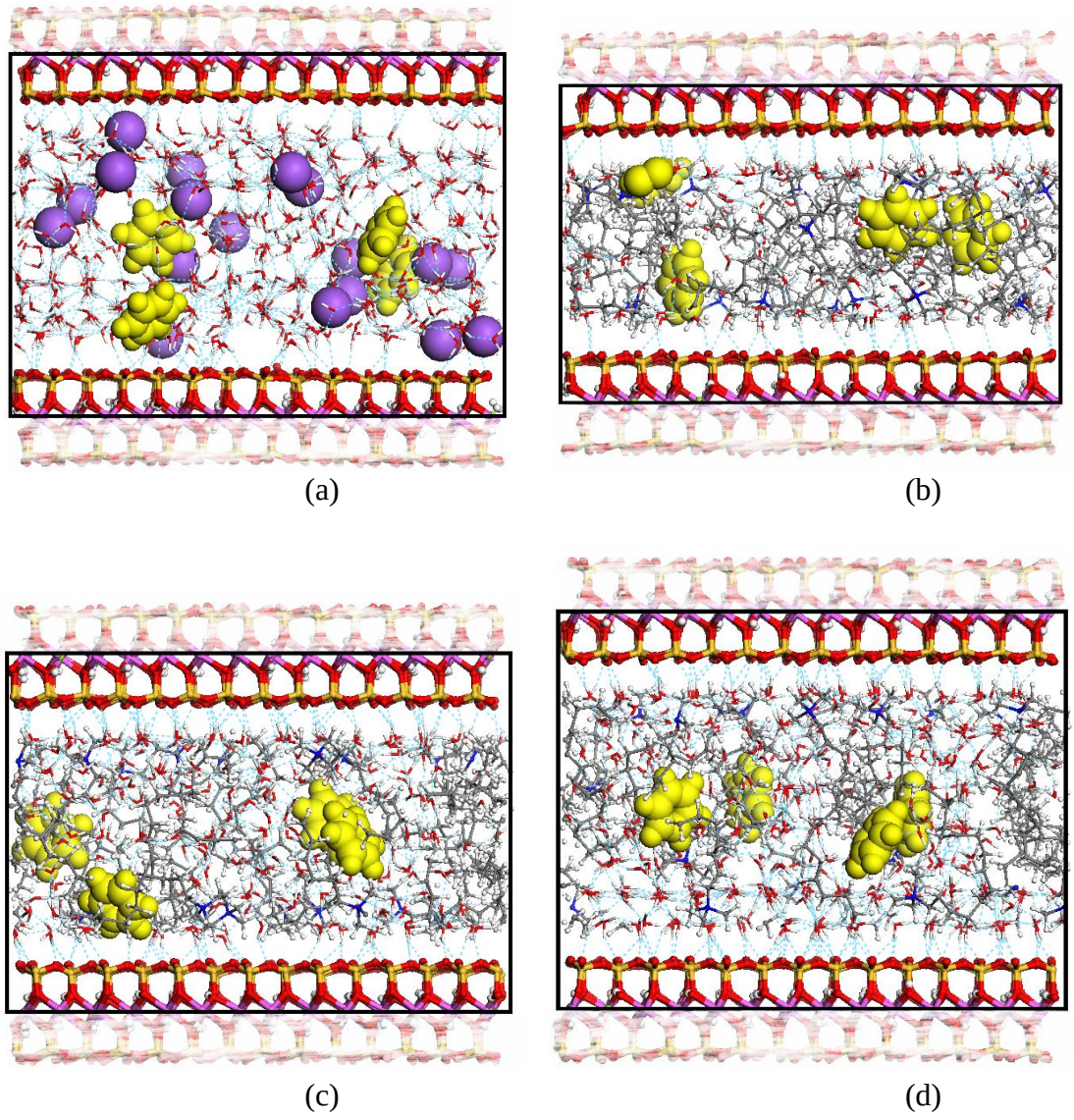

Figure 5-3. Interlayer species of simulated system after equilibrium. (a) Pure montmorillonite. (b) Interlayer water equivalent to 5 per unit cell. (c) Interlayer water equivalent to 10 per unit cell. (d) Interlayer water equivalent to 15 per unit cell. Note: for all species, C = gray, N = blue, H = white, O = red, Si = yellow, Na = purple, Al = pink, Mg = green. Benzene molecules are highlighted, and blue dashed line = hydrogen bond.

The dominant interaction type of HDTMA clay vs. benzene was the HDTMA cation vs. benzene, instead of clay vs. benzene, which can be the dominant type for adsorptive clays (e.g., TMA clay). Because the aliphatic chain has relatively larger mobility than the nitrogen head group, benzene molecules would have mobility with the chain even if they are sorbed via short-range force.

Interlayer diffusion coefficients calculated from MSD

The mean-squared displacement (MSD) of benzene molecules during NVT time integration in all simulated systems were recorded and their interlayer diffusion coefficient was calculated based on Einstein relation:

$$D_{\text{interlayer}} = \frac{dMSD}{4dt} \quad \text{..... (5.7)}$$

For each simulated system, the apparent interlayer diffusion coefficients of interested species were obtained from 5~5000ps of simulation time, the mean value was calculated as the slop of MSD vs. time at 5, 6, 7..10ps; 20, 30.. 100ps; 200, 300.. 1000ps; 2000, 3000…5000ps. The standard deviation is too small to be shown in log-log scale. The diffusion coefficients plotted versus time were shown in Figure 5.4. (standard deviation too small to be shown on log-log scale).

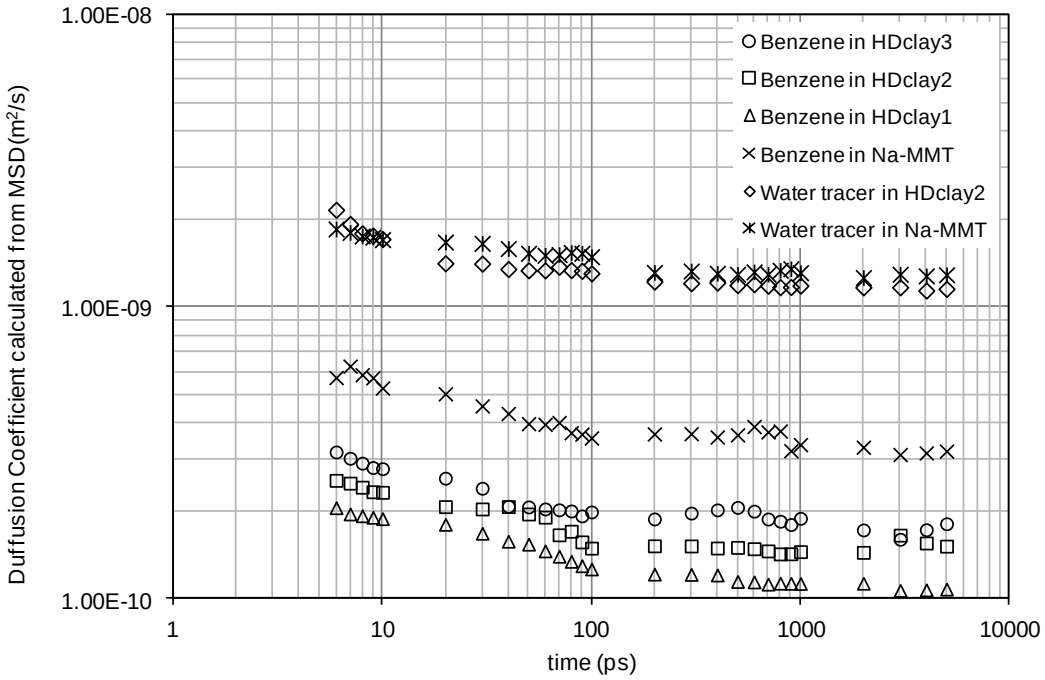

Figure 5-4. MD estimated diffusion coefficient of water tracer in Na-MMT; HDTMA clay2 and benzene in: Na-MMT; HDTMA clay1; HDTMA clay2; HDTMA clay3.

The calculated diffusion coefficient for all species clearly showed "hindered diffusion" stage before 100ps of simulation time, as demonstrated in previous study (Bourg and Sposito, 2010). Consequently the calculated diffusion coefficients after 100ps were considered to be true values for the following analysis. The calculated diffusion coefficients indicated that the diffusion rate in interlayer nanopores is a function of both solute and interlayer pore characteristic. It can be noticed that water tracer diffuses much faster than benzene in both Na-MMT and HDTMA clays but slower than in bulk water, while benzene also diffuses much slower than in aqueous solution. The slow motion of water tracer or benzene in interlayer nanopore is caused by constrain imposed by the interlayer pores with limited scale length. For non-interactive species, when Knudsen diffusion dominated in interlayer pores, their interlayer diffusion coefficients can be

described directly by a single "constrictivity factor" times diffusion coefficients in aqueous solution, as suggested by Bourg and Sposito (2010):

$$D_{\text{interlayer}} = D_{\text{aq}}\delta \quad \text{..... (5.8)}$$

As interlayer pore size increased, solute molecules would have increased apparent diffusion rate, corresponds to an increased volume for motion. This is also valid for benzene diffusion in HDTMA clays: the HDTMA loading on the clay surface is constant, while interlayer spacing increased, the diffusion rate of benzene also increased. The first reason for higher diffusion rate of water tracer than benzene was its relatively smaller molecule size. Another reason for faster diffusion of water tracer was that benzene molecules were subjected to the interaction with the intercalated HDTMA cations. The evidence is benzene diffuses faster in Na-MMT than in HDTMA clay2, when their interlayer pores have similar size. For benzene diffusion in HDTMA clays, however, even if the size effect of water and benzene were taken into account (in "constrictivity" part), the diffusion of benzene were still inherently lower than that calculated from equation (5.8). It is important to note that equation (5.8) is only valid for non-interacting species. For benzene diffusion in HDTMA clay pores, the sorption of a fraction of benzene to the HDTMA phases would cause lower average movement of benzene, which was reflected in equation (5.4): before sorption-diffusion equilibrium was completed within macro and interlayer pores, the diffusion pattern has been proved to be transient. This effect will be discussed in the following part.

Confined movement of benzene caused by sorption and diffusion dynamics

Comparison of the simulations of benzene molecules diffusing in pure montmorillonite with benzene molecules diffusing in HDTMA clay clearly showed significant differences. At the nanoscale, the intercalation of the HDTMA cation increased the hydrophobic carbon content in interlayer; consequently, a fraction of benzene molecules had the tendency to be sorbed onto the aliphatic chains via short-range forces, which resulted in a lower average diffusion rate for all benzene molecules. At the macro-scale, the increased organic surfactant loading into the clay interlayer often results in a higher uptake capacity of organic compounds (Redding et al., 2002), and a larger retardation factor for partitioning clays. In this study for the three simulated HDTMA clays, the simulations with lower quantity of water also demonstrated higher packing density of aliphatic carbons in the interlayer, which resulted in even slower motion of benzene molecules.

Because of preferential interaction with aliphatic carbon chains of HDTMA cations, benzene diffusion in the HDTMA clay interlayer is not only subjected to the influence of the clay surface but also to the HDTMA cations, with the latter becoming even more significant at intermediate to large amounts of cation loading. In addition to the possible interaction with the organic compound, the existence of HDTMA cations in MMT interlayer may have other impacts on their diffusive movement. The increased packing density of HDTMA cations in the HDTMA clay interlayer also increased the tortuosity of the pore space and decreased the mean width of available free-path, which was reflected in a decreased rate of diffusion of benzene molecules from HDTMA clay3 to HDTMA clay1 (Figure 5.4). When the amount of interlayer water increased, HDTMA

cations behaved more like “pillars” than “compartment walls” (Figure 5.5). For constant loading of HDTMA cations, because such influence on effective diffusion path was insignificant compared with sorption, its impact on the diffusivity was combined with influence of the pore wall and included in the “constrictivity” term. Consequently, HDTMA clays with same amount of organic loading were assumed to have the same “sorption factor” R, which accounted for the fraction of interlayer sorbates that became relatively immobile. To separate the R factor from other factors, HDTMA clay2 and Na-MMT were compared on the basis of their similar pore sizes. The normalized benzene diffusion coefficient for the Na-MMT interlayer to the HDTMA clay2 interlayer yielded (Figure 5.6):

$$R_t = \frac{D_{\text{Na-MMT},t}}{D_{\text{HDclay2},t}} \quad \text{..... (5.9)}$$

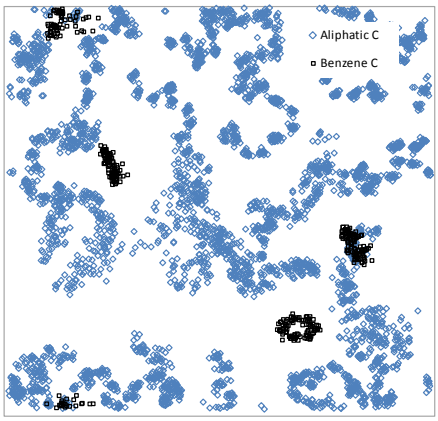

(a)

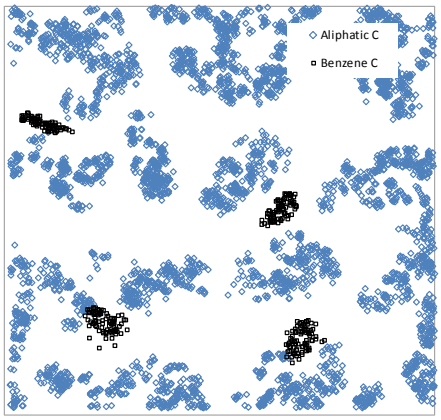

(b)

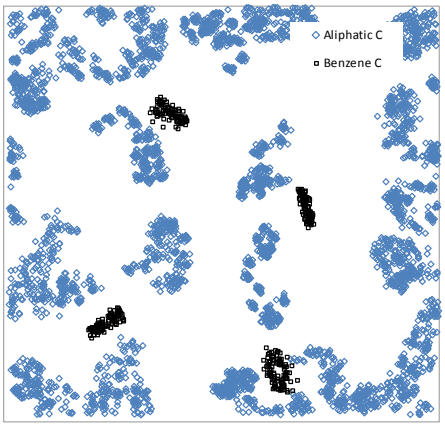

(c)

Figure 5-5. Top view of interlayer species density cloud (stage 2, 1~1.05ns): blue = aliphatic carbon; black = benzene carbon.

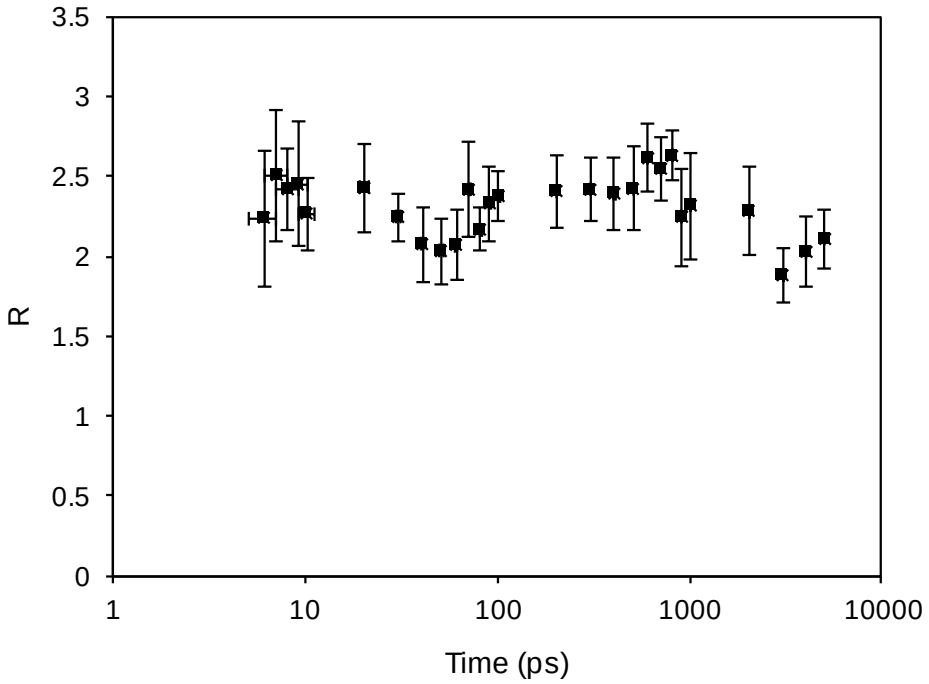

Figure 5-6. "Sorption factor" R plotted versus simulation time

Note that R is approximately 2~2.5, which suggested that a fraction of benzene molecules had very low mobility and the averaged mobility of all benzene molecules was decreased, when compared with the benzene molecules in Na-MMT. The remaining fraction of benzene molecules that desorbed or dissolved in interlayer water had faster rates of diffusion.

"Constrictivity" imposed by interlayer pores

Previous studies showed that interlayer water and cations exhibit decreased apparent diffusion coefficient in nanopores filled with liquid, compared with that in bulk aqueous solution. This restricted movement of sorbate results from increased viscosity of the solvent and will be more pronounced as the pore size is small enough compared with mean free path of the sorbate. Although the adsorbed HDTMA cations also occupy

considerable interlayer pore space and they also impose drag force on benzene, they might contribute to the restricted movement of benzene, but it will be considered as pure sorption which was included in the R term. Consequently, in this study for water tracer and benzene diffusion in clay interlayer nanopore, it was assumed that the constrictivity only corresponds to the proximity of the 2:1 clay surface. The "constricitivty factor" δ will be herein referred to the constrained imposed by the mineral phase only:

$$D_{\text{interlayer}} = \frac{D_{\text{aq}}\delta}{R} \quad \text{..... (5.10)}$$

Where R=1 for non-interacting species: e.g. water tracer.

Empirical estimate of constrictivity factor for both steady state and transient state diffusion have been proposed by Beck and Schultz (1970) (equ.5.11); Satterfield and Colton (1973) (equ.5.12):

$$\delta = (1-\lambda_p)^4 \quad \text{..... (5.11)}$$

$$\delta = \exp(-4.6\lambda_p) \quad \text{..... (5.12)}$$

Where: $\lambda_p = \dfrac{\text{molecule diameter}}{\text{pore diameter}} < 1$.

In this study movement of water tracer and benzene molecules in interlayer nanopore were recorded, and the constrictivitiy of water tracer was calculated by normalizing $D_{\text{interlayer,water}}$ (t >100ps) with $D_{\text{aq,water}}$; while the constrictivitiy for benzene was calculated by normalizing $D_{\text{interlayer,benzene}}$ (t >100ps) with $R_{\text{avg}}D_{\text{aq,benzene}}$ (Figure 5.7).

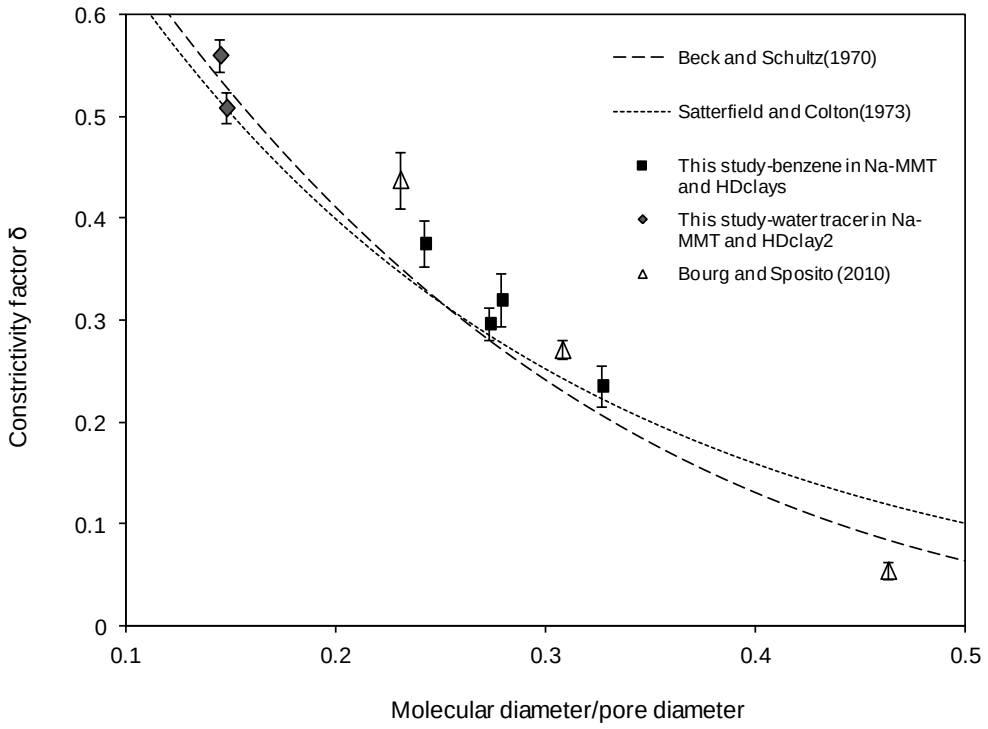

Figure 5-7. Constrictivity factor for solutes vs. ratio of solutes diameter to interlayer pore diameter.

Because HDTMA clay had larger interlayer spacing as the number of interlayer water molecules increased, there was less constriction imposed on the diffusion of the interlayer species, including both water and benzene. HDTMA clay, with very small interlayer spacing (e.g., HDTMA clay1), had very limited effective interlayer pore space for intermolecular collision, and subsequently demonstrated the strongest constriction on the mobility of benzene molecules. This demonstrated that increasing the water molecules in the interlayer of organoclays increased the rate of diffusion; however, the diffusion rate of benzene through organoclay would be slowed by decreasing the interlayer pore size of the synthesized clays or by increasing the size of the diffusing molecular species.

Bulk diffusion coefficient estimated from MD simulations

The bulk diffusion coefficient of each species of interest in HDTMA clay was calculated based on Equation (6). It is important to note that the equation is only applicable to organoclays with concentrated solids, as opposed to slurries or low solids content suspensions. The molar fraction in the macropore ($\alpha_{macropore}$) was used as the only variable, and for water tracers it was calculated as the percentage of water molecules in the macropore. The bulk diffusion coefficient in Figure 5.8 was calculated based on an assumed geometric factor (G) equal to 4, which was equivalent to a bulk totuosity factor of 0.25. G values range from 2.4~5.6, and corresponded to totuosity factors of 0.18~0.42, typical for geomaterials. It is important to note that benzene molecules had much higher concentration in the sorbent than in aqueous phase; consequently, their concentration in macropores was much smaller than that in interlayer pores. However, because the water molecules in the interlayer pores was insignificant compared that in the macorpores, $\alpha_{macropore,water}$ was close to 1. Overall, $\alpha_{macropore,benzene} << \alpha_{macropore,water}$. This suggested that for transient diffusion like benzene through HDTMA clays, the bulk diffusion rate was controlled by interlayer diffusion ($\alpha_{macropore,benzene} \sim 0$).

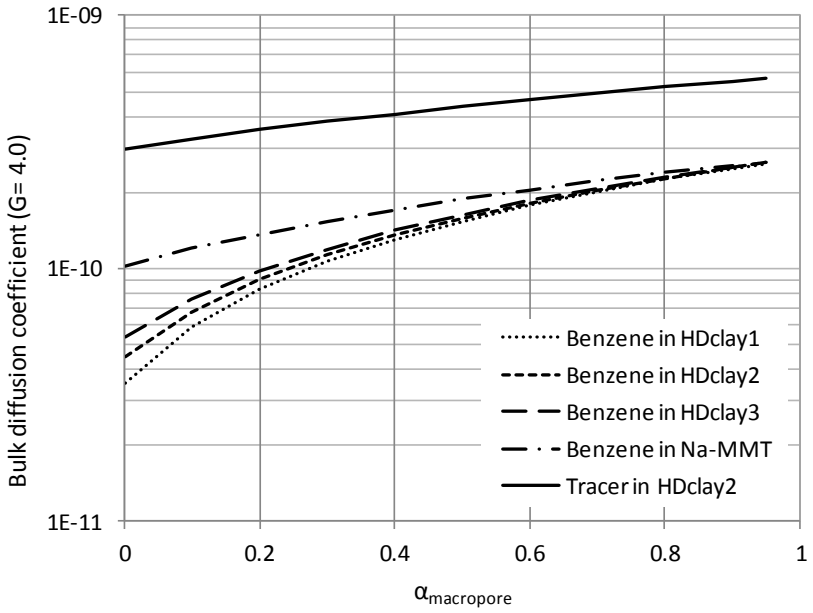

Figure 5-8. Estimates of bulk diffusion coefficients based on simulation.

The benchmark to examine the simulation results was the water tracer diffusion rate, which was compared with water tracer diffusion in an HDTMA clay amended GCL (Lorenzetti et al., 2005). The effective diffusion coefficient for water tracer in HDTMA clay amended GCLs as determined by diffusion testing ranged from $3.6\sim4.0\times10^{-10}$ m^2/s, which agrees well with the bulk value extrapolated from this MD simulation result. Furthermore, because the molar fraction of tracer could be dominant in the macropores of both MMT and HDTMA modified MMT, the calculated bulk apparent diffusion coefficient for water tracers should demonstrate no significant difference, as it was controlled by the transport in macropores. This explained the fairly consistent values of measured effective diffusion coefficients for water tracer diffusion in GCLs with varying organobentonite amendment as observed by Lorenzetti et al. (2005). Additionally, the bulk diffusion rate of benzene in Na-MMT estimated from this study was 10-10 m2/s, which agreed with previous observations of benzene diffusion through geosynthetic clay

liners (Lake and Rowe, 2004). The trend of slowed diffusion of interacting species in organophilic clays was also consistent with organic sorbate diffusion in organic-rich clays (Grathwohl, 1998).

In summary, this study simulated benzene sorption and diffusion in the interlayer of Na-MMT and HDTMA clays that were intercalated with different quantities of interlayer water. It was shown that the factors that controlled the diffusion of organic compounds in the interlayer of the clays included the constrictivity factor, which accounted for the Knudsen diffusion, and the sorption factor that accounted for the immobile fraction of sorbate that was taken up by the intercalated surfactant. A modified model that averaged the diffusion in the clay macropore and the interlayer pore was proposed, and it can be used for the estimate of bulk diffusion behavior of different species.

CHAPTER 6
MOLECULAR DYNAMICS SIMULATIONS OF SURFACE ELECTROKINETICS OF HDTMA COATED CLAYS

Introduction

The immersion of a charged soil particle in an aqueous electrolyte solution leads to the accumulation of oppositely charged ions and formation of a structures water/ion formation surrounding the particle that is known as the double layer (Sridharan and Jayadeva, 1982; Kjellander et al., 1988; McBride, 1997; Chang et al., 1998). The double layers are composed of the region known as the Stern layer, which consists of counterions that are tightly sorbed to the particle surface, and the region known as the diffuse layer, which consists of counterions sorbed by Coulombic forces, and can be represented using the electrical double layer (EDL) model (Gupta et al., 2007).

The Stern layer, adjacent to the negatively charged solid surface, can be divided into two regions known as the “inner Helmholtz” layer and “outer Helmholtz” layer. The inner Helmholtz plane represents the first layer near the solid surface where cations are attracted to the solid surface as bare cations without hydration shells (assuming a negative particle layer charge), while the outer Helmholtz plane represents the volume where cations in the fully hydrated state are sorbed to the solid surface. The diffuse layer lies outside the Helmholtz layer (moving away from the particle surface),where hydrated ions or other species have higher mobility but are still under the influence of surface long-range electric forces and thermal motion, the ionic concentration is higher than that of the bulk (Figure 6-1).

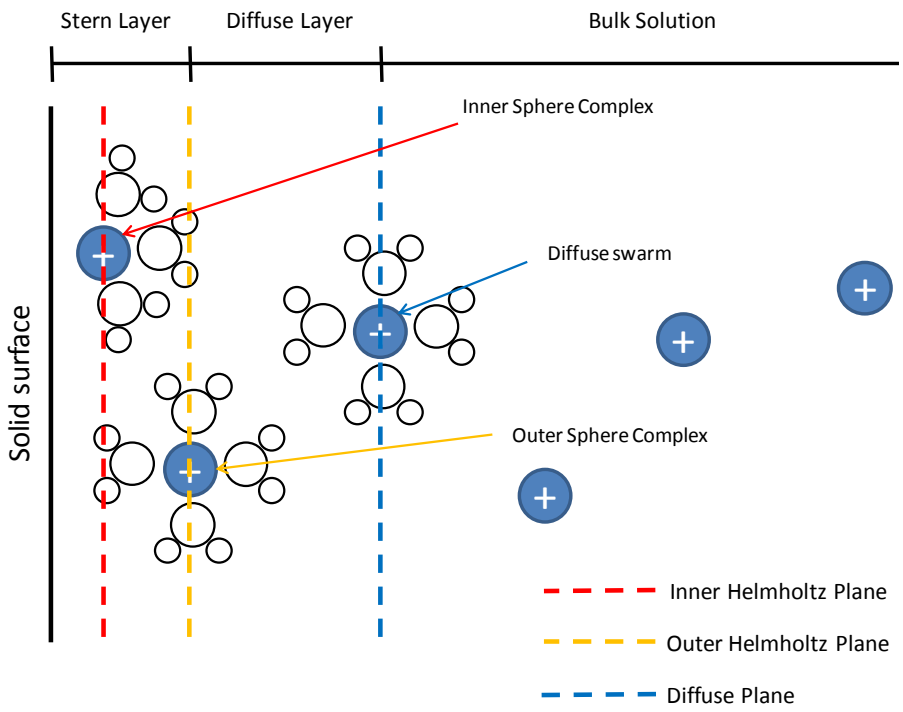

Figure 6-1. Sorbed and diffusive species near a charged surface.

Montmorillonite particles, which can be colloidal, tend to flocculate or disperse at a rate that depends on the interaparticle net force in a suspension or slurry (Gofenberg et al., 1979; Gerischer and Sanderson, 1981a; Gerischer and Sanderson, 1981b; Miyanishi, 1995). Interparticle net forces are a function of the layer charge of the clay particles, distance between particles, ionic strength, and pH value of the solution. Given the same fluid conditions, interparticle force is controlled by the effective surface charge of the particles, which is often correlated with surface electrical potentials of the particles. Defined as the electrical potential at the slipping plane, the zeta potential is a good indicator of the surface charge of the colloidal particle and repulsion between particles, as well as a good indicator of the stability of the suspension (Gungor and Tulun, 1994; Zarzycki et al., 2006).

While the electrical double layer (EDL) model has been proven to work well for pure montmorillonite particles, the surface electrokinetics of an organoclay, a montmorillonite particle that has had its interlayer inorganic cations exchanged for organic cations, will exhibit significantly different behavior. For the clay surface interacting with a long chain surfactant (e.g., $HDTMA^+$), the organic cation entity will not form hydration shells. Instead, the hydrophilic heads, which carry the positive charge of the cations, will be attracted to the montmorillonite surface oxygen plane, while the cation's hydrophobic tails (when the intercalated HDTMA was at lower density) will be pushed away from surface due to the preferential hydration of mineral surface. Consequently, the surface electrokinetic potential of the clay will be altered, as suggested by previous experimental studies (Bate and Burns, 2010). It has been demonstrated that the measured zeta potential can be decreased by incorporating more organic carbon on the clay surface, with this effect being more pronounced for organic cations with a single long carbon chain.

This study investigated the impact of sorption of organic carbon to the surface of montmorillonite particles on the electrokinetic behavior of the clay. The sorbed organic phase was modeled using the quaternary ammonium cation, $HDTMA^+$, and the resulting structure of the double layer, surface charge, and electrical potential near the surface in presence of water, inorganic cations, and anions was modeled. The density of water molecules, cations, and anions along the z direction (normal to the clay surface) were quantified and used as evidence to indicate the location of the interfacial boundaries within the double layer. Water alignment was also used to indicate differences between

the interfacial regions. The effective surface charge at each plane was calculated, and used as the basis for the calculation of electrical potential at each plane.

Simulation details

Molecular dynamics simulations were performed for a pore space between two half montmorillonite particles (approximately 80 Å wide); simulations were performed in LAMMPS (Plimpton, 1995). The modeled system consisted of an interlayer between one unmodified montmorillonite particle and one montmorillonite particle with $HDTMA^+$ cations sorbed to the surface, with diffuse species present in the interlayer. Five nanoseconds of constant volume and constant energy (NVE) time integration were performed on the system, which consisted of approximately 10,000 atoms. The simulation cell was periodic in 3 directions, and each half particle was composed of 14 duplicates of unit cells ($0.643Na\ (Mg_{0.571}Al_{3.429})(Al_{0.071}Si_{7.929})O_{20}(OH)_4$) with 37.68Å×35.96 Å in xy plane. The negative structural charge of montmorillonite resulted from x isomorphic substitutions, following Loewenstein's rule (Loewenstein, 1954). The pore between the two half clay platelets was filled with approximately 2900 water molecules, 24 sodium cations and 15 chloride anions, such that the number of different species was large enough to represent bulk solution, adsorbed, and diffuse layer. The bulk concentration of sodium and chloride was approximately 0.1 mol/L.

Prior to the NVT integration, cell z dimensions were determined by equilibrating the system for 1000 ps at 298 K and 1 atm (Figure 6-2a), with initial zero velocity for all atoms/ions, then 5000 ps of NVE integration were performed (Figure 6-2b). Average z cell dimensions after NPT and NVE equilibration were 79.89 Å and 80.48 Å, respectively. Total energy conservation during simulations was monitored. Long-range

Coulomb interactions were treated by Ewald summation with the precision of the k-space vector at 1.0×10^{-4}. In this study, the basis for the simulation was the combined force field of ClayFF, CVFF, SPC water model, and solute water potential for sodium and chloride (Smith and Dang, 1994), which has been demonstrated to work well for the mineral-liquid interface, mineral-organic cation, bulk liquid , and inorganic cation solutions.

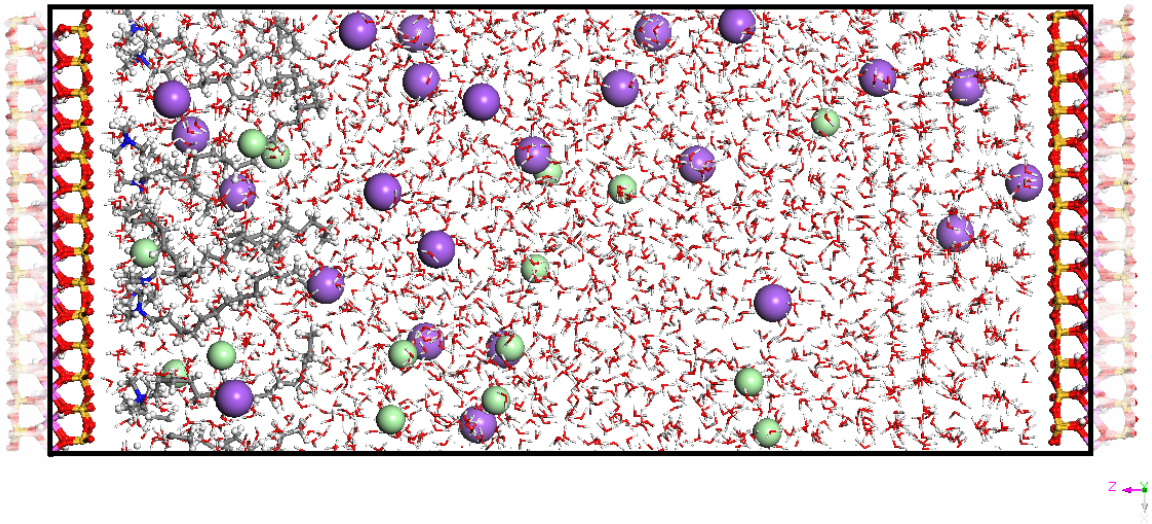

(a)

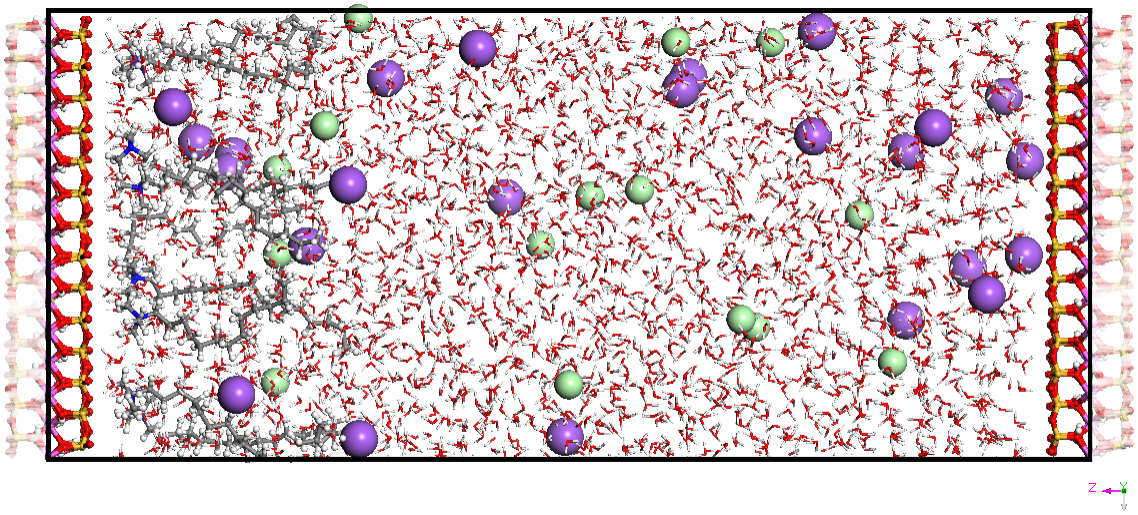

(b)

Figure 6-2. (a) Simulated system after NPT integration; (b) Simulated system after NVE integration. System include: MMT surface, HDTMA+ coated MMT surface, water, sodium and chloride ions. Note: for all species, C = gray, N = blue, H = white, O = red, Si = yellow, Na = purple, Al = pink, Mg = green, Cl = light green.

Results & Conclusions

Counter-ion adsorption

Simulation results showed that in the adsorbed layers near the two surfaces (clay surface to the outer Helmholtz plane), sodium cations sorbed to the clay surface as both inner-sphere and outer-sphere surface complexes; however, the chloride anion, only formed outer-sphere surface complexes. The distances from the inner Helmholtz plane of sodium to both surfaces were fairly consistent, in the range of 2.4-2.5Å and the outer Helmholtz plane of both sodium and chloride were at about 4.4-4.6 Å. This suggested that the location of the inner Helmholtz and the outer Helmholtz plane were independent of the electrolyte type for the simulated system (except chloride did not appear in the inner Helmholtz plane) (Figure 6-3).

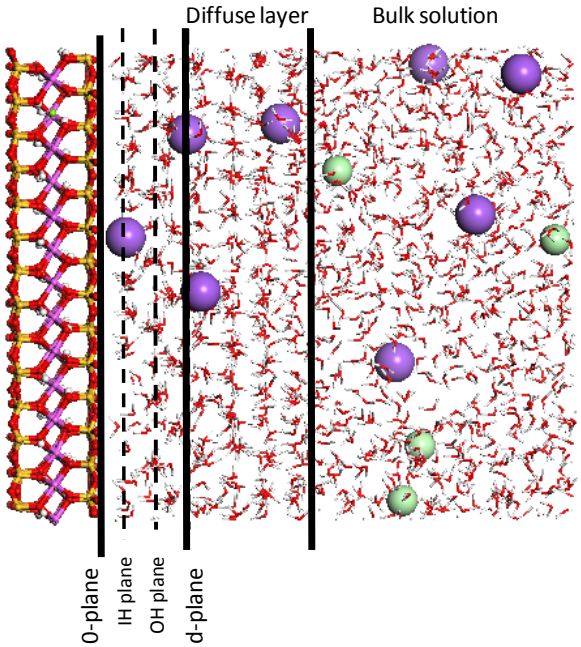

Figure 6-3. Inner Helmholtz, outer Helmholtz and diffusive plane locations near pure MMT surface.

The distance between the clay surface and the center of the nitrogen head group of the HDTMA cation was 4.3Å, which was significantly larger than the distance between the sodium cation and the clay surface. The increased distance was due to the larger size of the organic cation head group, as well as the fact that the head group also formed an inner-sphere complex via the direct interaction between the clay surface and the methyl group in the nitrogen head. It is important to note that although the center of the HDTMA cation was further away from the clay surface due to its larger size, when compared with the sodium cation, there were no observed outer sphere complex formed by HDTMA cations. HDTMA cations only formed inner-sphere complexes, which suggested that the HDTMA cations were more tightly bonded to the surface within the adsorbed layer. In contrast, part of the sodium cations were located in the diffuse layer and behaved more like a diffuse swarm. The distance to the interfacial planes of the inner sphere complexes, outer sphere complexes, and diffuse swarm of all species are given in Table 6-1.

Table 6-1. Inner Helmholtz, Outer Helmholtz and Diffusive Plane Locations Near Two Surfaces

Distance to clay surface (Å)			
Na-MMT surface		HD-MMT surface	
water O		water	
1st layer	2.7	1st peak	2.7
2nd layer	5.9	2nd peak	5.8
3rd layer	8.4	3rd peak	8.2
Na^+		Na^+	
IHP	2.4	IHP	2.5
OHP	4.5	OHP	4.5
DS	6.5	DS	6.7
Cl^-		Cl^-	
IHP	N/A	IHP	N/A
OHP	4.6	OHP	4.4
DS	9.3	DS	7.5
		$HDTMA^+$	
		IHP	4.3
		OHP	N/A
		DS	N/A

Species density profile

The density profile of oxygen (water), sodium, chloride, and nitrogen (HDTMA) were recorded every 0.1ns over 10 ns of NVE simulation time. In the space between the two clay surfaces, the density of each type of atom or ion X_i was quantified as its frequency histogram along the Z direction, normal to the clay basal surface:

$$N(X_i, z) = n(z - \frac{\delta}{2}, z + \frac{\delta}{2})$$

Where z is the coordinate of the atom along Z direction; n is the count of atom type X_i; δ = 0.2 Å is the interval of bin array.

The density of oxygen (water), sodium, and chloride showed distinct differences between the bulk water and water in adsorbed and diffuse layers (Figure 6-4). While the density in the bulk solution for the three species was fairly consistent, the density varied significantly in the layers near the clay surfaces. The peaks in the sodium density profile at approximately 2.4 Å and 4.5 Å near the clay surface confirmed that inner and outer sphere complexes formed during the simulation, with a gradual decrease in density observed in the diffuse layer until reaching the density of the bulk solution. The chloride anions were primarily observed in the outer Helmholtz plane and diffusive layers, due to the repulsion imposed by the negative surface charge of the clay particles. Consequently, the quantity of chloride anions near the sodium montmorillonite surface were lower than the quantity of sodium cations in the adsorbed and diffuse layers, but slightly higher in concentration with respect to the bulk solution. The higher concentration of chloride near the HDTMA clay surface resulted from the presence of the tightly sorbed HDTMA cation on the montmorillonite surface (indicated by the peaks of nitrogen in the range of 3.8~4.2 Å from the surface).

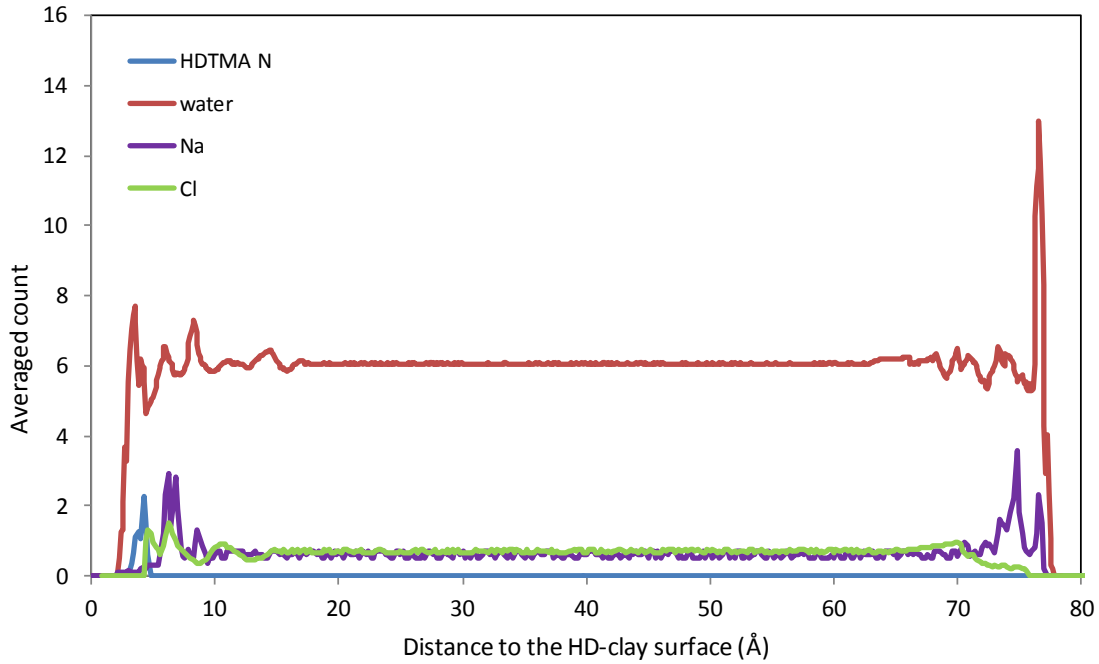

Figure 6-4. Averaged species density profile along z-direction (perpendicular to the clay basal surface).

The water density profile was similar to the profile observed for the sodium and chloride ions. The layering of water molecules was significant at the interface of both particles, while their density essentially remained constant in the bulk solution. The sharp peak of water near the sodium montmorillonite surface was due to the presence of the first layer of water that hydrated mineral surface, with the alternating layers of water as distance away from the surface increased caused by the influence of long-range forces imposed by the clay and ion hydration in the adsorbed and diffuse layers. However, the peak of the first water layer near the HDTMA clay surface was lower when compared to the sodium montmorillonite surface because the clay surface was partially occupied by methyl hydrogen, instead of water.

Based on the density profiles, the boundaries of the different layers (adsorbed, diffuse, bulk) were estimated. Interfaces were determined using the domain which had a

constant density of water interpreted as the bulk solution, while the layered arrangement of water was taken as the adsorbed layer and the diffuse layer. The first layer of water (first peak) adjacent to the mineral surface coincided with the inner Helmholtz plane.

Effective surface charge

The electrical neutrality of the overall system was maintained by summing the clay structural charge (σ_0 = -0.322e per unit cell in our simulations) with the charge carried by the cations and anions in the system:

$$\sigma_0 + q_{cation} + q_{anion} = 0$$

However, the presence on an adsorbed cation (or anion) near the clay surface acted to partially neutralize the surface charge, resulting in an "apparent" surface charge density to the diffusing species. The "effective" surface charge of the clay, after considering the adsorbed ions, equals the sum over all ions (cations or anions) of the magnitude of the valence Z_i times the specific surface excess relative to water $n_i^{(w)}$ (Sposito, 1984):

$$\sigma_{surf} = \sigma_0 + \sum_i Z_i n_i^{(w)} = \sigma_0 + \sum_i Z_i (n_i - \frac{n_w x_i}{x_w})$$

where:

n_i and n_w are the numbers of molecules of solute i and water per unit cell of clay in the adsorbed region (z < 20 A), and x_i and x_w are the mole fractions of i and water in the bulk solution (z > 20 A) (Table 6-2).

Table 6-2. Estimated "Effective" Surface Charge Near Two Surfaces

		HD-MMT Surface				Na-MMT Surface			
		Na^+	Cl^-	$HDTMA^+$	water	Na^+	Cl^-	$HDTMA^+$	water
χ_i		0.0078	0.0056	0.0000	0.9865	0.0078	0.0056	0.0000	0.9865
n_i	(count/unit cell)	0.2857	0.4286	0.6429	34.7857	0.4286	0.2143	0.0000	40.7143
$n^{(w)}_i$	(count/unit cell)	0.0090	0.2309	0.6429	N/A	0.1047	-0.0170	0.0000	N/A
σ_{surf}	(e/unit cell)	0.0994				-0.1997			

It is clear that adsorbed ions have a significant impact on the effective or "apparent" surface charge of the simulated clay. Using the same clay framework revealed that the montmorillonite surface coated with adsorbed HDTMA+ cations clearly showed a decreased number of co-adsorbed sodium cations but increased chloride anions when compared with that of clay without sorbed organic cations. When HDTMA cations sorbed directly as inner-sphere cations, the clay's structural charge was more effectively neutralized, and resulted in an almost positively charged surface, which is consistent with previous experimental results (Bate and Burns, 2010). A relatively small fraction of inorganic sodium cations were sorbed as diffuse swarm species, and the screening effect on the clay surface charge was not as significant as was observed for HDTMA cations. Consequently, the effective surface charge of the sodium montmorillonite clay surface had a value somewhat lower than the structural charge of the clay.

Because the density of adsorbed and diffusive ions is a function of distance from the clay surface, the local density of ions affects the "apparent" charge density at a given distance. A hypothetical probe can move perpendicular to the surface to yield the measured "screening function" of surface charge (Bourg and Sposito, 2011):

$$\Gamma(d) = \sigma_0 + \int_0^d \sum_{i=HD^+,Na^+,Cl^-} Z_i \rho_i(z) dz$$

where $\rho_i(z)$ is the local density of species i. Taking the average density of species into account, the calculated $\Gamma(d)$ for the sodium montmorillonite and the HDTMA montmorillonite demonstrated that the interfacial boundary is sharper and more pronounced in the case of HDTMA montmorillonite when compared to sodium montmorillonite (Figure 6-5):

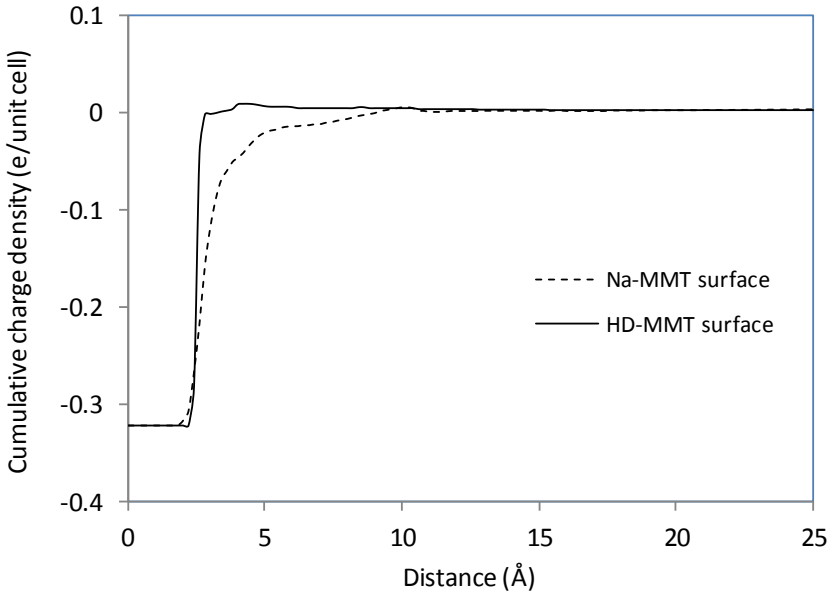

Figure 6-5. "Effective" surface charge as a function of distance from two clay surfaces.

Water alignment and plane boundaries

In addition to the concentration of ions, the alignment of water molecules between two particle surfaces was studied to help identify the boundaries of the planes within the diffuse double layer. One trajectory during the final one nanosecond was selected for study, and the orientation of the water molecules was recorded as vectors pointing at the direction of the angular bisectors of the H-O-H angles (Figure 6-6).

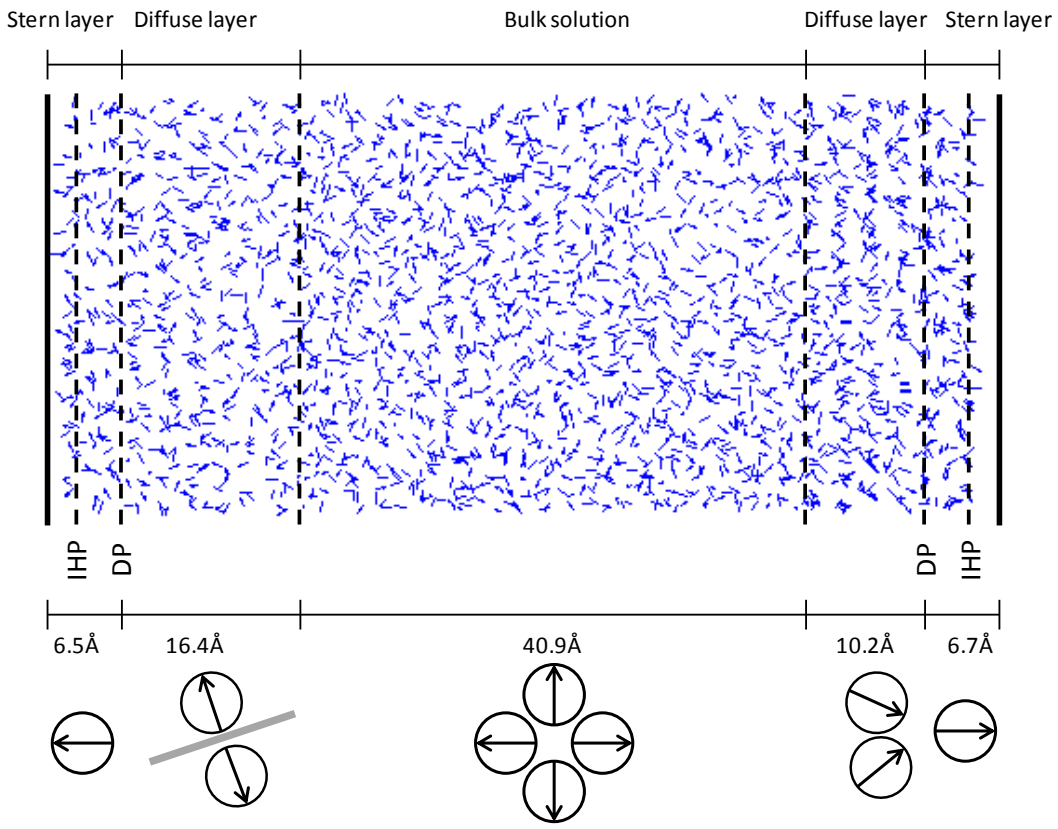

Figure 6-6. Water alignment and interfacial plane location near both surfaces. The vector indicates the direction of angular bisector of each water molecular angle.

The patterns of water alignment varied as a function of distance from the clay surface. At the clay surface, the force on water in the adsorbed layer resulted in the orientation of the water molecules by attracting the water hydrogen to the surface and pushing the water oxygen away from the surface. In the diffuse layer, the hydrogen of the water molecules was attracted to the clay surface, but the water molecules were also subjected to the influence of ions nearby; consequently, the alignment vectors were likely to be tilted, but still aligned to the mineral surface. In the case where the organic cations were also present in the diffuse layer, some of the water molecules were likely to be parallel to the clay surface because the hydrophobic tails of the organic cations were oriented perpendicular to the surface and they pushed the adjacent water molecules away

from the surface. In the bulk water, the water molecules were randomly oriented, which was consistent with the assumption that the influence of the mineral in the bulk solution was minimal (Figure 6-6).

If the two boundaries of the clay mineral planes are taken as capacitors using the proposed location of boundaries in the interparticle domain, the electrical potential can be estimated according to the following:

$$\psi_{DP} - \psi_{OHP} = \sigma_{DP} / C_2$$
$$\psi_{OHP} - \psi_{IHP} = -\sigma_{IHP} / C_1$$

where ψ_{DP}, ψ_{OHP}, ψ_{IHP} are the electrostatic potentials at the diffuse plane, outer Helmholtz plane, and inner Helmholtz plane, respectively, σ_{IHP} and σ_{DP} are the effective charge on the planes, and C_1 and C_2 are the capacitance of space between two planes, calculated as:

$$C_i = \varepsilon_i \varepsilon_0 / \Delta z_i$$

where ε_i is the dielectric constant of solution in each "capacitor", ε_0 is the permittivity of vacuum, and Δz_i is the distance between two planes.

Calculated potential was plotted as a function of distance from the surfaces (Figure 6-7). Similar to the observations for surface charge, the electrical potential was closer to zero near the surface of the HDTMA clay compared to the sodium montmorillonite in both the adsorbed and diffuse layers. Consequently, the resulting HDTMAclay would be more likely to flocculate and settle in suspension, when compared to sodium montmorillonite in similar fluid conditions.

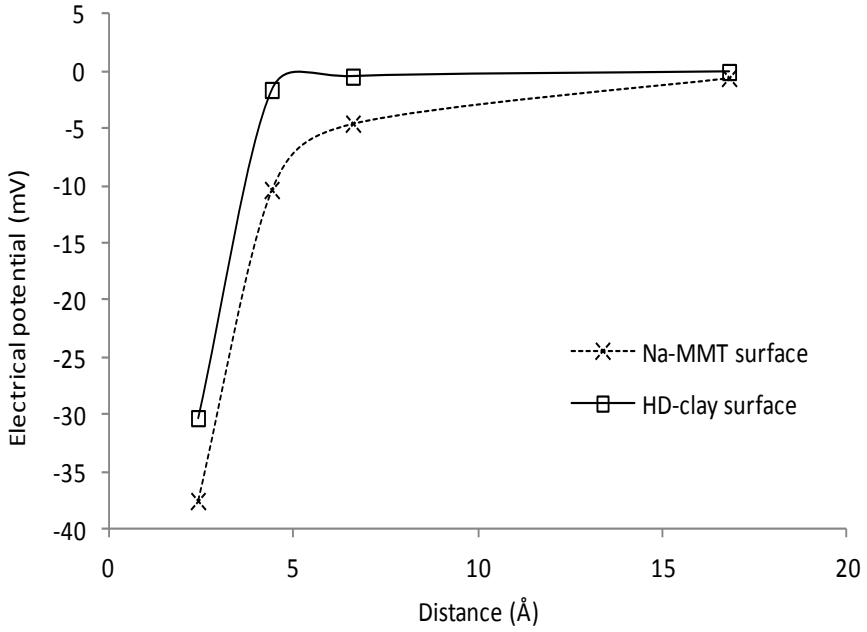

Figure 6-7. Calculated electrical potential near both surfaces.

Conclusions

The surface electrokinetics of both pure sodium montmorillonite and QAC coated montmorillonite was simulated in a system that contained water molecules, inorganic cations, and anions. Adjacent to both surfaces (sodium sorbed and HDTMA sorbed), an adsorbed layer and a diffuse layer formed, although the organic coating on the clay surface had significant impact on the surface electrokinetics of the clay. HDTMA surfactant effectively neutralize surface charge of montmorillonite, as indicated by less negative values of both "effective" surface charge and electrical potential near the mineral surface. The sorbed layers, including inner and outer Helmholtz layers, were positioned independent of the coating; however, the "thickness" of the diffuse layer varied due to the influence of the HDTMA cations.

CHAPTER 7
CONCLUSIONS

This work used molecular dynamics modeling to simulate the behavior of montmorillonite modified with an organic phase consisting of a series of single chain quaternary ammonium cations (QACs). Several geochemical processes in the organoclay interlayer and on the external surface were simulated, including organic cation arrangement, organic molecule sorption and diffusion in interlayer, and the surface electrokinetics of the organoclay and sodium montmorillonite clay particles. Simulated systems included 2:1 clay minerals, inorganic ions (sodium and chloride), organic cations (QACs), organic molecules (benzene), and water. The effect of increasing the length of carbon chain on the QAC molecule, as well as increasing the density of QAC molecules in the interlayer were studied and analyzed (Table 7-1).

Table 7-1. Summary of Simulated Organoclay Properties and Corresponding Mechanisms

Simulated properties	QAC type			Mechanism
	TMA	DTMA	HDTMA	
Surface coverage[a] (%)	~15	~62	~100	Carbon layer shifts from monolayer to bilayer, paraffin structure as surface coverage increased. Transition of different layers starts from the surface coverage of 100%
	~19	~80	~100	
	~32	~100	~100	
Basal spacing[b] (Å)	14.08	14.36	18.21	Carbon layer shifts from monolayer to bilayer, paraffin strcuture as organic loading increased. Increased basal spacing indicates more carbon layers: 13.0~ 15.0Å, monolayer; 17.7~ 19.8Å, bilayer; >22Å, trilayer or paraffin structure
	14.12	17.71	18.79	
	14.19	19.44	24.12	
Interaction with organic molecule	Surface adsorption	Both surface adsorption and partitioning	Partitioning	For adsorptive clay (e.g., TMA clay), dominant interaction is organic compound vs. clay surface; for organophilic clay (e.g., HDTMA clay), dominant interaction is organic compound vs. aliphatic chain
Organic molecule interlayer diffusion rate[c] (m^2/s)	N/A	N/A	$\sim 1.4 \times 10^{-10}$	Non-polar organic molecule has lower diffusion rate in HDTMA clay interlayer pore because of the interaction with the HDTMA cation; this diffusion rate can be slowed by increasing HDTMA loading or decreasing pore size
			$\sim 1.8 \times 10^{-10}$	
			$\sim 2.2 \times 10^{-10}$	
Surface electrokinetcs	N/A	N/A	surface charge and electrical potential almost zero	HDTMA cations bonded with surface as inner sphere complex, the surface indicated less "effective" charge and less negative electrical potential.

[a] Charge density for clay prototype: first row, 0.5e/unit cell; second row, 0.643e/unit cell; last row, 1.071e/unit cell.

[b] Charge density for clay prototype: first row, 0.5e/unit cell; second row, 0.643e/unit cell; last row, 1.071e/unit cell.

[c] Same amount of $HDTMA^+$ loading but different amount of interlayer water: first row, approximately 5 water molecules/unit cell; second row, 10 water/unit cell; last row, 15 water/unit cell

The interlayer arrangement of QAC was proven to depend on both the number and type of intercalated organic cations, or more simply, total organic carbon loading. Increased organic carbon loading in the QAC clay interlayer caused increased basal spacing and interlayer aliphatic carbon density. The increased basal spacing often corresponded to increased layering of carbon. The transition from monolayer of carbon coverage to multiple layers of carbon was controlled by the saturation of the clay basal plane coverage. A rough estimate of the number of organic carbon layers was performed by comparing the van der Waals area versus basal surface area per unit charge. Consequently, when the interlayer organic coating was known, the interlayer surfactant microstructure could be estimated.

The interlayer sorption of a model organic compound, benzene, to different types of organoclays showed two major types of sorption mechanism: adsorption, with the dominant sorption mechanism being interaction between the clay surface and the organic molecule. Adsorption was observed for organoclays synthesized from smaller QACs, and demonstrated that as the number of small QACs decreased, the synthesized clay had a higher number of surface sites available for sorption, resulting in increased sorption capacity as the cation density decreased. In contrast. partitioning behavior was observed for organoclays synthesized with long chain cations, with the dominant mechanism of interaction between the surfactant chain and the organic molecule. For these organophilic clays, as the organic carbon content increased, the organic carbon matrix formed from the cation chains had larger volume to dissolve organic molecules, resulting in increased sorption capacity.

For mass transport of the benzene molecules through HDTMA coated clay (or similar organophilic clays), the interlayer diffusion rate was slowed due to constraints of both the clay pore wall and the interaction with the interlayer organic carbon matrix. When diffusion dominated the overall mass transport of organic molecules, the bulk diffusion rate of organic molecules in organoclays could be controlled by the interlayer diffusion rate. Simulation results demonstrated that either decreased pore space of QAC clay or increased density of QAC loading (e.g., base clay with higher charge density or longer chain QAC) may be favorable in terms of slowing down the organic molecule diffusion.

Simulations of the surface electrokinetics of suspended HDTMA clay particles demonstrated that HDTMA cations can neutralize clay surface charge more effectively than inorganic cations such as sodium, as indicated by both increased "effective" surface charge and surface electrical potential. Because HDTMA cations were more likely to form inner-sphere complexes near the surface, the head groups that carried counter-charge stayed in adsorbed layer, instead of diffuse layer, resulting in more neutralization of the surface charge. The organic coating also had an impact on the thickness of the diffuse layer, the distribution of inorganic anions, and on the alignment of water molecules.

APPENDIX

 # Input file

```
# uptake of benzene by HDTMAclay

dimension       3
units          real
boundary        p  p  p


atom_style full

# LJ/coul potentials

read_data  data.HDTMAbenzene

pair_style lj/cut/coul/long 9.5
pair_coeff 1     1     1.5540E-01 3.166      9.5
pair_coeff 2     2     1.8405E-06 3.3020     9.5
pair_coeff 3     3     1.3298E-06 4.2712     9.5
pair_coeff 4     4     0.0000E+00 3.166       9.5
pair_coeff 5     5     0.1554     3.1655     9.5
pair_coeff 6     6     9.0298E-07 5.2643     9.5
pair_coeff 7     7     0.1554     3.1655     9.5
pair_coeff 8     8     0.1554     3.1655     9.5
pair_coeff 9    9    0.036      2.4651     9.5
pair_coeff 10   10    0.1478     3.6170     9.5
pair_coeff 11   11    0.1478     3.6170    9.5
pair_coeff 12   12    0.1478     3.6170     9.5
pair_coeff 13   13    0.1668    3.5000    9.5
pair_coeff 14    14    0.038      2.4500     9.5
pair_coeff 15    15    0.16       3.4745     9.5
pair_coeff 16    16    1.5540E-01 3.166      9.5

pair_modify shift yes mix arithmetic



bond_style  hybrid  harmonic  morse
bond_coeff 1    harmonic 554.1349  1.000
bond_coeff 2     morse 108.6       1.171     1.105
bond_coeff 3     morse 88.00       1.915     1.526
bond_coeff 4     morse 72.00       2.290     1.460
#bond coeff 5   C-C (benzene)
bond_coeff 5   harmonic   480.00  1.34
#bond coeff 6   C-H (benzene)
bond_coeff 6   harmonic   363.42  1.08



angle_style  harmonic
angle_coeff      1    30.0  109.47
```

```
angle_coeff     2     44.4  110
angle_coeff     3     46.6  110.5
angle_coeff     4     50    109.5
angle_coeff     5     37    120
angle_coeff     6     51.5  109.5
angle_coeff     7     39.5  106.4


#angle coeff 8    H-O-H (H2O)
angle_coeff  8    45.77 109.47

#angle coeff 9    C-C-H  (benzene)
angle_coeff  9    37.0     120.0

#angle coeff 10    C-C-C  (benzene)
angle_coeff  10   90.0     120.0

dihedral_style  harmonic


dihedral_coeff  1   0.14225   1    3
dihedral_coeff  2   0.14225    1    3
dihedral_coeff  3   0.14225     1    3
dihedral_coeff  4   0.0000   1    3
dihedral_coeff  5   0.0000   1    3
dihedral_coeff  6   0.14225      1    3
dihedral_coeff  7   0.14225     1    3
dihedral_coeff  8    12.000     -1    2
dihedral_coeff  9    12.000     -1    2
dihedral_coeff  10   12.000     -1    2

improper_coeff  1     ....
...

kspace_style ewald 1.0e-4


neighbor 4.0 bin
neigh_modify every 1 delay 10 check yes page 100000

group mont    molecule 1 2
group HDTMA   molecule 3 4 5 6 7 8 9 10 11 12 13 14 15 16 17 18
19 20 21 22 23 24 25 26 27 28 29 30 31 32
group Benzene molecule 33 34 35 36

...


velocity        all   zero linear

timestep       1.0
thermo         100
```

```
minimize        0.0   1.0e-8  10000 1000000


fix             1 all npt 298.0 298.0 100.0 xyz 1.0 1.0 1000.0
dump            1 all xyz 1000 dump.nptxyz
dump            2 all atom 1000 dump.nptatom
run            500000


unfix           1

fix             2 all nvt 298.0 298.0 100.0 drag 0.2

...

run             5000000
dump           3 all xyz 100000 dump.nvtxyz
dump            4 all atom 10000 dump.nvtatom
run             1000000
```

 # Data file

```
# LAMMPS data file for Benzene- HDTMA

6056   atoms
3980   bonds
7748   angles
10452  dihedrals
10452  impropers

16    atom types
6      bond types
10      angle types
10    dihedral types
4    improper types

-0.265624 36.4155 xlo xhi
-0.153133 36.2413 ylo yhi
-48.8571 2.78224 zlo zhi

Masses

1 16
2 28
3 27
4 1
5 16
6 24
7 16
8 16
9 1
```

```
10 12
11 12
12 12
13 14
14 1
15 12
16 16


Atoms

1     1     3     1.575 0.24914    1.11594    -0.213716
2     1     2     2.1   0.978215   8.88872    2.30592
3     1     2     2.1   0.860866   2.72349    2.30425
…….
Bonds

1     1     10    4
2     1     21    15
3     1     32    26
4     1     43    37
5     1     54    48
......

Angles

1     1     22    10    4
2     1     44    32    26
3     1     375   43    37
4     1     66    54    48
5     1     397   65    59
......

Dihedrals

......

Impropers

......
```

REFERENCES

Allen, M. P. and D. J. Tildesley (1987). Computer simulation of liquids. Oxford, Clarendon Press.

Azam, S. S.; Hofer, T. S.; Randolf, B. R.; Rode, B. M. (2009). "Hydration of Sodium(I) and Potassium(I) Revisited: A Comparative QM/MM and QMCF MD Simulation Study of Weakly Hydrated Ions." Journal of Physical Chemistry A **113** (9): 1827-1834.

Barrer, R. M. (1989). "Shape-selective sorbents based on clay-minerals-a review " Clays and Clay Minerals **37**(5): 385-395.

Bartelt-Hunt, S. L., et al. (2003). "Nonionic organic solute sorption onto two organobentonites as a function of organic-carbon content." Journal of Colloid and Interface Science **266**(2): 251-258.

Bate, B. and S. E. Burns (2010). "Effect of total organic carbon content and structure on the electrokinetic behavior of organoclay suspensions." Journal of Colloid and Interface Science **343**(1): 58-64.

Beck, R. E. and J. S. Schultz (1970). "Hindered diffusion in microporous membranes with know pore geometry " Science **170**(3964): 1302-&.

Bedding, N. D., et al. (1982). "Organic contaminants in the aquatic environment. 1. Source and occurrence " Science of the Total Environment **25**(2): 143-167.

Berendsen, H. J. C., et al. (1981). Interaction models for water in relation to protein hydration. Riedel, Dordrecht, The Netherlands.

Bhattacharyya, K. G. and S. Sen Gupta (2006). "Kaolinite, montmorillonite, and their modified derivatives as adsorbents for removal of Cu(II) from aqueous solution." Separation and Purification Technology **50**(3): 388-397.

Bourg, I. C., et al. (2003). "Modeling diffusion and adsorption in compacted bentonite: a critical review." Journal of Contaminant Hydrology **61**(1-4): 293-302.

Bourg, I. C. and G. Sposito (2010). "Connecting the Molecular Scale to the Continuum Scale for Diffusion Processes in Smectite-Rich Porous Media." Environmental Science & Technology **44**(6): 2085-2091.

Boving, T. B. and P. Grathwohl (2001). "Tracer diffusion coefficients in sedimentary rocks: correlation to porosity and hydraulic conductivity." Journal of Contaminant Hydrology **53**(1-2): 85-100.

Boyd, S. A., et al. (1988). "Sorption characteristics of organic-compounds on hexadecyltrimethylammonium-smectite." Soil Science Society of America Journal **52**(3): 652-657.

Burns, S. E., et al. (2006). "Coupled mechanical and chemical behavior of bentonite engineered with a controlled organic phase." Journal of Geotechnical and Geoenvironmental Engineering **132**(11): 1404-1412.

Cases, J. M., et al. (1992). "Mechanism of adsorption and desorption of water-vapor by homoionic montmorillonite. 1. The sodium-exchanged form." Langmuir **8**(11): 2730-2739.

Celis, R., et al. (1997). "Sorption of thiazafluron by iron- and humic acid-coated montmorillonite." Journal of Environmental Quality **26**(2): 472-479.

Chang, F. R. C., et al. (1998). "Monte Carlo and molecular dynamics simulations of electrical double-layer structure in potassium-montmorillonite hydrates." Langmuir **14**(5): 1201-1207.

Chiou, C. T., et al. (1983). "Partition equilibria of non-ionic organic-compounds between soil organic-matter and water." Environmental Science & Technology **17**(4): 227-231.

Cummings, P. T. (2002). "Molecular modeling of nanoscale systems: Overview and applications in geochemistry." Abstracts of Papers of the American Chemical Society **223**: U615-U615.

Cygan, R. T. (2001). "Molecular modeling in mineralogy and geochemistry." Molecular Modeling Theory: Applications in the Geosciences **42**: 1-35.

Cygan, R. T., et al. (2004). "Molecular models of hydroxide, oxyhydroxide, and clay phases and the development of a general force field." Journal of Physical Chemistry B **108**(4): 1255-1266.

Dauberosguthorpe, P., et al. (1988). "Structure and energetics of ligand-binding to proteins-escherichia-coli dihydrofolate reductase trimethoprim, a drug-receptor system." Proteins-Structure Function and Genetics **4**(1): 31-47.

Fetter, C. W. (1999). Contaminant hydrogeology. Upper Saddle River, NJ :, Prentice Hall.

Focazio, M. J., et al. (2008). "A national reconnaissance for pharmaceuticals and other organic wastewater contaminants in the United States - II) Untreated drinking water sources." Science of the Total Environment **402**(2-3): 201-216.

Fuller, M., et al. (2007). "Sorption of nonionic organic solutes from water to tetraalkylammonium bentonites: Mechanistic considerations and application of the Polanyi-Manes potential theory." Journal of Colloid and Interface Science **313**(2): 405-413.

Fu, X. A. and S. Qutubuddin (2005). "Swelling behavior of organoclays in styrene and exfoliation in nanocomposites." Journal of Colloid and Interface Science **283**(2): 373-379.

Gerischer, G. F. R. and R. D. Sanderson (1981). "The use of zeta-potential as a quantitative stability-criterion for concentrated clay suspensions .1. Specific electrokinetic properties of south-african kaolin suspensions and the determination of zeta-potential." Paperi Ja Puu-Paper and Timber **63**(8): 477-&.

Gerischer, G. F. R. and R. D. Sanderson (1981). "The use of zeta potential as a quantitative stability-criterion for concentrated clay suspensions. 2. Interrelation of the electrophoretic mobility of suspended kaolin particles with their flow behavior in concentrated suspensions." Paperi Ja Puu-Paper and Timber **63**(9): 561-&.

Gofenberg, I. V., et al. (1979). "Relationship between zeta-potential of clay particles and conditions for production of aluminum hydroxide coagulants." Colloid Journal of the Ussr **41**(2): 267-270.

Grathwohl, P. (1998). Diffusion in natural porous media : contaminant transport, sorption/desorption and dissolution kinetics. Boston :, Kluwer Academic Publishers.

Greathouse, J. A. and R. T. Cygan (2005). "Molecular dynamics simulation of uranyl(VI) adsorption equilibria onto an external montmorillonite surface." Physical Chemistry Chemical Physics **7**(20): 3580-3586.

Gungor, N. and T. Tulun (1994). "Studies on the zeta-potential of bentonite clay in aqueous-solution." Revue Roumaine De Chimie **39**(2): 177-182.

Gupta, A. K., et al. (2007). "Influence of the Stern layer on electrokinetic phenomena in porous media." Journal of Colloid and Interface Science **316**(1): 140-159.

He, H. P., et al. (2004). "Conformation of surfactant molecules in the interlayer of montmorillonite studied by C-13 MAS NMR." Clays and Clay Minerals **52**(3): 350-356.

He, H. P., et al. (2005). "Molecular simulation of the interlayer structure and the mobility of alkyl chains in HDTMA(+)/montmorillonite hybrids." Journal of Physical Chemistry B **109**(27): 13301-13306.

He, H. P., et al. (2004). "Infrared study of HDTMA(+) intercalated montmorillonite." Spectrochimica Acta Part a-Molecular and Biomolecular Spectroscopy **60**(12): 2853-2859.

Headley, J. V., et al. (2001). "Determination of diffusion and adsorption coefficients for volatile organics in an organophilic clay-sand-bentonite liner." Canadian Geotechnical Journal **38**(4): 809-817.

Heinz, H., et al. (2003). "Structure and phase transitions of alkyl chains on mica." Journal of the American Chemical Society **125**(31): 9500-9510.

Heinz, H., et al. (2005). "Force field for mica-type silicates and dynamics of octadecylammonium chains grafted to montmorillonite." Chemistry of Materials **17**(23): 5658-5669.

Heinz, H., et al. (2004). "Analysis of the phase transitions in alkyl-mica by density and pressure profiles." Journal of Chemical Physics **120**(8): 3847-3854.

Heinz, H., et al. (2007). "Self-assembly of alkylammonium chains on montmorillonite: Effect of chain length, head group structure, and cation exchange capacity." Chemistry of Materials **19**(1): 59-68.

Hinchliffe, A. (2003). Molecular modelling for beginners. Chichester, West Sussex, England ;, Wiley.

Hou, T. J., et al. (2000). "Adsorption and diffusion of benzene in ITQ-1 type zeolite: Grand canonical Monte Carlo and molecular dynamics simulation study." Journal of Physical Chemistry B **104**(39): 9356-9364.

Jaynes, W. F. and S. A. Boyd (1991). "Clay minerals type and organic-compound sorption be hexadecyltrimethylammonium-exchanged clays." Soil Science Society of America Journal **55**(1): 43-48.

Jaynes, W. F. and G. F. Vance (1999). "Sorption of benzene, toluene, ethylbenzene, and xylene (BTEX) compounds by hectorite clays exchanged with aromatic organic cations." Clays and Clay Minerals **47**(3): 358-365.

Johnson, R. L., et al. (1989). "Diffusive contaminant transport in natural clay-a field example and implications for clay-lined waste-disposal sites." Environmental Science & Technology **23**(3): 340-349.

Kjellander, R., et al. (1988). "Attractive double-layer interactions between calcium clay particles." Journal of Colloid and Interface Science **126**(1): 194-211.

Koneshan, S.; Rasaiah, J. C.; Lynden-Bell, R. M.; Lee, S. H. (1998). "Solvent structure, dynamics, and ion mobility in aqueous solutions at 25 degrees C." Journal of Physical Chemistry B **102** (21): 4193-4204.

Kraepiel, A. M. L., et al. (1999). "A model for metal adsorption on montmorillonite." Journal of Colloid and Interface Science **210**(1): 43-54.

Lagaly, G. (1981). "Characterization of clays by organic-compounds." Clay Minerals **16**(1): 1-21.

Lagaly, G., et al. (1976). "Problems in layer-charge determination of montmorillonites." Clay Minerals **11**(3): 173-187.

Lake, C. B.; Rowe, R. K. (2004). "Volatile organic compound diffusion and sorption coefficients for a needle-punched GCL." Geosyntetics International 11 (4), 257-272.

Lee, S., et al. (2012). "Organoclays as Variably Permeable Reactive Barrier Media to Manage NAPLs in Ground Water." Journal of Geotechnical and Geoenvironmental Engineering **138**(2): 115-127.

Lee, S. Y., et al. (2005). "Microstructural changes of reference montmorillonites by cationic surfactants." Applied Clay Science **30**(3-4): 174-180.

Liu, X., et al. (2009). "Molecular dynamics insight into the cointercalation of hexadecyltrimethyl-ammonium and acetate ions into smectites." American Mineralogist **94**(1): 143-150.

Lo, I. M. C. (2001). "Organoclay with soil-bentonite admixture as waste containment barriers." Journal of Environmental Engineering-Asce **127**(8): 756-759.

Lo, I. M. C. and X. Y. Yang (2001). "Use of organoclay as secondary containment for gasoline storage tanks." Journal of Environmental Engineering-Asce **127**(2): 154-161.

Loewenstein, W. (1954). "The distribution of aluminum in the tetrahedra of silicates and aluminates." American Mineralogist **39**(1-2): 92-96.

Lorenzetti, R. J., et al. (2005). "Hydraulic conductivities and effective diffusion coefficients of geosynthetic clay liners with organobentonite amendments." Geotextiles and Geomembranes **23**(5): 385-400.

McBride, M. B. (1997). "A critique of diffuse double layer models applied to colloid and surface chemistry." Clays and Clay Minerals **45**(4): 598-608.

Miyanishi, T. (1995). "Effects of zeta-potential on flocculation measurement in microparticle systems." Tappi Journal **78**(11): 135-141.

Mortland, M. M., et al. (1986). "Clay-organic complexes as adsorbents for phenol and chlorophenols." Clays and Clay Minerals **34**(5): 581-585.

Osman, M. A., et al. (2004). "Structure and properties of alkylammonium monolayers self-assembled on montmorillonite platelets." Journal of Physical Chemistry B **108**(8): 2580-2588.

Osman, M. A., et al. (2005). "Gas permeation properties of polyethylene-layered silicate nanocomposites." Journal of Materials Chemistry **15**(12): 1298-1304.

Park, J. W. and P. R. Jaffe (1993). "Partitioning of 3 nonionic organic-compounds between adsorbed surfactants, micelles, and water." Environmental Science & Technology **27**(12): 2559-2565.

Perret, D., et al. (2000). "The diversity of natural hydrous iron oxides." Environmental Science & Technology **34**(17): 3540-3546.

Pignatello, J. J. and B. S. Xing (1996). "Mechanisms of slow sorption of organic chemicals to natural particles." Environmental Science & Technology **30**(1): 1-11.

Plimpton, S. (1995). "Fast parallel algorithms for short-range molecular dynamics." Journal of Computational Physics **117**(1): 1-19.

Rapaport, D. C. (1995). The art of molecular dynamics simulation. Cambridge ;, Cambridge University Press.

Redding, A. Z., et al. (2002). "Organoclay sorption of benzene as a function of total organic carbon content." Journal of Colloid and Interface Science **250**(1): 261-264.

Richards, S. and A. Bouazza (2007). "Phenol adsorption in organo-modified basaltic clay and bentonite." Applied Clay Science **37**(1-2): 133-142.

Sastre, G., et al. (1999). "Diffusion of benzene and propylene in MCM-22 zeolite. A molecular dynamics study." Journal of Physical Chemistry B **103**(25): 5187-5196.

Satterfi.Cn, et al. (1973). "Restricted diffusion in liquids within fine pores " Aiche Journal **19**(3): 628-635.

Sharma, H. D. (2004). Geoenvironmental engineering : site remediation, waste containment, and emerging waste management technologies. Hoboken, N.J. :, Wiley.

Sheng, G. Y. and S. A. Boyd (1998). "Relation of water and neutral organic compounds in the interlayers of mixed Ca/trimethylphenylammonium-smectites." Clays and Clay Minerals **46**(1): 10-17.

Sheng, G. Y. and S. A. Boyd (2000). "Polarity effect on dichlorobenzene sorption by hexadecyltrimethylammonium-exchanged clays." Clays and Clay Minerals **48**(1): 43-50.

Skipper, N. T., et al. (1995). "Monte-carlo simulation of interlayer molecular-structure in swelling clay-minerals .1. methodology." Clays and Clay Minerals **43**(3): 285-293.

Skipper, N. T., et al. (1995). "Monte-carlo simulation of interlayer molecular-structure in swelling clay-minerals .2. monolayer hydrates." Clays and Clay Minerals **43**(3): 294-303.

Smith, D. E. and L. X. Dang (1994). "Computer-simulations of nacl association in polarizable water." Journal of Chemical Physics **100**(5): 3757-3766.

Smith, J. A. and P. R. Jaffe (1994). "Adsorptive selectivity of organic-cation-modified bentonite for nonionic organic contaminants." Water Air and Soil Pollution **72**(1-4): 205-211.

Smith, J. A. and P. R. Jaffe (1994). "Benzene transport through landfill liners containing organophilic bentonite " Journal of Environmental Engineering-Asce **120**(6): 1559-1577.

Smith, J. A., et al. (1990). "Effect of 10 quaternary ammonium cations on tetrachloromethane sorption to clay from water." Environmental Science & Technology **24**(8): 1167-1172.

Soule, N. M. and S. E. Burns (2001). "Effects of organic cation structure on behavior of organobentonites." Journal of Geotechnical and Geoenvironmental Engineering **127**(4): 363-370.

Sposito, G. (1984). The surface chemistry of soils. New York :, Oxford University Press ;.

Sridharan, A. and M. S. Jayadeva (1982). "Double-layer theory and compressibility of clays." Geotechnique **32**(2): 133-144.

Stadler, M. and P. W. Schindler (1993). "Modeling of h+ and cu2+ adsorption on calcium-montmorillonite." Clays and Clay Minerals **41**(3): 288-296.

Tambach, T. J., et al. (2006). "Molecular order and disorder of surfactants in clay nanocomposites." Physical Chemistry Chemical Physics **8**(23): 2700-2702.

Tambach, T. J., et al. (2006). "Hysteresis in clay swelling induced by hydrogen bonding: Accurate prediction of swelling states." Langmuir **22**(3): 1223-1234.

Thomas, M. M. and J. A. Clouse (1990). "Primary migration by diffusion through kerogen .1. model experiments with organic-coated rocks." Geochimica Et Cosmochimica Acta **54**(10): 2775-2779.

Thomas, M. M. and J. A. Clouse (1990). "Primary migration by diffusion through kerogen .2. hydrocarbon diffusivities in kerogen." Geochimica Et Cosmochimica Acta **54**(10): 2781-2792.

Thomas, M. M. and J. A. Clouse (1990). "Primary migration by diffusion through kerogen .3. calculation of geologic fluxes." Geochimica Et Cosmochimica Acta **54**(10): 2793-2797.

Upson, R. T. and S. E. Burns (2006). "Sorption of nitroaromatic compounds to synthesized organoclays." Journal of Colloid and Interface Science **297**(1): 70-76.

Vaia, R. A., et al. (1994). "Interlayer structure and molecular environment of alkylammonium layered silicates." Chemistry of Materials **6**(7): 1017-1022.

Weber, W. J., et al. (1991). "Sorption phenomena in subsurface systems - concepts, models and effects on contaminant fate and transport." Water Research **25**(5): 499-528.

Wen, X. Y., et al. (2006). "Arrangement, conformation, and mobility of surfactant molecules intercalated in montmorillonite prepared at different pillaring reagent concentrations as studied by solid-state NMR spectroscopy." Journal of Colloid and Interface Science **299**(2): 754-760.

Xie, W., et al. (2002). "Thermal stability of quaternary phosphonium modified montmorillonites." Chemistry of Materials **14**(11): 4837-4845.

Yang, L. Y., et al. (2003). "Chemical and biological regeneration of HDTMA-modified montmorillonite after sorption with phenol." Environmental Science & Technology **37**(21): 5057-5061.

Yariv, S. (2004). "The role of charcoal on DTA curves of organo-clay complexes: an overview." Applied Clay Science **24**(3-4): 225-236.

Yariv, S. and H. Cross (2002). Organo-Clay Complexs and Interactions. New York, Marcel Dekker.

Yeung, A. T., et al. (1996). "Field investigation of potential contamination by bitumen-coated piles." Journal of Geotechnical Engineering-Asce **122**(9): 736-744.

Young, D. A. and D. E. Smith (2000). "Simulations of clay mineral swelling and hydration: Dependence upon interlayer ion size and charge." Journal of Physical Chemistry B **104**(39): 9163-9170.

Zarzycki, P., et al. (2007). "Modelling of zeta-potential of the montmorillonite/electrolyte solution interface." Applied Surface Science **253**(13): 5791-5796.

Zeng, Q. H., et al. (2003). "Molecular dynamics simulation of organic-inorganic nanocomposites: Layering behavior and interlayer structure of organoclays." Chemistry of Materials **15**(25): 4732-4738.

Zhao, Q. and S. E. Burns (2012). "Molecular Dynamics Simulation of Secondary Sorption Behavior of Montmorillonite Modified by Single Chain Quaternary Ammonium Cations." Environmental Science & Technology **46**(7): 3999-4007.

Zhou, Q., et al. (2007). "Adsorbed para-nitrophenol on HDTMAB organoclay - A TEM and infrared spectroscopic study." Journal of Colloid and Interface Science **307**(2): 357-363.

Zhou, Q., et al. (2008). "Application of near infrared spectroscopy for the determination of adsorbed p-nitrophenol on HDTMA organoclay-implications for the removal of organic pollutants from water." Spectrochimica Acta Part a-Molecular and Biomolecular Spectroscopy **69**(3): 835-841.

Zhao, Z.; Rogers, D. M.; Beck, T. L. (2010). "Polarization and charge transfer in the hydration of chloride ions." Journal of Chemical Physics **132** (1).

Zhu, J. X., et al. (2003). "Arrangement models of alkylammonium cations in the interlayer of HDTMA(+) pillared montmorillonites." Chinese Science Bulletin **48**(4): 368-372.

Zhu, J. X., et al. (2005). "Characterization of organic phases in the interlayer of montmorillonite using FTIR and C-13 NMR." Journal of Colloid and Interface Science **286**(1): 239-244.

Zhu, R. L., et al. (2011). "Sorptive Characteristics of Organomontmorillonite toward Organic Compounds: A Combined LFERs and Molecular Dynamics Simulation Study." Environmental Science & Technology **45**(15): 6504-6510.